THICK AXISYMMETRIC TURBULENT BOUNDARY LAYER AND NEAR WAKE OF A LOW-DRAG BODY OF REVOLUTION

by
V. C. Patel and Y. T. Lee

Sponsored by
General Hydromechanics Research Program
of the Naval Sea Systems Command
David W. Taylor Naval Ship Research & Development Center
Contract No. N00014-75-C-0273

IIHR Report No. 210

Iowa Institute of Hydraulic Research
The University of Iowa
Iowa City, Iowa

December 1977

ABSTRACT

Detailed measurements of pressure distributions, mean velocity profiles and Reynolds stresses were made in the thick, axisymmetric boundary layer and the near wake of a low-drag body of revolution. The data are presented in graphical as well as tabular form for convenience in later analysis. These measurements shed some light on the joint influence of transverse and longitudinal surface curvatures and pressure gradients on the boundary-layer development and on the manner in which an axisymmetric boundary layer becomes a fully-developed wake. Apart from giving a complete set of data on such an important flow configuration, the measurements should provide a fairly rigorous test case for some of the recent turbulence closure models which claim a level of generality not achieved by the older phenomenological models. The present data have been used to provide an independent check on the accuracy of the simple, integral boundary-layer method proposed by Patel, and its extension to the calculation of the near wake made by Nakayama, Patel and Landweber. Preliminary calculations have also been performed using the differential equations of the thick axisymmetric turbulent boundary layer and a rate equation for the Reynolds stress derived from the turbulent kinetic-energy equation along the lines suggested by Bradshaw and others. By inclusion of recently proposed modifications to account for the effects of the extra rates of strain on the turbulence length scale arising from longitudinal and transverse surface curvatures, it is shown that the boundary layer in the tail region of a body of revolution is dominated by the extra strain rates and that more research is needed to account for them properly even in the most recent calculation procedures.

ACKNOWLEDGEMENTS

This research was carried out under the sponsorship of the Naval Sea Systems Command, General Hydro-Mechanics Research Program, Subproject SR023 01 01, administered by the David W. Taylor Naval Ship Research and Development Center, Contract N00014-75-C-0273. The authors are also indebted to Dr. A. Nakayama, who initiated the present experiment, to Dr. O. Guven, who assisted in the turbulence measurements and to Professor J.R. Glover for his assistance with hot-wire anemometry. The authors acknowledge the assistance of Professor B.R. Ramaprian through several stimulating discussions on the influence of longitudinal surface circulation on the turbulent boundary layers.

TABLE OF CONTENTS

LIST OF FIGURES

LIST OF TABLES

LIST OF SYMBOLS

a_1	structure parameter ($= -\overline{uv}/\overline{q^2}$)
C_D	drag coefficient ($= D/\frac{1}{2}\rho U_o^2 S$)
C_E	entrainment coefficient
C_f	skin-friction coefficient
C_p	pressure coefficient
D	drag force
e	extra rate of strain
e_{eff}	effective rate of strain
e_ℓ	rate of strain due to longitudinal curvature
e_t	rate of strain due to transverse curvature
G	diffusion function
h_1	metric coefficient in x-direction
H	axisymmetric shape factor ($= \Delta_1/\Delta_2$)
$\bar{H}$	planar shape factor ($= \bar{\delta}_1/\bar{\delta}_2$)
$\bar{H}^*$	entrainment shape parameter ($= \frac{\delta - \bar{\delta}_1}{\bar{\delta}_2}$)
I_k	integral defined by equation (20)
I_p	integral defined by equation (21)
k_1, k_2, k_3	constants
ℓ	mixing length or length scale
ℓ_A	mixing length (axisymmetric definition)
ℓ_o	length scale with no extra rate of strain
L	body length
p	static pressure
p_o	free-stream static pressure
q	$(u^2 + v^2 + w^2)^{1/2}$
Q	$(U^2 + V^2)^{1/2}$
r	radial distance
r_o	local radius of body
r_m	maximum r_o
Re	Reynolds number ($= U_o L/\nu$)
S	a representative area (maximum cross-sectional area of the body)

u	fluctuating velocity in x-direction
U	mean velocity in x-direction
U_c	mean velocity in axial direction at wake center
$\bar{U}_c$	$1 - U_c/U_\delta$
U_d	defect velocity $(= U_o - U)$
$U_{d_{max}}$	maximum U_d
U_o	velocity of the approach stream
U_δ	U at $y=\delta$
v	fluctuating velocity in y-direction
V	mean velocity in y-direction
w	fluctuating velocity in the azimuthal direction
x	coordinate parallel to the body surface and the centerline of the wake
X	axial coordinate
X_m	X where $r_o=r_m$
y	coordinate normal to the surface
$y_{1/2}$	y where $U_d = 1/2\ U_{d_{max}}$
α	constant
δ	boundary-layer thickness or radius of the wake
δ^*	radius of the displacement surface
$\bar{\delta}_1$	planar displacement thickness (equation 2)
$\bar{\delta}_2$	planar momentum thickness (equation 2)
Δ_1	mass-deficit area (equation 3)
Δ_2	momentum-deficit area (equation 3)
$\Delta_{2\infty}$	asymptotic value of Δ_2
ε	eddy viscosity
ε_A	eddy viscosity (axisymmetric definition)
θ	angle between axis and tangent to the body surface
κ	longitudinal curvature of the body surface
λ	constant
Λ	Pohlhausen parameter
ν	kinematic viscosity
ξ_1	X/X_m

ξ_2	$\frac{L-X}{L-X_m}$
ρ	density
τ	$\mu\frac{\partial u}{\partial y} - \rho\overline{uv}$

Subscripts

c	quantities evaluated at the wake centerline
δ	quantities evaluated at the edge of the boundary layer or wake
w	quantities evaluated at the wall

THICK AXISYMMETRIC TURBULENT BOUNDARY LAYER
AND NEAR WAKE OF A LOW-DRAG BODY OF REVOLUTION

I. INTRODUCTION

In some previous work at Iowa [1], measurements were made in the thick axisymmetric boundary layer over the tail region of a spheroid whose tail was modified by attaching a short conical piece in order to avoid separation. Those measurements have been used [2,3] in the development of simple integral entrainment methods for the calculation of thick boundary layers in which there exists a substantial variation of static pressure in the direction normal to the surface. Since the measurements indicated that a proper theoretical treatment of the flow in the tail region should consider the interaction between the boundary layer and the external potential flow, a more refined iterative technique was developed [4,5]. During the course of this latter study it became apparent that a successful interaction scheme must also take the flow in the near wake of the body into consideration. The lack of detailed mean-flow and Reynolds-stress data in the near wake of an unseparated body of revolution provided the incentive to perform the present experiments. The results of these experiments provide an opportunity to independently verify some of the assumptions that have been made in the previous theoretical developments.

II. EXPERIMENTAL ARRANGEMENT AND INSTRUMENTS

A. Wind Tunnel and Model. The experiments were performed in the large wind tunnel of the Iowa Institute of Hydraulic Research. The working section of the tunnel is 7.3 m long with a cross-section in the form of a 1.5 m octagon provided by throating a 3.7 m square approach section.

The selection of the model shape was based on a number of considerations and experience gained from the previous experiments [1]. First of all, it was desirable to select a practically important configuration rather than a simple geometric shape. Secondly, in order to highlight the influence of strong transverse surface curvature it was necessary to maintain a thick boundary layer over an extended region of the body. Thirdly, it was essential to avoid separation in the tail region so that the near wake could be explored in detail. Finally, in order to avoid the experimental [1] and theoretical [5] difficulties encountered in earlier work with a conical tail, it was thought convenient to consider a cusped-tail body so that the transition from the boundary layer to the wake would be smooth.

Parsons and Goodson [6] have considered a variety of shapes within a five-parameter family of bodies of revolution and used well known potential-flow and boundary-layer calculation methods and optimization techniques to recommend optimum low-drag shapes. The so-called F-57 body was selected out of these shapes as one which gave minimum resistance (at zero-incidence and practical Reynolds numbers) and, at the same time, met most of the requirements set out above. The coordinates of this body are given by

For $0 \leq X \leq X_m$ (fore-body)

$$\frac{r_o}{r_m} = \{-1.1723\ \xi_1^4 + 0.7088\ \xi_1^3 + 1.0993\ \xi_1^2 + 0.3642\ \xi_1\}^{1/2}$$

For $X_m \leq X \leq L$ (pointed aft-body)

$$\frac{r_o}{r_m} = \{-0.11996\ \xi_2^5 - 2.58278\ \xi_2^4 + 3.52544\ \xi_2^3 + 0.17730\ \xi_2^2\}^{1/2}$$

where $\xi_1 = X/X_m$, $\xi_2 = \frac{L-X}{L-X_m}$, X is the axial distance measured from the nose, r_o is the local radius, X_m is the axial location of the maximum radius r_m, and L is the total length of the body. The location of maximum radius is thus $X_m/L = 0.4446$ and the length to maximum diameter ratio, $L/2r_m = 4.2735$

For the present experiments, a model was constructed with L = 1.219 m (4.0 ft) so that $r_m = 0.1426$ m (0.4680 ft). The model was made hollow and in two parts in order to accomodate a scanivalve which was connected to the forty eight, 0.117 cm (0.046 in) diameter, pressure taps on the surface. Thirty two pressure taps lay on a single generator on the surface while the other fifteen were spaced circumferentially at three axial locations X/L = 0.104, 0.445 and 0.771, for use in model adjustment. The main body of the model was made of seasoned wood but metal nose- and tail-pieces, 5.08 cm and

12.70 cm in length, respectively, were used to provide accuracy and durability. The major features of the model are shown in Figure 1.

B. Model Alignment. The model was mounted in the wind tunnel by means of eight 0.84 mm diameter steel wires in tension, four at each end (Figure 1). Each wire was provided with a screw coupling so that its length could be adjusted and the model located at the desired position.

The model was placed in the tunnel with its axis coincident with the tunnel axis. Minor adjustments were then made to obtain axisymmetric flow conditions. Several means were employed to ascertain axial symmetry:

1. The static pressures measured along the circumference at the three axial locations were used to guide the preliminary positioning of the model.
2. Three 1.651 mm outside-diameter Preston tubes were then mounted on the surface at X/L = 0.771 at 120-degree intervals. The final position of the model was achieved by making small adjustments in the lengths of the rear support wires until the Preston tubes gave identical readings.
3. The final check on axial symmetry was provided by traversing a total pressure tube and a hot wire across the wake of the body at X/L = 1.10 and 1.20. Satisfactory symmetry was observed in terms of the profiles of the total pressure, the average velocity and the turbulence intensity.

All measurements reported here were made without further adjustments, the model being kept in the tunnel until the experiment was completed.

C. Instrumentation. The measurements in the boundary layer and the wake of the model were made with basically the same transverse mechanism as was described in [1]. The range of axial distances over which measurements could be made was, however, extended for the present experiments by making suitable modifications to the transverse mounting system situated outside the wind tunnel.

The total and static pressures were measured using micro-manometers and probes of standard design made from hypodermic tubing. In view of the uncertainities experienced earlier [1] in making static pressure measurements across the thick boundary layer where the mean-flow streamlines diverge appreciably from the surface, a special mechanism was built to rotate the head of the static probe into the direction of the local on-coming stream. Such a device was of course not required for the total pressure measurements due to the yaw-insensitivity of the pitot tube. Preston tubes of different diameters were used, in conjunction with the calibration of Patel [7], to measure the wall shear stress on the body. As indicated earlier, the surface pressure distribution was measured by means of the pressure taps on the model. The scanivalve was located inside the model primarily to avoid flow interference associated with a large number of pressure tubes running from the model to outside the tunnel. The scanivalve was driven by power supplied through the rear cables supporting the model. Thus, only one pressure tube had to be taken out of the model. The flow disturbance caused by this was considered negligible.

Mean velocities and Reynolds stresses within the boundary layer and the wake were measured by means of single-wire and cross-wire probes using the two-channel, constant-temperature, "Old-Gold-Model, Type 4-2H Hot-Wire Anemometer" and "Type 2 Mean-Product Computer" [8]. For the purposes of the present experiments, these instruments were modified to make them compatible with the gold-plated series of probes made by DISA. In order to ascertain that proper matching had been achieved and, at the same time, to establish measurement procedures to be used, a series of preliminary tests was conducted in fully-developed turbulent flow in a 5.08 cm diameter pipe. The measurements on the body of revolution were commenced only after achieving consistent and satisfactory agreement with the data of Laufer at a pipe Reynolds number of 50,000.

D. Transition Device. The computations [6] of Parsons and Goodson had indicated that transition on the F-57 body would occur naturally at X/L = 0.475, i.e. a short distance downstream of the location of maximum diameter, over a range of Reynolds numbers. Surface pressure distributions and other flow diagnostics on the model at a Reynolds number of 1.2×10^6 ($Re = U_o L/\nu$, where U_o is the velocity of the freestream approaching the body, L is the axial length of the body and ν is the kinematic viscosity) indicated that in reality transition occurred as a result of laminar separation followed by a turbulent reattachment, the bubble being in the neighborhood of the predicted location of transition. In order to eliminate this somewhat unsteady separation bubble and establish well defined conditions for the subsequent development of the turbulent boundary layer, a circular trip wire of 1.664 mm diameter was wrapped around the body at $X/L = 0.475$. Subsequent analysis of data revealed that the choice of such a relatively large trip wire was somewhat unfortunate since its downstream influence (say 100 diameters) may have persisted upto $X/L = 0.6$, where the first set of detailed measurements was made. Nevertheless, since the main body of data of interest here was collected from stations further downstream, the overall influence of the trip wire may be considered negligible.

III. MEAN FLOW MEASUREMENTS

All measurements reported here were made at a Reynolds number, based on the approach velocity U_o and the body length L, of 1.2×10^6, which corresponded to a nominal approach velocity 15.24 m/s (50 fps). U_o and the static pressure P_o at the end of the tunnel contraction were monitored throughout the experiments and have been used as reference conditions to nondimensionalize the data.

A. Surface Pressure Distribution. The static pressure distribution on the body surface is shown in Figure 2. Also shown for comparison is the potential-flow pressure distribution computed using the method of Landweber [9]. The close agreement between the two over most of the body indicates that the influence of wind-tunnel bockage is quite small. The departure of the measured pressure distribution from the theoretical one over the rear 25 percent of the body length is a result of the large thickness of the boundary layer in that region and its interaction with the external inviscid flow. It is seen that the influence of the increasing boundary layer thickness is to relieve the inviscid pressure gradients.

B. Upstream Laminar Boundary Layer. A single set of measurements was made in the laminar boundary layer upstream of the trip wire at the axial location $X/L = 0.433$. The velocity profile obtained by means of a flattened pitot tube is shown in Figure 3 along with two members of the Pohlhausen family of profiles, the values of the Pohlhausen parameter Λ being chosen to span the value of -1.65 estimated from the local boundary layer thickness, which was 1.93 mm, and the local pressure gradient.

C. Static Pressure Field. Figure 4 shows the variation of static pressure across the boundary layer and the wake at several axial positions in the range $0.551 < X/L < 2.472$. The convex longitudinal curvature of the body surface in the range $0.45 < X/L < 0.76$ apparently leads to the substantial increase in static pressure along the outward normal not only within the boundary layer but also for some distance beyond the edge of the boundary layer (which was determined from the distribution of total pressure and is indicated by the dotted line $y = \delta$). As the longitudinal curvature becomes concave and the boundary layer thickens as a result of the decreasing transverse radius r_o over the rear one-quarter of the body length, the trends of the static pressure variation are reversed, indicating that the mean streamlines are concave. The data in the near wake suggest that the streamlines become nearly straight within a short distance downstream of the tail.

The axial variation of static pressure at the edge of the boundary layer and wake inferred from these measurements is compared in Figure 2 with the surface pressure distribution. The magnitude of the pressure difference between the surface of the body and the edge of the boundary layer is apparent from Figure 2.

The present data have been used to assess the importance of the static pressure variation across the near wake in the prediction of the overall drag coefficient of bodies of revolution using the conventional Squire-Young type formula [10]. Further analysis of the pressure measurements in the thick boundary layer over the tail would undoubtedly shed some light on the magnitude of the extra terms in the momentum-integral equation which were found to be important in the previous experiments and analysis [2,5]. This aspect is considered in a later section.

D. Mean Velocity Profiles. Figures 5 shows the mean velocity profiles across the boundary layer and the wake at several axial stations. Here U and V are the components of velocity in the directions tangent and normal to the body surface, respectively, and Q is the resultant velocity, i.e. $(U^2 + V^2)^{1/2}$. Q was measured by means of a single hot-wire probe and was also obtained from the separate pitot and static probe traverses. It is seen that the two sets of data are in close agreement. The U and V components were measured by means of a cross-wire probe. It is known that this technique is not altogether satisfactory insofar as accuracy of the mean flow quantities is concerned. Nevertheless, the data show the relative magnitudes of the two components and indicate that the normal component attains maximum values in the neighborhood of X/L = 0.92, where it is roughly 12 to 13 percent of the tangential component. The implication of this with regard to the validity of the thin boundary-layer assumptions is obvious.

The velocity and shear-stress profiles measured at the most downstream station in the wake, namely X/L = 2.472, are compared in Figure 6 with the most downstream measurements of Chevray [11] and Schetz and others [12,13], and with the asymptotic axisymmetric wake profiles. It would be recalled that the measurements of Chevray were made in the wake of a prolate spheroid of axis ratio 6:1, where the boundary layer separated some distance upstream of the tail. The measurements of Schetz and others were made in the wake of an elongated body of axis ratio 12:1, consisting of a parabolic nose, a cylindrical middle body and a pointed stern, and it is not clear whether boundary layer separation was encountered before the tail. The velocity distribution in the far wake is assumed to be (see, for example, Schlichting [14])

$$\frac{U_d}{U_{d_{max}}} = \left\{1 - 0.293\left[\frac{y}{y_{1/2}}\right]^{3/2}\right\}^2 \qquad (1)$$

where U_d $(=U_o-U)$ is the velocity defect, $U_{d_{max}}$ is its value at the wake center and $y_{1/2}$ is the radial distance to the point where U_d is one-half of the maximum value $U_{d_{max}}$. The corresponding shear-stress profile is deduced by assuming a constant mixing length across the wake. It would be seen from Figure 6 that the present measurements at X/L = 2.472 may be regarded as those corresponding to a fully-developed axisymmetric far wake where the memory of the body which generated it is almost eliminated. It is, however, known (see, for example, Rodi [15]) that the mean velocity distribution in an axisymmetric wake continues to depend on body shape for quite large axial distances.

Figure 7 shows the variations of the velocity Q_c along the centerline of the wake and the total velocity Q_δ at the edge of the boundary layer and the wake. It is observed that the velocity at the edge of the wake reaches the freestream value by about X/L = 1.25. This is roughly 2.3 initial wake diameters, or one maximum body diameter, downstream of the tail. The wake develops under the influence of a small favorable axial pressure gradient over this region. The maximum velocity defect in the wake, $Q_\delta - Q_c$, is also seen to decrease rapidly within this distance. On the basis of these observations it may be conjectured that the so-called near wake is confined to this region, and we may expect the measurements further downstream to conform with the asymptotic wake behavior discussed above.

E. Integral Parameters. The velocity profiles deduced from the pitot and static+ traverses were integrated to determine the various types of integral parameters discussed earlier in [1]. The overall shape of the velocity profile is best described by the so-called "planar" displacement and momentum thicknesses:

$$\overline{\delta_1} = \int_o^\delta \left(1 - \frac{U}{U_\delta}\right) dy, \qquad \overline{\delta_2} = \int_o^\delta \frac{U}{U_\delta}\left(1 - \frac{U}{U_\delta}\right) dy \tag{2}$$

which do not take the axial symmetry of the flow into account. On the other hand, the physical mass- and momentum-flux deficits in the boundary layer and the wake are given by the integral areas

$$\Delta_1 = \int_o^\delta \left(1 - \frac{U}{U_\delta}\right) r dy, \qquad \Delta_2 = \int_o^\delta \frac{U}{U_\delta}\left(1 - \frac{U}{U_\delta}\right) r dy \tag{3}$$

respectively+. Here, U_δ is the velocity component at the edge of the boundary layer and wake ($y = \delta$), tangent to the body surface for the boundary layer and parallel to the axis for the wake, r is the radial distance from the axis of symmetry and y is measured normal to the surface of the body. Thus, $r=r_o+y \cos\theta$, where θ is the angle between the axis and the tangent to the body surface, for the boundary layer, and r=y for the wake.

The variations of $\overline{\delta_2}$ and Δ_2 with X/L in the turbulent boundary layer

+ In view of the inaccuracies in the direct measurement of U, the integral parameters have been determined using Q. The error is negligible for practical purposes.

and wake, and the corresponding shape parameters, defined by

$$\bar{H} = \overline{\delta_1}/\overline{\delta_2}\ , \qquad H = \Delta_1/\Delta_2 \tag{4}$$

are shown in Figure 8. It should be noted that the total drag coefficient C_D of the body is related to the asymptotic value $\Delta_{2\infty}$ of the momentum-deficit area in the far wake via

$$C_D = \frac{D}{\frac{1}{2}\rho U_o^2 S} = \frac{4\pi\ \Delta_{2\infty}}{S} \tag{5}$$

where D is the drag force and S is a representative area of the body. The measurements at X/L = 2.472 indicate that the drag coefficient, based on frontal area, of the present body (with the trip wire) is 0.0092. $\overline{\delta_2}$, on the other hand, has no special physical significance, but the parameter $\bar{H}$ indicates the shape of the velocity distributions.

Finally, the normal distance by which the external inviscid-flow streamlines are displaced outward due to the presence of the boundary layer and the wake, i.e. the displacement thickness δ^*, may be obtained from the relation [1]

$$r_o\ \delta^*\ (1 + \frac{1}{2}\frac{\delta^*}{r_o}\cos\ \theta) = \Delta_1 \tag{6}$$

for the boundary layer, and

$$\frac{1}{2}\ \delta^{*2} = \Delta_1 \tag{7}$$

for the wake. The displacement surface deduced in this manner is shown in Figure 9 along with the physical edge of the boundary layer and the wake. It should be emphasized here that this figure was drawn to scale without any distortion so that it clearly illustrates what is meant by a <u>thick boundary layer</u>. It is particularly interesting to note the magnitude of the displacement effect of the boundary layer over the rear one-quarter of the body and that in the near wake. The implication of this with regard to the boundary layer and near wake computations is discussed later on.

F. Wall Shear Stress. Three different Preston tubes of external diameters 1.651, 1.270 and 0.711 mm were used to measure the wall shear-stress distribution on the body. Figure 10 shows the results obtained with the largest and the smallest tubes. The data from the intermediate size tube lay between these. The use of Preston tubes of course pre-supposes the validity of the usual law of the wall even in the thick axisymmetric boundary layer. The small but systematic variation in the wall shear stress obtained with the three tubes indicated the need for an alternative approach. The velocity profile data were therefore replotted in the form suggested by Clauser, but using the extended law of the wall proposed by Patel [16], to determine the wall shear stress compatible with that law. These results are also shown in Figure 10. It will be seen that substantial departures from the usual law of the wall (over the distance occupied by the Preston tubes) are indicated only in the neighborhood of the tail ($X/L > 0.94$, say).

IV. TURBULENCE MEASUREMENTS

Hot-wire traverses were made at six axial stations in the boundary layer (X/L = 0.60, 0.80, 0.88, 0.92, 0.96 and 1.00) and six stations (X/L = 1.02, 1.06, 1.20, 1.30, 1.40 and 2.47) in the wake. The mean-velocity profiles obtained in this manner were discussed earlier. The distributions of the four non-zero Reynolds stresses, namely $\overline{u^2}$, $\overline{v^2}$, $\overline{w^2}$, and $\overline{uv}$, are shown in Figures 11, 12, 13 and 14, respectively. It will be observed that two sets of data are shown in each figure for the station $X/L = 1.00$, which corresponds to the tail of the body. The only difference between these is the direction of traverse. Initially, a traverse was made normal to the axis of the body and the wake ($\theta=0$), but since the semi-angle of the body tail is 5.7 degrees, another traverse was made ($\theta=5.7°$) in the direction normal to the surface of the body at the tail. Figures 11, 12 and 14 show that the results of the two traverses differ appreciably in the distributions of $\overline{v^2}$ and $\overline{uv}$, and that the data in terms of the boundary-layer coordinates ($\theta=5.7°$) are more consistent. It is obvious that this ambiguity would not have arisen had the tail been exactly cusped. However, the present data indicate the need for a very careful treatment of the flow in the neighborhood of pointed tails where the change from the boundary layer to the wake coordinates occurs abruptly. The data corresponding to $\theta=5.7°$ is used in the subsequent analysis.

Insofar as the measurements of the Reynolds stresses in the thick boundary layer are concerned, it is observed that they are qualitatively similar to those made earlier in the tail region of a modified spheroid [1]. Quantitatively, however, the present data are expected to be quite different from the earlier set due to the different pressure gradient and surface curvature histories.

The distributions of shear stress $\overline{uv}$ were used in conjunction with the mean-velocity profiles to calculate the variation of eddy viscosity according to the planar (ε) and the axisymmetric (ε_A) definitions

$$-\overline{uv} = \varepsilon\left(\frac{\partial U}{\partial y}\right) \quad , \qquad -\overline{uv} = \varepsilon_A \frac{1}{r}\frac{\partial}{\partial y}(Ur) \tag{8}$$

and the corresponding variation of mixing length

$$-\overline{uv} = \ell^2\left(\frac{\partial U}{\partial y}\right)^2 \quad , \qquad -\overline{uv} = \ell_A^2 \left[\frac{1}{r}\frac{\partial}{\partial y}(Ur)\right]^2 \tag{9}$$

The values of ε_A and ℓ_A were found to be substantially lower than those of ε and ℓ which are shown in Figures 15 and 16, respectively. The boundary-layer data are again in general agreement with the observations made on the modified spheroid [1] (reproduced here as Figures 17 and 18) insofar as they indicate a substantial reduction of eddy viscosity and mixing length as the boundary layer thickens towards the tail. They increase again with axial distance in the wake. The mixing length reaches a nearly constant value in the range $0.08 < \ell/\delta < 0.10$ at the most downstream station $X/L = 2.47$, where, as indicated earlier, the wake approaches a nearly fully-developed state. The major conclusion to be drawn from these measurements is that the characteristics of the turbulence in the region where the boundary layer is thick, and in the near wake, i.e. over $0.75 < X/L < 1.25$, say, are markedly different from those of a thin turbulent boundary layer and the asymptotic far wake.

Yet another quantity that is of interest in the discussion of the characteristics of the turbulence is the so-called structure parameter

$a_1 \equiv -\overline{uv}/\overline{q^2}$. It would be recalled that for most thin turbulent shear layers this is nearly constant across the flow and equal to about 0.15. The distributions of a_1 across the boundary layer and the wake of the low-drag body are shown in Figure 19. The corresponding results deduced from the modified spheroid boundary layer [1] are shown in Figure 20. From Figure 19 it is seen that a_1 remains nearly constant around 0.14 in the inner one-half of the boundary layer on the low-drag body and indicates some reduction with normal distance over the outer half. The data in the wake, however, appear to indicate nearly constant values again. Examination of Figure 20, corresponding to the boundary layer on the modified spheroid, indicates that in those experiments a_1 undergoes a drastic reduction right across the boundary layer, the minimum values of a_1 being reached at $X/L = 0.93$.

Possible reasons for the above observations on ℓ and a_1 are discussed in a subsequent section.

V. TABULATION OF DATA

Since the main thrust of this report is to present the results of the experimental study, the complete set of data is tabulated. Table 1 provides a summary of the body geometry, pressure and freestream-velocity distributions, and the integral parameters of the boundary layer and the wake. Tables 2 through 26 contain the total- and static-pressure as well as mean-velocity distributions across the boundary layer and wake at the 25 axial measuring stations. For the 12 stations at which hot-wire traverses were made, the corresponding tables contain the distributions of the mean as well as turbulence quantities.

VI. SOME PRELIMINARY ANALYSIS OF DATA

As remarked upon earlier, the measurements of Patel, Nakayama and Damian [1] in the tail region of a modified spheroid provided the impetus to the development of some theoretical methods for the calculation of thick axisymmetric turbulent boundary layers [2,3] and the interaction between the boundary layer, the wake and the external potential flow [4,5] in the tail region of bodies whose shapes are such that the boundary layer does not separate. The main objective of the present experiment was therefore to obtain data from a body of significantly different shape so as to provide an independent check on some of the observations that had been made earlier and the assumptions that were made in the theoretical models. This section is devoted to a preliminary discussion of these topics.

A. Influence of Transverse and Longitudinal Curvatures. Figure 21 shows the conventional transverse and longitudinal curvature parameters for the present and the earlier spheroid experiments. The ratio of the boundary-layer thickness to the transverse radius of curvature, δ/r_o, is seen to be more than twice as large in the present experiments as in the previous ones. In both cases, however, δ/r_o is less than 0.4 upto $X/L = 0.75$ so that the boundary layers may be regarded as thin upto that station. Over the rear one-quarter of the body length, the influence of transverse curvature would prevail not only through the geometrical terms in the equations of motion (e.g. the term $U \frac{\partial r}{\partial x}$ in the equation of continuity or $\frac{\Delta_2}{r_o} \frac{dr_o}{dx}$ in the integral momentum equation) but also through any direct effect on the turbulence. The precise nature of the latter is not known at the present time since the turbulence is also affected by the longitudinal curvature of the streamlines associated with the curvature of the surface as well as the curvature induced by the rapid thickening of the boundary layer over the tail.

The longitudinal surface curvature parameter $\kappa\delta$ is seen to be quite different for the two bodies. In the case of the modified spheroid the curvature is convex upto $X/L = 0.933$ and zero thereafter, while that of the low-drag body is initially convex and becomes concave for $X/L > 0.772$. Now, several recent studies with nominally two-dimensional turbulent boundary layers [17-26] have indicated that even mild ($\kappa\delta \sim 0.01$) longitudinal surface curvature exerts a dramatic influence on turbulence structure. In particular, it is noted that quantities such as the mixing length ℓ, the structure parameter $a_1 \equiv -\overline{uv}/\overline{q^2}$ and the shear-stress correlation coefficient $\overline{uv}/(\sqrt{\overline{u^2}}\sqrt{\overline{v^2}})$ are influenced markedly, and experiments indicate that convex streamline curvature leads to a reduction in these, whereas concave curvature has an opposite effect. While these studies in thin boundary layers, where the streamline curvature is dictated by that of the surface, would tend to indicate that the somewhat larger reduction in ℓ (compare Figure 18 with 16) and the drastic reduction in a_1 (compare Figure 20 with 19) observed on the modified spheroid may be attributed to the large, prolonged, convex longitudinal curvature of the surface, it should be noted that the rapid growth of the boundary layer over the tail tends to cancel out some of the convex curvature of the streamlines. Nevertheless, in view of the fact that the longitudinal streamline curvature in both experiments is large, it is possible that a part, if not all, of the changes in parameters such as ℓ and a_1 may be due to that factor.

In reference [18] Bradshaw has argued that whenever a thin shear layer experiences an extra rate of strain, i.e. in addition to the usual one $\partial U/\partial y$, the response of the turbulence parameters is an order of magnitude greater than one would expect from an observation of the appropriate extra terms in the mean-flow equations of momentum and continuity. For THIN shear layers and SMALL extra rates of strain he proposed a simple linear correction for the length scale of the turbulence, viz.

$$\frac{\ell}{\ell_o} = 1 + \frac{\alpha e}{\partial U/\partial y} \qquad (10)$$

where ℓ_o is the length scale with the usual rate of strain $\partial U/\partial y$, ℓ is the length scale with the extra rate of strain e and α is a constant of the order of 10. For the axisymmetric boundary layer being considered here, there are two extra rates of strain:

$$e_\ell = -\frac{\kappa U}{1 + \kappa y} \qquad (11)$$

due to the longitudinal curvature, and

$$e_t = \frac{U}{1 + \kappa y}\frac{1}{r}\frac{\partial r}{\partial x} = \frac{U}{r}\frac{dr_o}{dx} \qquad (12)$$

due to the convergence or divergence of the streamlines (in planes parallel to the surface) associated with the changes in the transverse curvature. The former is a shearing strain while the latter is a plain strain, and it is not certain whether the two effects can be added simply in using equation (10) as recommended by Bradshaw [18]. If this is the case, however, we would expect a greater reduction in ℓ in the tail region of the modified spheroid, where κ is positive and dr_o/dx is negative, than on the low-drag body, where κ becomes negative and would therefore tend to offset the influence of the negative dr_o/dx. Although the data shown in Figures 16 and 18 appear to bear this out to some extent, a direct comparison between equations (10), (11) and (12) and the data has not been attempted, especially in view of Bradshaw's [27] assertion that equation (10) should be used in conjunction with a simple rate equation which accounts for the upstream extra rate-of-strain history. He proposes

$$\frac{\ell}{\ell_o} = 1 + \frac{\alpha e_{eff}}{\partial U/\partial y} \tag{13}$$

and

$$\frac{d}{dx}(e_{eff}) = \frac{e-e_{eff}}{10\,\delta} \tag{14}$$

where e is the actual rate of strain, e_{eff} is its effective value and 10δ represents the "lag length" over which the boundary layer responds to a change in e. Now, in order to determine the merit of this proposal, it is of course necessary to incorporate it in an actual calculation and make a comparison between the predictions and measurement. Such an attempt has been made here.

B. Solutions of the Differential Equations. As shown by Patel [28] and Nakayama, Patel and Landweber [5], the differential equations of a thick axisymmetric turbulent boundary layer may be written

$$\frac{U}{h_1}\frac{\partial U}{\partial x} + V\frac{\partial U}{\partial y} + \frac{\kappa}{h_1}UV + \frac{1}{\rho h_1}\frac{\partial p}{\partial x} - \frac{1}{rh_1}\frac{\partial}{\partial y}\left(\frac{h_1 r\tau}{\rho}\right) = 0 \tag{15}$$

$$\frac{U}{h_1}\frac{\partial V}{\partial x} + V\frac{\partial V}{\partial y} - \frac{\kappa}{h_1}U^2 + \frac{1}{\rho}\frac{\partial p}{\partial y} = 0 \tag{16}$$

$$\frac{\partial}{\partial x}(Ur) + \frac{\partial}{\partial y}(rh_1V) = 0 \tag{17}$$

where U and V are the components of mean velocity in the x and y directions, along and normal to the body surface, respectively, $h_1 = 1 + \kappa y$, κ being the longitudinal surface curvature, $\tau = -\rho\overline{uv} + \mu\frac{\partial U}{\partial y}$, ρ and μ are the density and dynamic viscosity of the fluid, and $r = r_o + y \cos\theta$ is the radial distance measured from the body axis. These equations allow for the variation of static pressure across the boundary layer. If the Reynolds stress $\overline{uv}$ is determined by a one-equation model using the turbulent kinetic-energy equation, as proposed by Bradshaw, Ferriss and Atwell [29], then the appropriate closure equation is

$$\frac{1}{2a_1}\{\frac{U}{h_1}\frac{\partial\tau}{\partial x} + V\frac{\partial\tau}{\partial y}\} - \tau\{\frac{\partial U}{\partial y} - \kappa U\} + \frac{1}{r}\frac{\partial}{\partial y}\{rG\frac{\tau}{a_1^{3/2}}\sqrt{\frac{\tau_{max}}{\rho}}\} + \frac{1}{\ell}\frac{\tau^{3/2}}{\rho^{1/2}} = 0 \qquad (18)$$

where a_1 is a constant (=0.15), $G(y/\delta)$ is a diffusion function and $\ell(y/\delta)$ is a length-scale function identified with the usual mixing length. It is assumed that ℓ is given by equations (13) and (14) where $\ell_o(y/\delta)$ is the universal function corresponding to a thin, flat-surface boundary layer [29] with no extra rate of strain.

A computer program available for the solution of equations corresponding to equations (15), (17) and (18) for a thin two-dimensional boundary layer was modified to introduce the longitudinal- and transverse-curvature terms and, instead of incorporating the y-momentum equation (16) into the solution procedure, changes were made such that a prescribed variation (in the y-direction) of the pressure gradient $\frac{\partial p}{\partial x}$ could be used. The computer program was then used to perform calculations for the two bodies of revolution for which detailed experimental data are available.

Preliminary calculations quickly indicated that the extra rates of strain in both experiments were much larger than those examined by Bradshaw [18] in support of the linear length-scale correction formula. In fact, the use of the linear formula led to a rapid decrease in ℓ and indicated almost total destruction of the Reynolds stress across the boundary layer. In view of this, recourse was made to a non-linear correction formula in the form

$$\frac{\ell}{\ell_o} = \{1 - \frac{\alpha e_{eff}}{\partial U/\partial y}\}^{-1} \qquad (13a)$$

which reduces to the linear one, equation (13), for small extra rates of strain. Equations (15), (17), and (18), together with (11), (12), (13a), and (14), were then solved with the following inputs:

A: the measured wall pressure distribution and $\ell(y/\delta) = \ell_o(y/\delta)$

B: the measured wall pressure distribution with $\ell(y/\delta)$ corrected for only the longitudinal curvature ($e = e_\ell$) according to equations (13a) and (14)

C: the measured wall pressure distribution with $\ell(y/\delta)$ corrected for only the streamline convergence ($e = e_t$) according to equations(13a) and (14)

D: As above, but with $e = e_\ell + e_t$

E: Using $e = e_\ell + e_t$ in equations (13a) and (14), and a variable $\frac{\partial p}{\partial x}$ across the boundary layer evaluated by assuming a linear variation in p from y=0 to y=δ and using the measured values of C_{pw}, $C_{p\delta}$ and δ.

The constant a_1 and the diffusion function G were maintained at their usual thin boundary-layer values [29] in all calculations. Thus, case A corresponds to an axisymmetric boundary layer with thin, two-dimensional boundary-layer physics. The other cases enable the evaluation of the influence of the extra rates of strain as well as the static-pressure variation through the boundary layer. The calculations were started with the velocity and shear-stress profiles measured at X/L = 0.662 for the modified spheroid and X/L = 0.601 for the low-drag body.

The major results of the aforementioned calculations are summarized in Figure 22 (a-i) for the low-drag body and in Figure 23 (a-i) for the modified spheroid. Each figure contains comparisons between the experimental and calculated velocity, shear-stress and mixing-length profiles at a few representative axial stations as well as the development of the integral parameters $\delta, \bar{\delta}_2, \Delta_2, \bar{H}$, H and C_f with axial distance. In the interest of clarity, the results of all the calculations (cases A through E) are shown only at one axial station (Figure 22c and 23c), those at other stations being qualitatively similar.

Considering the most detailed figures, 22c and 23c, first, it is clear that the predictions are rather poor when the length scale ℓ is assumed to be the same as that in a thin boundary layer (case A). This is particularly evident in the prediction of the shear-stress profiles. Incorporation of the correction to ℓ to account for the extra rate of strain due to longitudinal curvature (case B) leads to a marginal improvement in the case of the low-drag body and a dramatic improvement for the modified spheroid. This is to be expected in view of the grossly different curvature histories of the two bodies as noted earlier (Figure 21). Nevertheless, it is clear that this correction by itself is not sufficient to account for the differences between the data and the calculations with thin boundary-layer turbulence models. The application of the correction for the extra rate of strain due to the transverse curvature (case C) appears to account for a major portion of these differences for both bodies. The influence of transverse curvature is in fact seen to be somewhat larger for the low-drag body as would be expected from the fact that δ/r_o is greater in that case (Figure 21). The simple addition of the effects of the two rate of strains (case D) leads to a significant improvement in the prediction of both the velocity profiles and the shear stress profiles. The incorporation of a variable pressure gradient across the boundary layer (case E), which is an attempt to account for the normal pressure gradients, appears to make a significant improvement in the prediction of the velocity profile in the case of the modified spheroid, but its influence is small, and confined to the outer part of the boundary layer, in the case of the low-drag body.

Examination of the velocity and shear-stress profiles at several axial stations shown in Figures 22b, c, d and 23b, c, d suggests that the incorporation of the non-linear length-scale correction of equation (13a), the associated rate equation (14) and the static-pressure variation in the equations of the thick boundary layer, which already include the direct longitudinal and transverse curvature terms, leads to satisfactory overall agreement with the data for both bodies. The predictions of the shear stress profiles are consistent with those of the mixing-length distributions shown in Figures 22e and 23e insofar as lower shear stresses correspond to an over correction in the mixing length.

It is interesting to note that, for both bodies the calculation procedure predicts normal components of mean velocity which are of the same order of magnitude as those measured. The relatively close agreement between the predictions and experiment for both components of velocity is perhaps a good indication of the axial symmetry achieved in the experiments. The large values of the normal velocity and the influence of static pressure variation noted above would appear to indicate that the incorporation of the y-momentum equation in the calculation procedure would be worthwhile. Note that this has been avoided in the present calculations by using the measured pressure distributions at the surface and the outer edge of the boundary layer.

Finally, the comparisons made in Figures 22(f-i) and 23(f-i) with respect to the integral parameters of the boundary layer show several interesting and consistent features. It is observed that the prediction of the physical thickness of the boundary layer is insensitive to the changes in ℓ as well as the inclusion of static pressure variation. The planar momentum thickness $\bar{\delta}_2$ and the momentum-deficit area Δ_2 are also insensitive to changes in ℓ. The variation of static pressure across the boundary layer appears to make a small but noticeable contribution to the development of Δ_2 in both cases. However, it is not large enough to account for the differences between the calculations and experiment. Indeed, the disagreement between the experimental results and calculations for Δ_2 are somewhat surprising in view of the excellent agreement shown by the planar momentum thickness $\bar{\delta}_2$. A closer examination of the predictions of the two quantities suggests, however, that the maximum percentage of error in both cases is about the same. The predictions for the shape parameters $\bar{H}$ and H, and the wall shear stress, shown in Figures 22h,i and 23h,i, again indicate that the best overall results are obtained with corrections to ℓ for both extra rates of strain and that inclusion of the static pressure variation makes only small contributions. The influence of the reduction in the mixing length, caused here by convex curvature and lateral convergence of streamlines, on the various integral parameters is similar to that shown earlier by Bradshaw [17] and others in connection with longitudinal surface curvature effects alone.

C. <u>Integral Correlations and Predictions</u>. One of the objectives of the on-going research is to investigate the possibilities of extending boundary-layer calculation methods into the near wake and recover the well known asymptotic axisymmetric wake behavior. One such attempt was made in

[5] where the simple entrainment method of Patel [2] was extended to calculate the development of the wake. It is therefore of interest not only to verify the assumptions made in the boundary-layer method but also the additional assumptions required for its extension to wakes.

The method of Patel is based on that of Head [30] for thin two-dimensional boundary layers. It involves the simultaneous solution of the momentum integral equation for the thick axisymmetric boundary layer [2,5],

$$\frac{d\Delta_2}{dx} + (H + 2)\frac{\Delta_2}{U_\delta}\frac{dU_\delta}{dx} - \frac{1}{2}C_f r_o - I_k - I_p = 0 \tag{19}$$

where $$I_k = \kappa\int_o^\delta \frac{UV}{U_\delta^2} r\, dy \tag{20}$$

and $$I_p = \frac{1}{U_\delta^2}\int_o^\delta r\frac{\partial}{\partial x}\left\{\frac{p-p_\delta}{\rho} - \frac{V_\delta^2}{2}\right\} dy \tag{21}$$

and an equation relating the rate of mass entrainment into the boundary layer to the shape of the velocity profile, together with a number of auxiliary relations between the planar and axisymmetric integral parameters deduced from assumed velocity profile shapes. For thick axisymmetric boundary layers, two additional assumptions are made: that the empirical correlation between the entrainment shape-parameter $\bar{H}^* = (\delta - \bar{\delta}_1)/\bar{\delta}_2$ and the usual shape parameter $\bar{H} = \bar{\delta}_1/\bar{\delta}_2$, and the correlation between the entrainment coefficient C_E and $\bar{H}^*$, are the same as in two-dimensional flow provided the shape parameters are based only on the shape of the velocity profile (i.e. planar definitions of equation (2) are used) and C_E is defined appropriately, viz

$$C_E = \frac{1}{U_\delta r_\delta h_{1\delta}}\frac{d}{dx}\left[U_\delta\left(r_o\delta - \Delta_1 + \frac{1}{2}\delta^2\cos\theta\right)\right]^{+} \tag{22}$$

where $r_\delta = r_o + \delta\cos\theta$, $h_{1\delta} = 1 + \kappa\delta$ and the quantity within the square brackets represents the mass flux within the boundary layer. The assumption concerning the shape-parameter correlation was verified directly in [5] using the then available data from boundary layers and wakes. Figure 24 shows that the data from the low-drag body supports this observation. Upon closer examination, however, it is seen that there is a systematic departure from the boundary-

---

+This definition of C_E differs slightly from that of Patel [2] and is in agreement with the improvement suggested by Nakayama, Patel and Landweber [5] and Granville [3].

layer correlation and that the data from the most downstream wake stations are in better agreement with the $\bar{H}^*$ vs $\bar{H}$ relation deduced from the asymptotic wake profile of equation (1). Wake calculations have been performed using both correlations to demonstrate their influence. An attempt was made to deduce the variation of C_E with $\bar{H}^*$ using equation (22) and the measured values of the quantities appearing therein. The inaccuracies associated with the differentiation in equation (22), however, masked any systematic trend, and therefore the previous assumption that the correlation of Head continues to apply in the wake has been retained. The influence of this could then be determined by the performance of the overall solutions.

The method of Patel [2], with the modification of C_E noted earlier, was used to predict the development of the boundary layer and the wake of the low-drag body. Since the tail of the low-drag body is nearly cusped, it was not necessary to change the coordinates abruptly at the tail, and make a special analysis as in Nakayama, Patel and Landweber [5], in order to continue the calculation into the wake. The assumption of an exponential velocity profile family in the wake, suggested in [5], namely

$$\frac{U}{U_\delta} = 1 - \bar{U}_c e^{-\lambda (y/\delta)^2} \qquad (23)$$

where

$$\bar{U}_c = 1 - \frac{U_c}{U_\delta}$$

U_c is the velocity at the wake center and λ is a parameter, was retained. The inter-relationships between the planar and the axisymmetric integral parameters were obtained in [5] by using $\lambda = 3.22$ in equation (23), performing the integrations in equations (2) and (3) upto $y/\delta=1$ and curve-fitting. In the present work, this procedure has been simplified by setting the outer limit of integration equal to infinity so that the necessary relations are obtained analytically. These are

$$\left.\begin{aligned} \Delta_1 &= \frac{k_2}{\bar{U}_c (k_1 - \bar{U}_c)^2} \bar{\delta}_2^2 \\ \Delta_2 &= \frac{k_2 - k_3 \bar{U}_c}{\bar{U}_c (k_1 - \bar{U}_c)^2} \bar{\delta}_2^2 \\ H &= \frac{k_2}{k_2 - k_3 \bar{U}_c} \end{aligned}\right\} \qquad (24)$$

and

$$\bar{H} = \frac{k_1}{k_1 - \bar{U}_c}$$

where $k_1 = \sqrt{2}$, $k_2 = 4/\pi$ and $k_3 = 2/\pi$. It is of interest to note that these relations are independent of λ and therefore a constant value of λ is not implied.

The boundary layer calculation was started at $X/L = 0.70$, where the boundary layer has recovered from the influence of the trip wire, and terminated at the tail. The initial conditions for the wake were provided by requiring the continuity of the physical mass and momentum deficits there, i.e. Δ_2 and H remain continuous in going from the boundary layer to the wake. Since the integral method is basically a two-parameter method, this leads to a discontinuity of the other parameters, such as the boundary layer thickness δ. The wake calculation was terminated in the far wake, where the momentum deficit approaches a constant value.

A set of calculations was first performed using only the pressure distribution along the body surface and wake centerline (i.e. with $I_k = I_p = 0$ in equation (19), as suggested by Patel [2]) and the two alternative shape-parameter relations $\bar{H}^*(\bar{H})$ (Figure 24) in the wake. The results of these are shown in Figure 25 and identified as curves A and B. It is seen that the method predicts most of the quantities reasonably well in the boundary layer. In fact, comparison of Figure 25 with Figure 22(f-i) shows that the simple integral method appears to do just as well as the differential one with respect to the prediction of the integral parameters δ, Δ_2, $\bar{\delta}_2$, H, $\bar{H}$ and C_f. The performance of the method in the wake is not as good as that for the boundary layer. This is due partly to the retention of the boundary layer entrainment correlation and more likely to the inadequacy of the exponential velocity profile family used to describe the velocity distribution in the near as well as far wake. The difference between curves A and B, which correspond to the two different shape-parameter relations, clearly indicate the need for the introduction of another parameter which would govern the gradual change from the boundary layer profile at the tail to the asymptotic wake profile in the far wake. Although such an additional parameter would eliminate the discontinuity in δ (Figure 25a) and improve the prediction of the near wake, it is not entirely clear what additional equation could be used to determine its streamwise distribution within the framework of an integral method.

Another possible source of the disagreement between the calculations and experiment is the use of the pressure distribution on the body surface and the wake centerline to compensate for the neglected static pressure and curvature integrals (I_p and I_k) in the momentum integral equation. An attempt has been made to evaluate these integrals from the experimental data. The procedure that has been adopted is described in the Appendix. Although this involves several approximations and inaccuracies stemming from the differentiation of ill-defined quantities such as the boundary layer and wake thicknesses and the normal velocity at the edge of the boundary layer and the wake, it is seen from Figure 26 that the two integrals are not small in comparison with some of the other terms in the momentum integral equation. A similar conclusion was drawn by Patel and Guven [10] from their analysis of the same data in order to explore the importance of the near wake in the calculation of the viscous resistance of axisymmetric bodies using conventional extrapolation formulae.

A second set of calculations was performed in which the momentum integral equation was solved using the estimated values of I_p and I_k and the velocity distribution measured at the edge of the boundary layer in place of that inferred from the pressure distribution on the body surface and the wake centerline. The effective value of I_k in the near wake was estimated simply by fairing the values at the tail to zero in the far wake, as shown in Figure 26. The results of these calculations are shown in Figure 25 as curves C and D, corresponding again to the two shape-parameter relations for the wake. The relatively small differences between this and the previous set of calculations suggest that the use of the pressure distribution on the surface and wake centerline to account for the effects of I_p and I_k, as recommended by Patel [2], is a good engineering approximation. However, the results of the calculations also indicate that such an approximation can be discarded in favor of the correct momentum integral equation, equation (19), provided the values of I_p and I_k can be determined a priori, as is the case in an interactive scheme such as that of Nakayama, Patel and Landweber [5].

VII DISCUSSION AND CONCLUSIONS

The data from the present experiments have been documented here in as much detail as possible so that they can be used by others to further investigate the various aspects of the thick axisymmetric turbulent boundary layer and near wake of a body of revolution. The boundary layer data are qualitatively similar to the earlier set obtained on a modified spheroid by Patel, Nakayama and Damian [1]. The two configurations are, however, sufficiently different to indicate the relative importance of longitudinal and transverse surface curvatures in the tail region. In both cases, the boundary layer grows rapidly towards the tail and interacts with the external potential flow. This interaction is strong enough to relieve the inviscid pressure gradients and avoid separation. The experiments with these two distinctly different shapes would appear to suggest that separation may be avoided on most slender axisymmetric bodies of practical interest by providing pointed tails and thus ensuring the growth of thick boundary layers.

The data in the wake are of considerable interest insofar as they document the transformation of a wall boundary layer into a free shear layer without the usual complication of flow reversal. To the authors' knowledge, the only other detailed set of data in a non-separated near wake is that of Chevray and Kovasznay [31], who made measurements in the wake of a two-dimensional flat plate. Such data are needed to examine the possibilities of continuing boundary layer solutions into the wake. Information on the wake is required, in turn, to develop practical methods for the treatment of the viscous-inviscid interaction in the tail region.

The boundary layer and wake data also afford the opportunity to verify the applicability of some of the recent turbulence closure models which claim to possess greater generality than the older phenomenological (mixing-length and eddy-viscosity) models. From the preliminary solutions of the differential equations, using the (one-equation) turbulent kinetic-energy model of Bradshaw, Ferriss and Atwell [29], presented in section VI.B, it is clear that methods developed for thin shear layers cannot be relied upon to predict the behavior of thick boundary layers. Although these calculations have demonstrated that a fairly satisfactory prediction procedure can be developed by incorporating ad hoc corrections to the model for the extra rates of strain, along the lines recommended by Bradshaw [18], it is indeed surprising that such modifications, proposed originally for small extra rates of strain and thin shear layers, work so well in the thick boundary layer on both bodies. In keeping with recent trends in the formulation of turbulence models, one inquires whether thick boundary layers ought to be treated by the so-called two-equation models. From the rapid changes in the mixing-length indicated by the data, this would appear to be desirable since it would provide an extra equation for the length-scale of the turbulence in addition to that for its intensity. This would also enable the incorporation of the variation in the structure parameter a_1 observed in the experiments. However, the recent work of Launder, Priddin and Sharma [32] and Chambers and Wilcox [33] indicates that even two-equation models, at least of the type available at the present time, require further modifications to account for the extra rates of strain stemming from such effects as streamline curvature, streamline convergence and rotation, two of which are present in the case examined here.

In addition to the problem of turbulence models, the thick boundary layer contains the complication of normal pressure gradients. Both sets of data show that there exist substantial variations of static pressure across the boundary layer. Examination of the momentum integral equation (19) suggests that it is the streamwise rate of change of this variation, and not the variation itself, which affects the growth of the boundary layer. The calculations made here with the differential as well as the integral method have shown that the normal pressure gradients are not negligible. If they are to be taken into account in a method based on the differential equations, it is then necessary to include the y-momentum equation in the solution procedure and regard the pressure as an additional unknown. This is perhaps best accomplished by means of an iterative scheme such as that proposed by Nakayama, Patel and Landweber [4,5], although other possibilities can be explored.

The calculations presented in section VI.C have demonstrated the overall reliability of the simple integral method of Patel [2] for the prediction of the thick boundary layer. Its extension to the wake is not altogether satisfactory and this is attributed largely to the lack of a systematic procedure for the description of the velocity profiles in the near wake. This method is ideally suited, however, for rapid calculations to determine the state of the boundary layer in the tail region for applications in the design of tail-mounted propellers, control surfaces and other appendages.

In view of the success of the differential method of section VI.B, it is now proposed to extend it beyond the tail to calculate the development of the wake. Comparisons of the results with near- and far-wake data would shed some light on the continued applicability of the one-equation turbulence model together with the extra rate-of-strain corrections, in the wake. If such an extension can be carried out successfully, the method would be incorporated in the iterative scheme of Nakayama, Patel and Landweber [4,5], in place of the integral method, to study the viscous-inviscid interaction in the tail region in greater detail.

REFERENCES

1. Patel, V.C., Nakayama, A. and Damian, R., "Measurements in the Thick Axisymmetric Turbulent Boundary Layer Near the Tail of a Body of Revolution," Journal of Fluid Mechanics, Vol. 63, 1974, pp. 345-362.

2. Patel, V.C., "A Simple Integral Method for the Calculation of Thick Axisymmetric Turbulent Boundary Layers," The Aeronautical Quarterly, Vol. 25, 1974, pp. 47-58.

3. Granville, P.S., "Similarity-Law Entrainment Method for Thick Axisymmetric Turbulent Boundary Layers in Pressure Gradients," David W. Taylor Naval Ship Research and Development Center, Rept. 4525, 1975.

4. Nakayama, A., Patel, V.C. and Landweber, L., "Flow Interaction Near the Tail of a Body of Revolution. Part I: Flow Exterior to Boundary Layer and Wake," ASME, Journal of Fluids Engineering, Vol. 98, 1976, pp. 531-537.

5. Nakayama, A., Patel, V.C. and Landweber, L., "Flow Interaction Near the Tail of a Body of Revolution. Part II: Iterative Solution for Flow Within and Exterior to Boundary Layer and Wake," ASME, Journal of Fluids Engineering, Vol. 98, 1976, pp. 538-549.

6. Parsons, J.S. and Goodson, R.E., "The Optimum Shaping of Axisymmetric Bodies for Minimum Drag in Incompressible Flow," Automatic Control Center, School of Mech. Eng., Purdue Univ., Rept. ACC-72-5, 1972.

7. Patel, V.C., "Calibration of the Preston Tube and Limitations On Its Use in Pressure Gradients," Journal of Fluid Mechanics, Vol. 23, 1965, pp. 185-208.

8. Glover, J.R., "Old Gold Model, Type 4-2H Hot-Wire Anemometer and Type 2 Mean-Product Computer," Iowa Institute of Hydraulic Research, IIHR Rept. No. 136, 1972.

9. Landweber, L., "Potential Flow About Bodies of Revolution and Symmetric Two-Dimensional Forms," IIHR, Report Buships Index NS 715-102, 1959.

10. Patel, V.C. and Güven, O., "Importance of the Near Wake in Drag Prediction of Bodies of Revolution," AIAA Journal, Vol. 14, 1976, pp. 1132-1133.

11. Chevray, R., "The Turbulent Wake of a Body of Revolution," ASME, Journal of Basic Engineering, Vol. 90, 1968, pp. 275-284.

12. Swanson, R.C., Schetz, J.A., Jr. and Jakubowski, A.K., "Turbulent Wake behind Slender Bodies Including Self-Propelled Configurations," VPI-Aero-024, Virginia Polytechnic Institute and State University, 1974.

13. Chieng, C.C., Jakubowski, A.K. and Schetz, J.A., "Investigation of the Turbulence Properties of the Wake behind Self-Propelled, Axisymmetric Bodies," VPI-Aero-025, Virginia Polytechnic Institute and State University, 1974.

14. Schlichting, H., Boundary-Layer Theory, 6th edition, McGraw-Hill Book Company, 1968, pp. 691-695.

15. Rodi, W., "A Review of Experimental Data of Uniform Density Free Turbulent Boundary Layers," Studies in Convection, Vol. I, ed. B.E. Launder, Academic Press, 1975, pp. 79-165.

16. Patel, V.C., "A Unified View of the Law the Wall Using Mixing-Length Theory", The Aeronautical Quarterly, Vol. 24, 1973, pp. 55-70.

17. Bradshaw, P., "The Analogy Between Streamline Curvature and Buoyancy in Turbulent Shear Flow," Journal of Fluid Mechanics, Vol. 36, 1969, pp. 177-191.

18. Bradshaw, P., "Effects of Streamline Curvature on Turbulent Flow," AGARDograph No. 169, 1973.

19. So, R.M.C. and Mellor, G.L., "An Experimental Investigation of Turbulent Boundary Layers Along Curved Surfaces," NASA-CR-1940, 1972.

20. So, R.M.C. and Mellor, G.L., "Experiment on Convex Curvature Effects in Turbulent Boundary Layers," Journal of Fluid Mechanics, Vol. 60, 1973, pp. 43-62.

21. So, R.M.C. and Mellor, G.L., "Experiment on Turbulent Boundary Layers on Concave Wall," The Aeronautical Quarterly, Vol. 26, 1975, pp. 35-40.

22. Meroney, R.N. and Bradshaw, P., "Turbulent Boundary Layer Growth Over Longitudinally Curved Surfaces," AIAA Journal, Vol. 13, 1975, pp. 1448-1453.

23. Ramaprian, B.R. and Shivaprasad, B.G., "Mean Flow Measurements in Turbulent Boundary Layers Along Mildly-Curved Surfaces," AIAA Journal, Vol. 15, 1977, pp. 189-196.

24. Shivaprasad, B.G. and Ramaprian, B.R., "Some Effects of Longitudinal Wall-Curvature on Turbulent Boundary Layers," Proc. of Symposium on Turbulent Shear Flows, Penn State Univ., April 18-20, 1977, pp. 9.21-9.28.

25. Shivaprasad, B.G. and Ramaprian, B.R., "Turbulence Measurements in Boundary Layers along Mildly Curved Surfaces," To be published in ASME, Journal of Fluids Engineering, 1977.

26. Ramaprian, B.R. and Shivaprasad, B.G., "The Structure of the Turbulent Boundary Layer Over Surfaces of Mild Longitudinal Curvature," To be published in Journal of Fluid Mechanics, 1977.

27. Bradshaw, P. and Unsworth, K., "Computation of Complex Turbulent Flows", in "Reviews of Viscous Flow," Proceedings of the Lockheed-Georgia Company Viscous Flow Symposium, June 22-23, 1976, pp. 448-498.

28. Patel, V.C., "On the Equations of a Thick Axisymmetric Turbulent Boundary Layer," Iowa Institute of Hydraulic Research, IIHR Report No. 143, 1973.

29. Bradshaw, P., Ferris, D.H. and Atwell, N.P., "Calculation of Boundary Layer Development Using the Turbulent Energy Equation," Journal of Fluid Mechanics, Vol. 28, 1967, pp. 593-616.

30. Head, M.R., "Entrainment in the Turbulent Boundary Layer," British ARC, R&M No. 3152, 1958.

31. Chevray, R and Kovasznay, L.S.G., "Turbulence measurements in the wake of a thin flat plate," AIAA Journal, Vol. 7, 1969, pp. 1641-1643.

32. Launder, B.E., Priddin, C.H. and Sharma, B.I., "The calculation of turbulent boundary layers on spinning and curved surfaces", ASME, J. Fluids Engineering, Vol. 99, No. 1, 1977, pp. 231-239. See also discussions by P. Bradshaw and G. Mellor, ASME, J. Fluids Engineering, Vol. 99, No. 2, 1977, pp. 435-439.

33. Chambers, T.L. and Wilcox, D.C., "Critical examination of two-equation turbulence closure models for boundary layers," AIAA Journal, Vol. 15, No. 6, 1977, pp. 821-828.

APPENDIX

Estimation of Integrals I_k and I_p from Data

These integrals are defined in the text by the following equations:

$$I_k = \kappa \int_o^\delta \frac{UV}{U_\delta^2} r \, dy \tag{20}$$

and

$$I_p = \frac{1}{U_\delta^2} \int_o^\delta r \frac{\partial}{\partial x} \left\{ \frac{p-p_\delta}{\rho} - \frac{V_\delta^2}{2} \right\} dy \tag{21}$$

The evaluation of I_k is straightforward since both U and V have been measured in the boundary layer and the wake. Since κ is the curvature of the surface, I_k becomes zero everywhere in the wake.

From physical considerations, it may be argued that I_k represents the influence of the curvature of the streamlines in the boundary layer rather than that of the surface. It may therefore be preferrable to use a representative streamline curvature for κ. For example, an appropriate choice may be the longitudinal curvature of the displacement surface shown in Figure 9. In the calculations presented in the text, however, the original definition of I_k has been retained and an "effective" value has been assigned in the near wake simply by reducing I_k to zero, from its value at the tail, exponentially over a distance X/L = 0.20 from the tail.

In order to simplify the evaluation of I_p, it is first observed that the measured static-pressure variations across the boundary layer and wake (Figure 4) may be approximated by linear distributions, viz

$$p - p_\delta = (p - p_w)(1 - y/\delta) \tag{A-1}$$

where p_w is the pressure at the body surface or the wake centerline. Substitution of this into equation (21) and integration leads to

$$\begin{aligned} I_p U_\delta^2 = {} & \frac{\delta^2}{12}\left(\frac{3r_o}{\delta} + \cos\theta\right) \frac{d}{dx}(C_{pw} - C_{p\delta}) \\ & + \frac{\delta}{12}\left(\frac{3r_o}{\delta} + 2\cos\theta\right) \frac{d\delta}{dx}(C_{pw} - C_{p\delta}) \\ & - \frac{\delta^2}{4}\left(\frac{2r_o}{\delta} + \cos\theta\right) \frac{d}{dx}(V_\delta^2) \end{aligned} \tag{A-2}$$

Using the Bernoulli equation, V_δ can be related to $C_{p\delta}$ and U_δ as follows

$$\frac{V_\delta^2}{U_o^2} = 1 - C_{p\delta} \frac{U_\delta^2}{U_o^2} \qquad \text{(A-3)}$$

I_p can now be evaluated using the measured values of δ, U_δ , $C_{p\delta}$ and C_{pw}.

The estimated values of I_k and I_p are shown in Figure 26, along with the axial variation of the terms $\frac{d\Delta_2}{dx}$ and $1/2\ c_f r_o$ appearing in the momentum integral equation. It is seen that both I_k and I_p make a substantial contribution to the rate of growth of the momentum deficit area. It should be noted that the accuracy of the solutions of the momentum equation using I_k and I_p is limited due not only to the approximations that are involved in the estimation of these integrals but also because they are large and of opposite signs over a substantial axial distance.

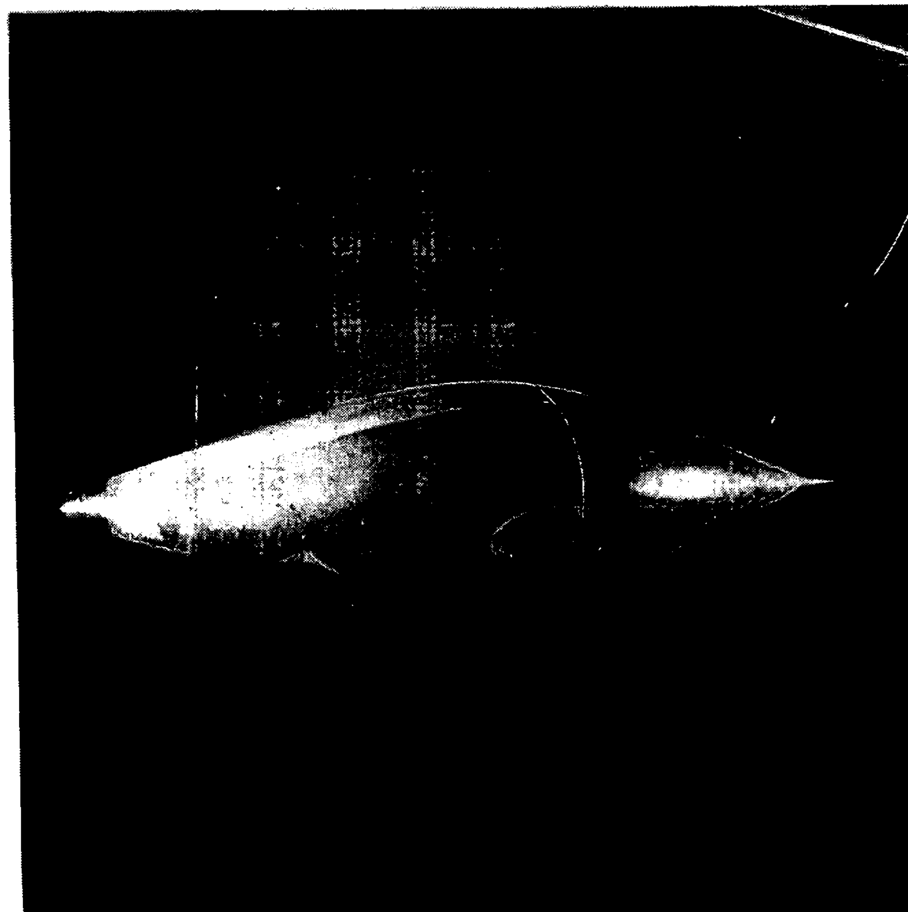

FIGURE 1 (a) THE F-57 BODY IN THE WIND TUNNEL

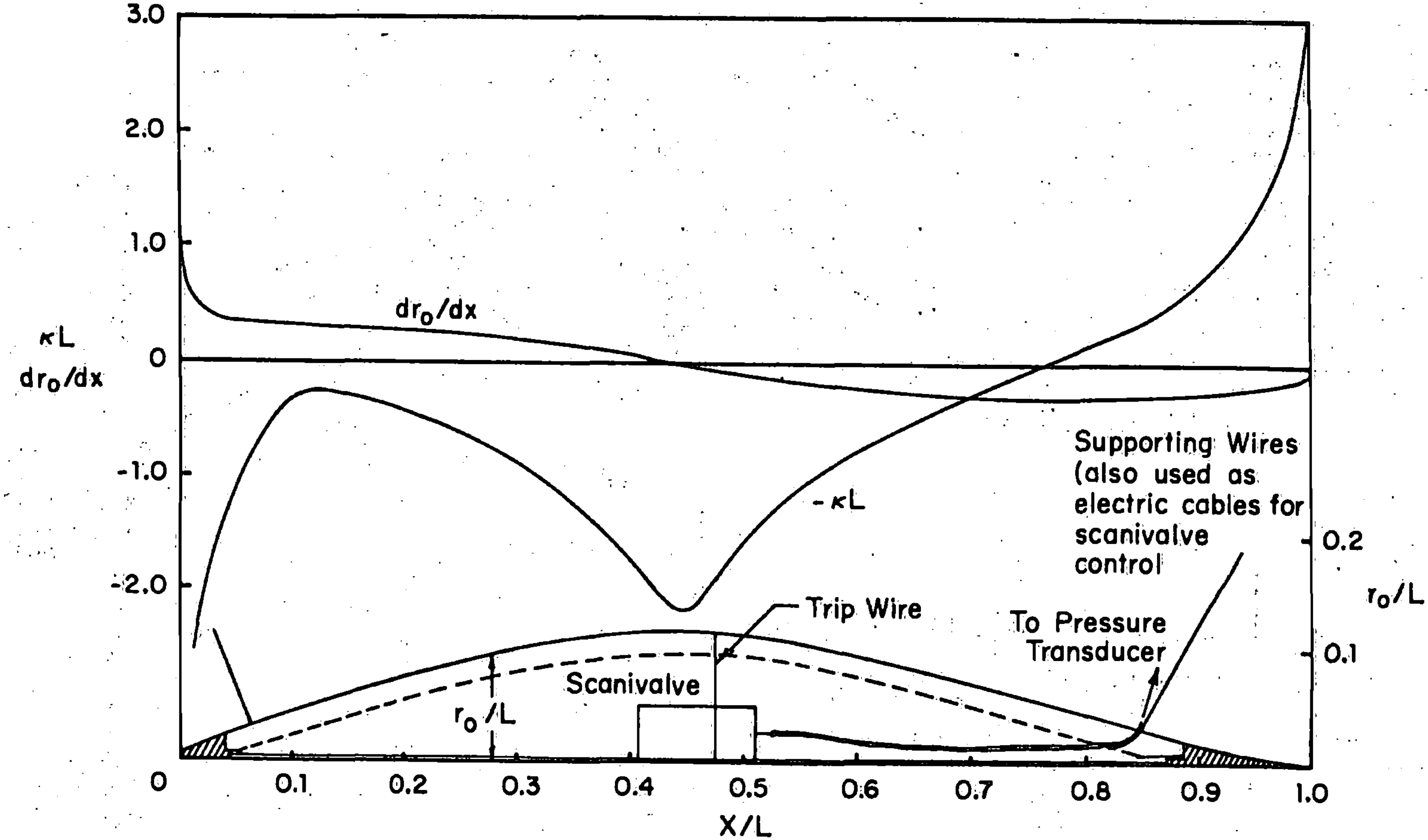

FIGURE 1 (b) DETAILS OF THE F-57 BODY

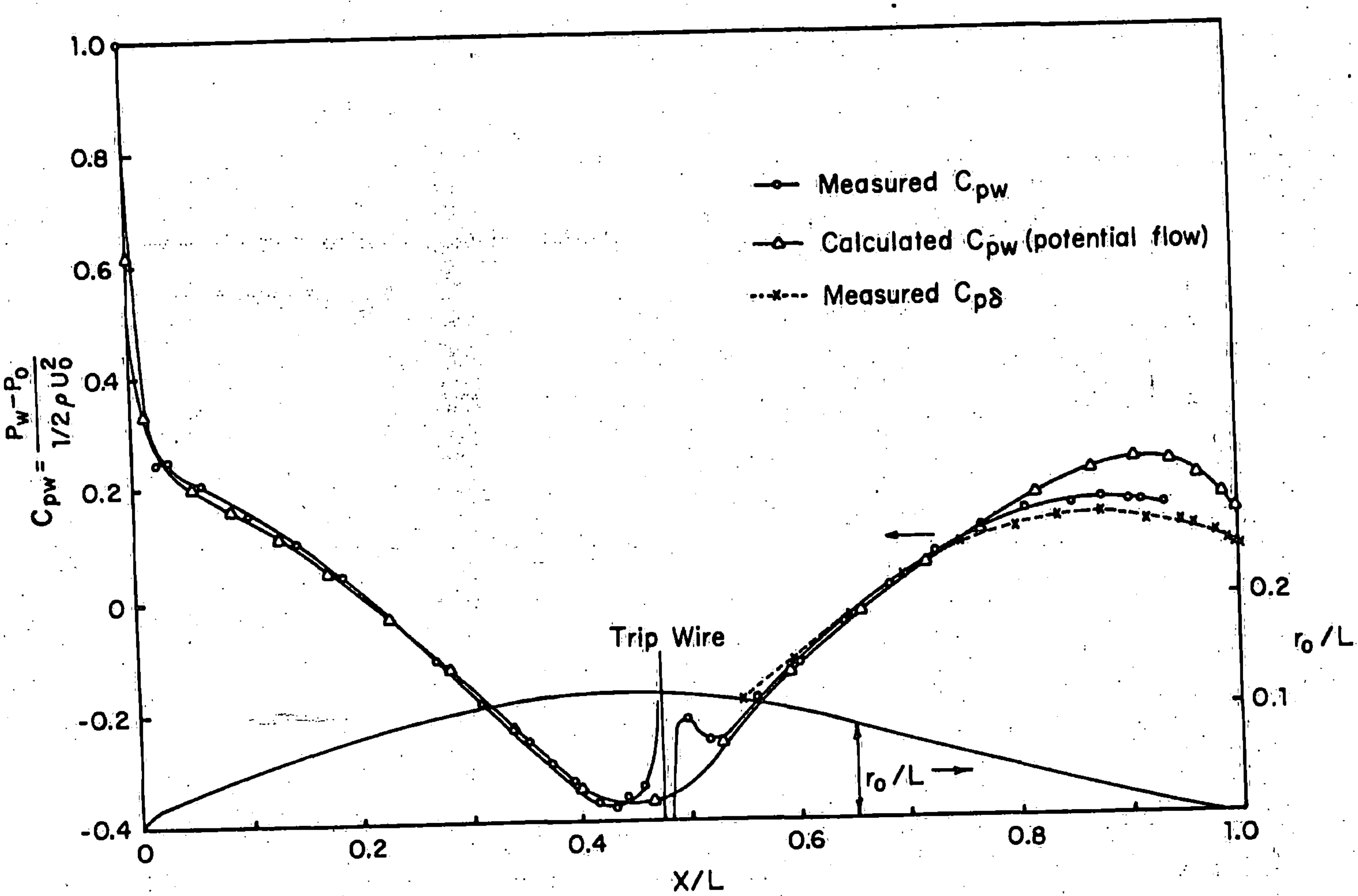

FIGURE 2 PRESSURE DISTRIBUTIONS ON THE BODY

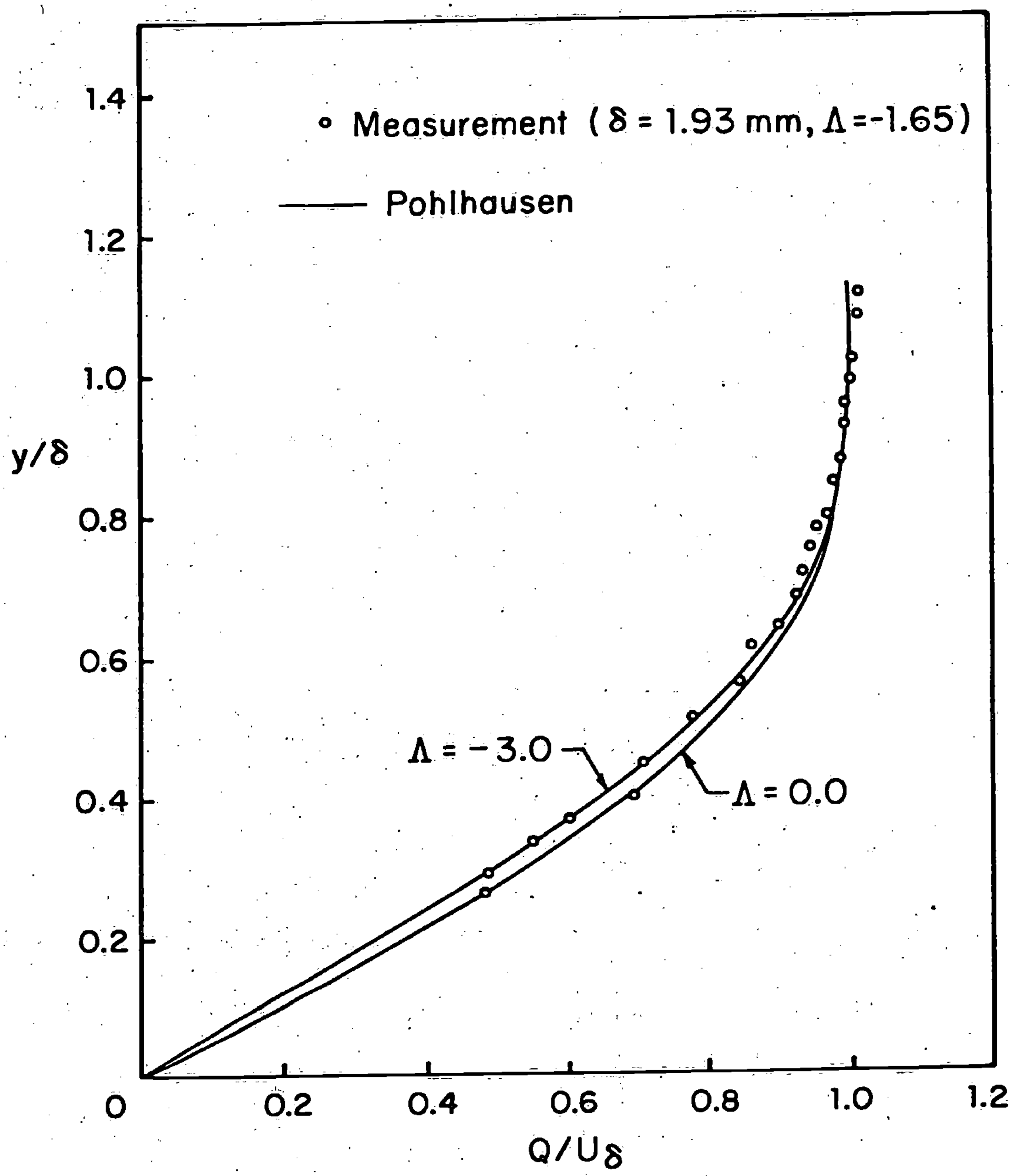

FIGURE 3 VELOCITY PROFILE AT X/L = 0.433

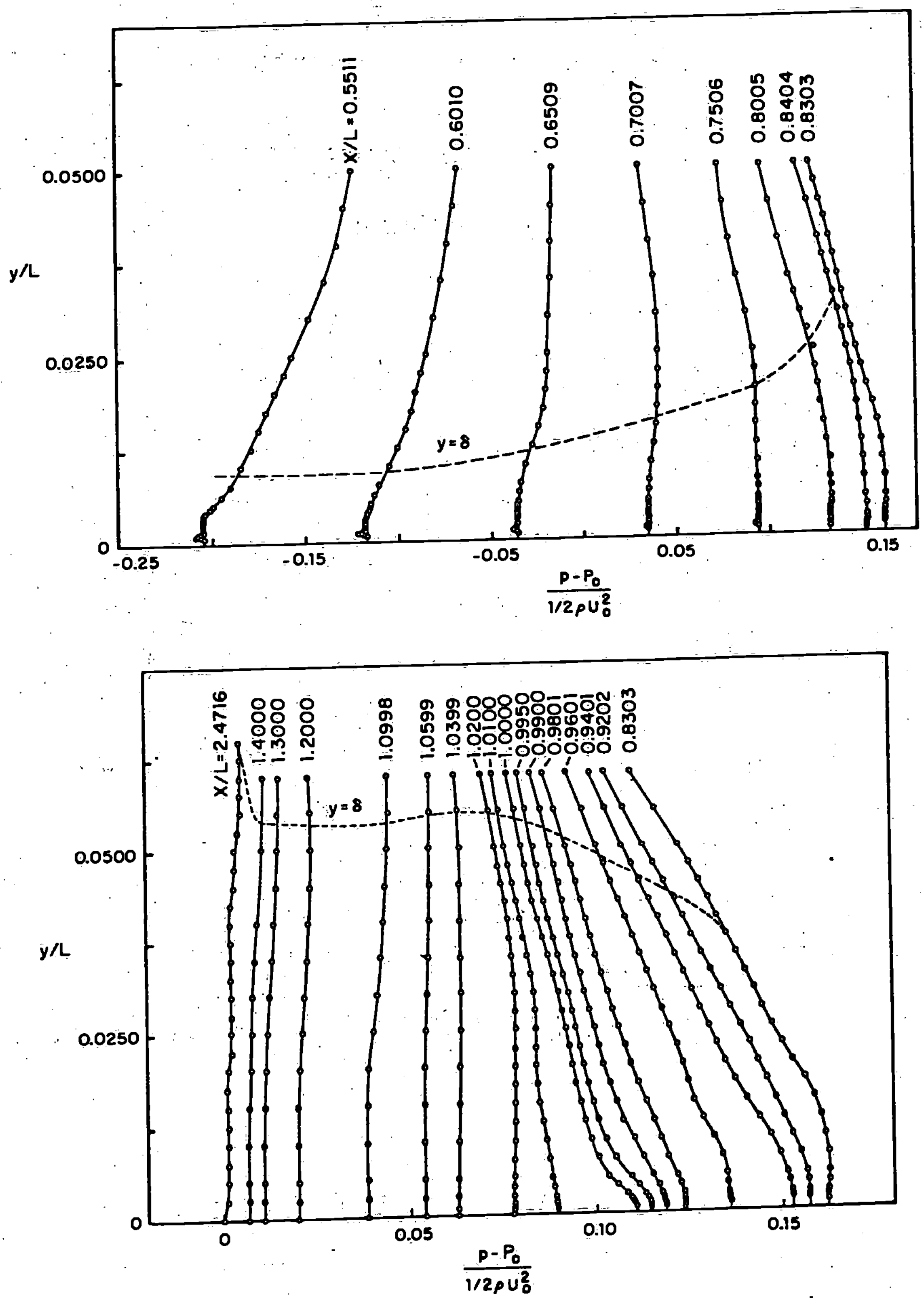

FIGURE 4 STATIC PRESSURE DISTRIBUTIONS

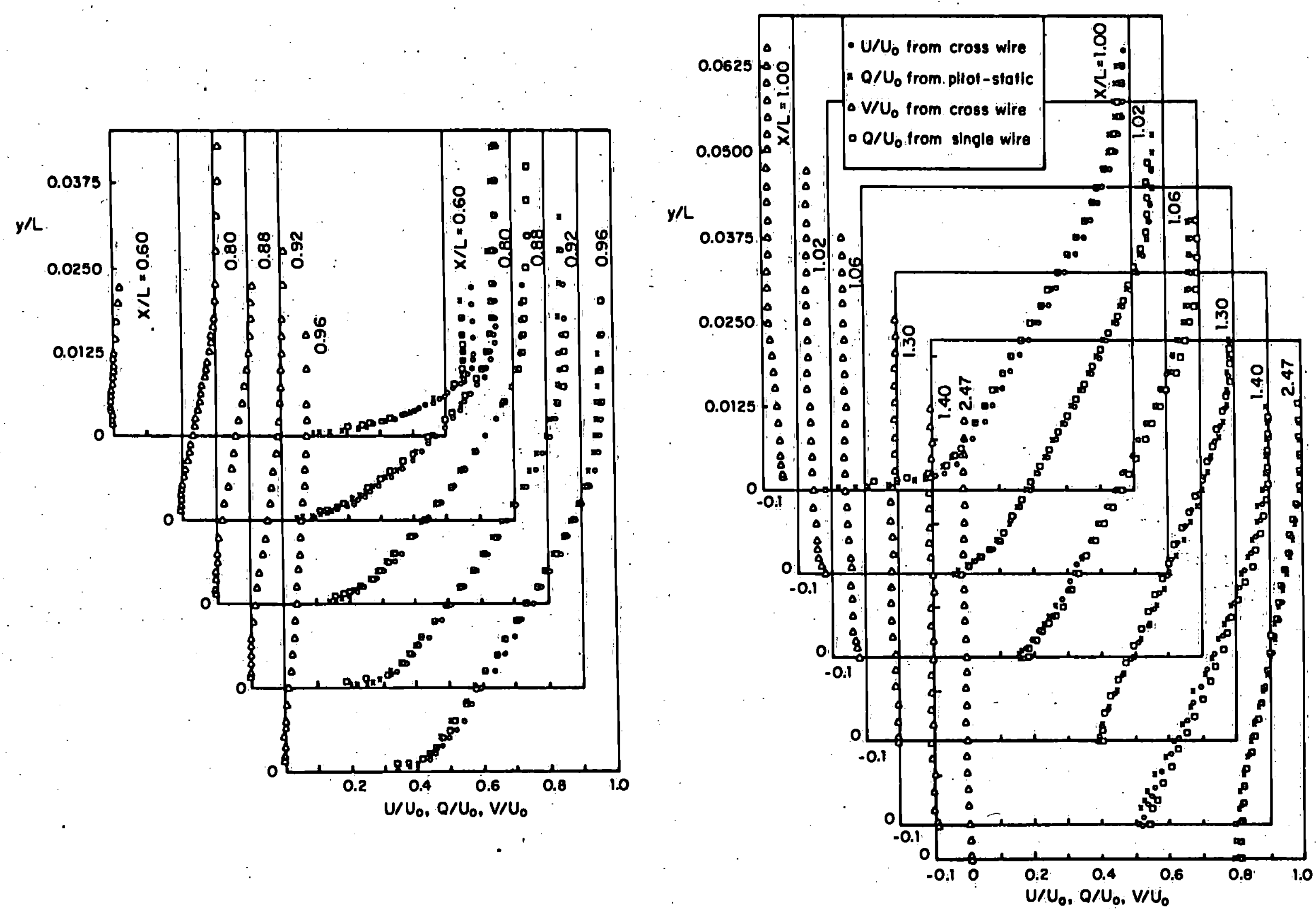

FIGURE 5 MEAN VELOCITY PROFILES

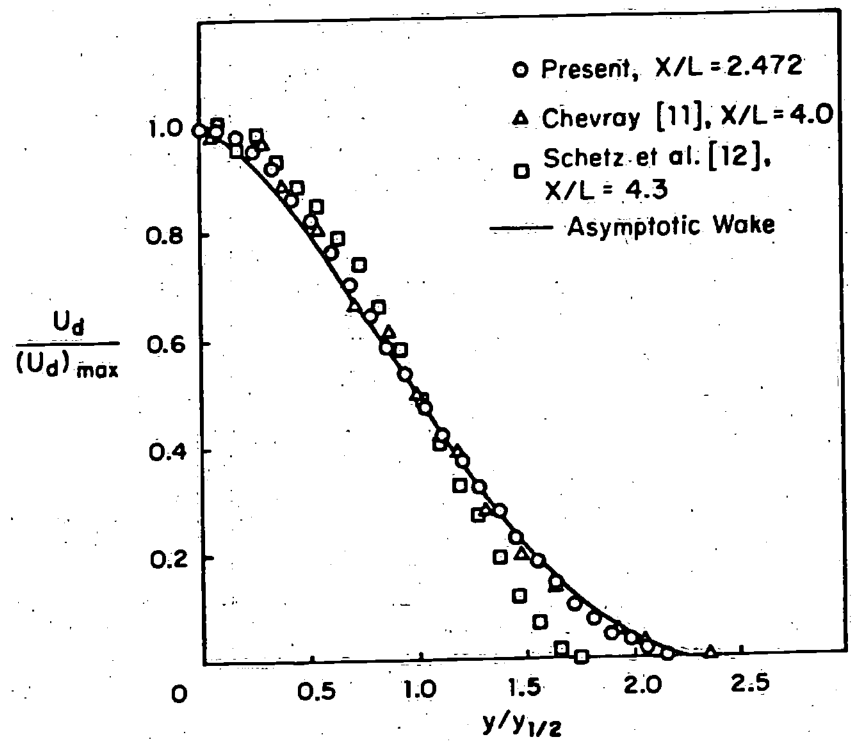

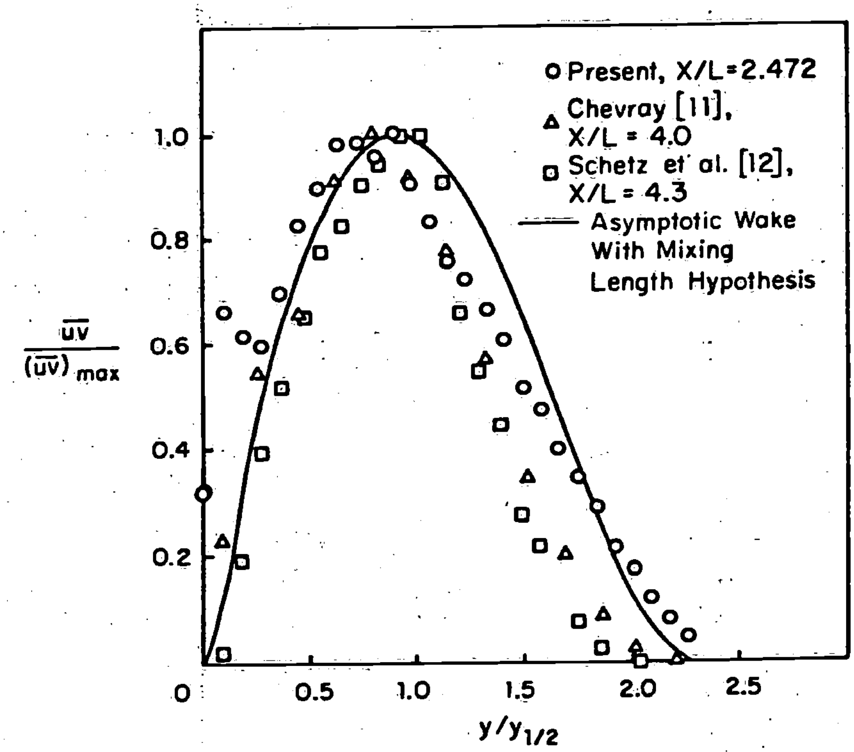

FIGURE 6 ASYMPTOTIC VELOCITY AND SHEAR STRESS PROFILES IN THE WAKE

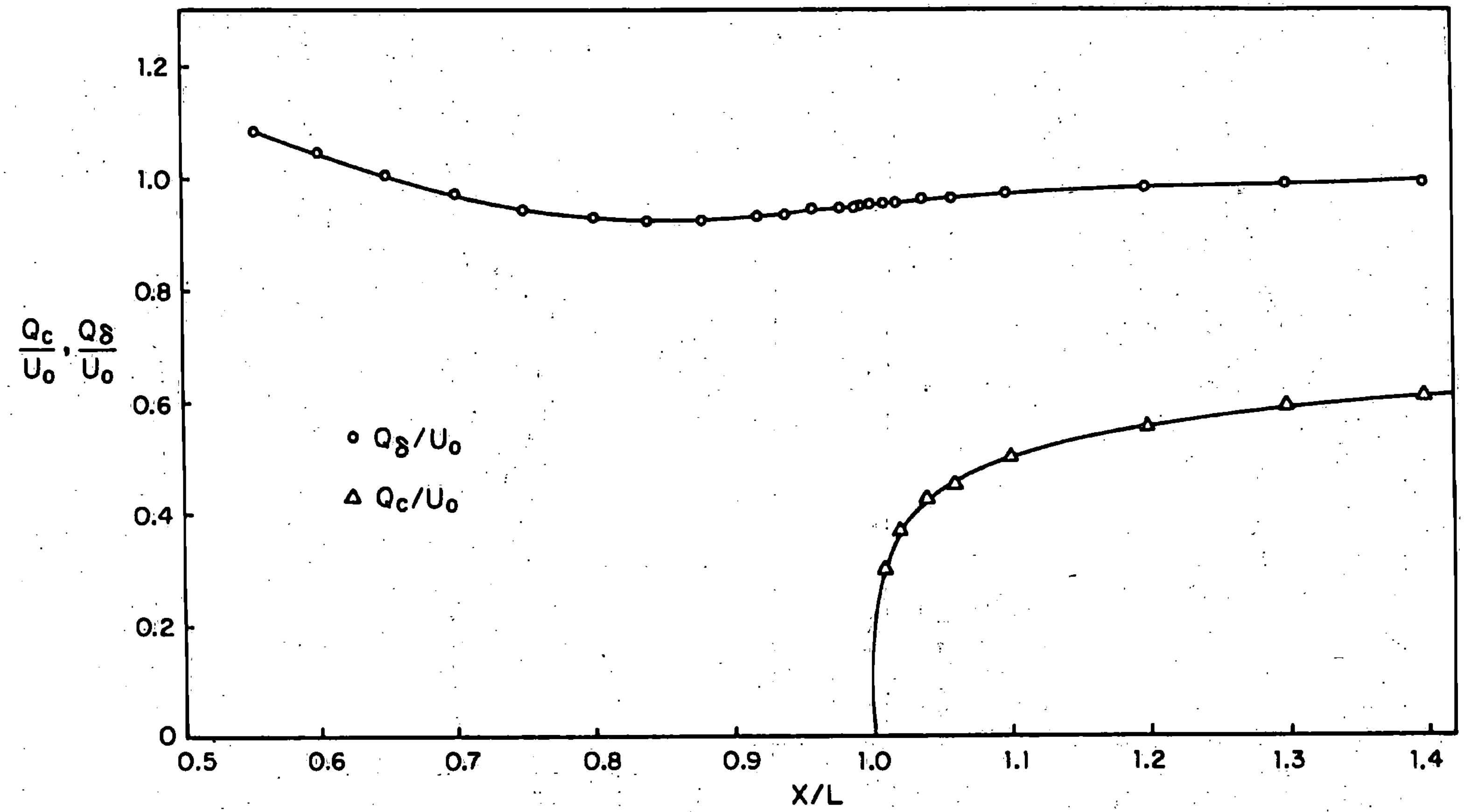

FIGURE 7 VELOCITY AT $y=\delta$ AND WAKE CENTERLINE

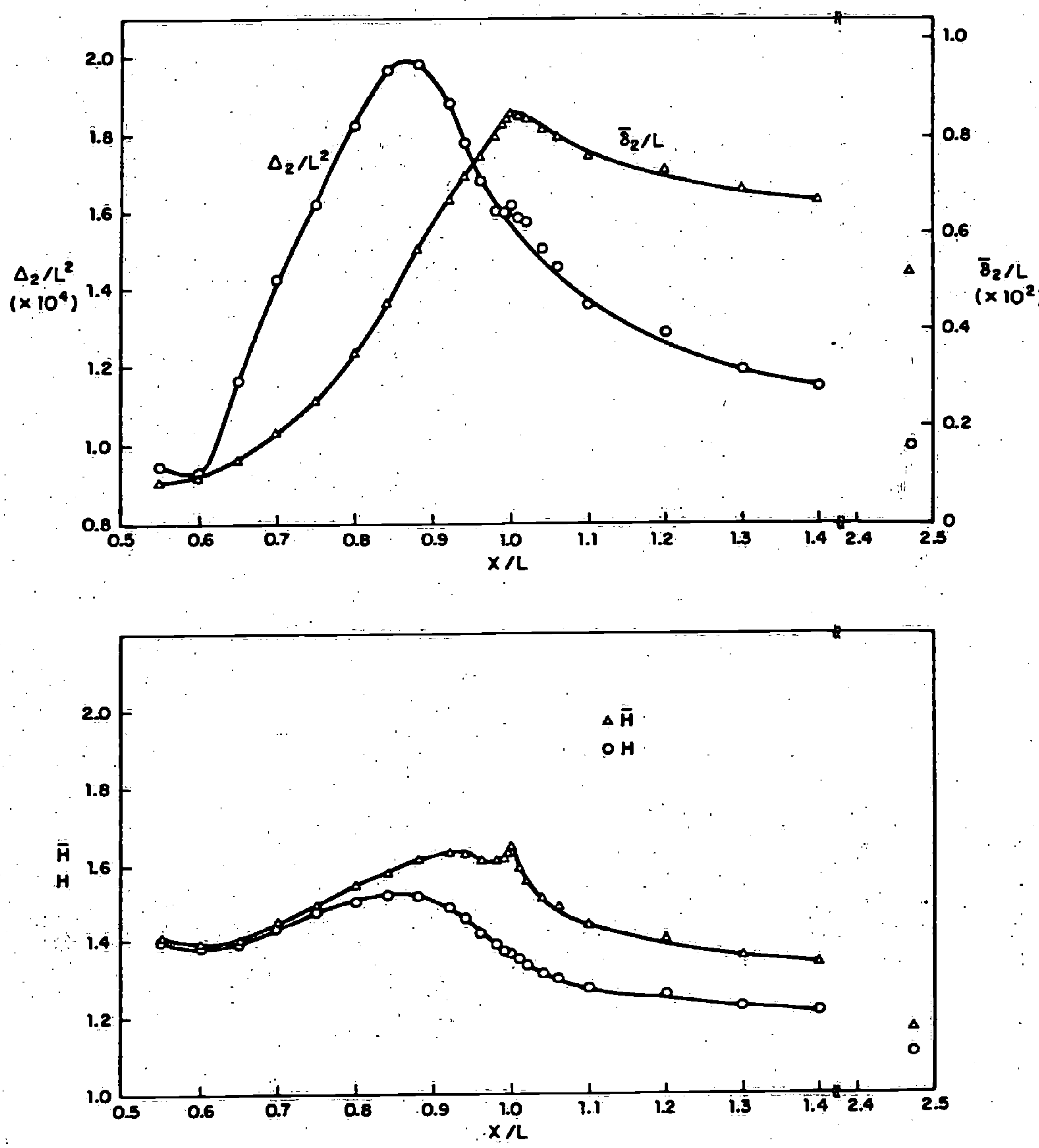

FIGURE 8 INTEGRAL PARAMETERS

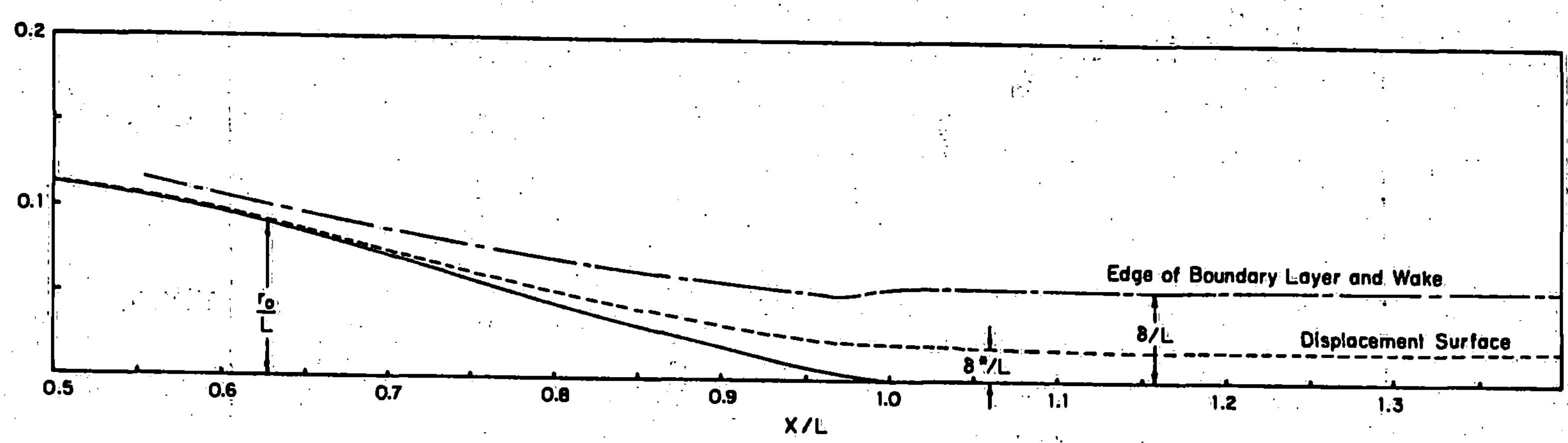

FIGURE 9 DISPLACEMENT SURFACE

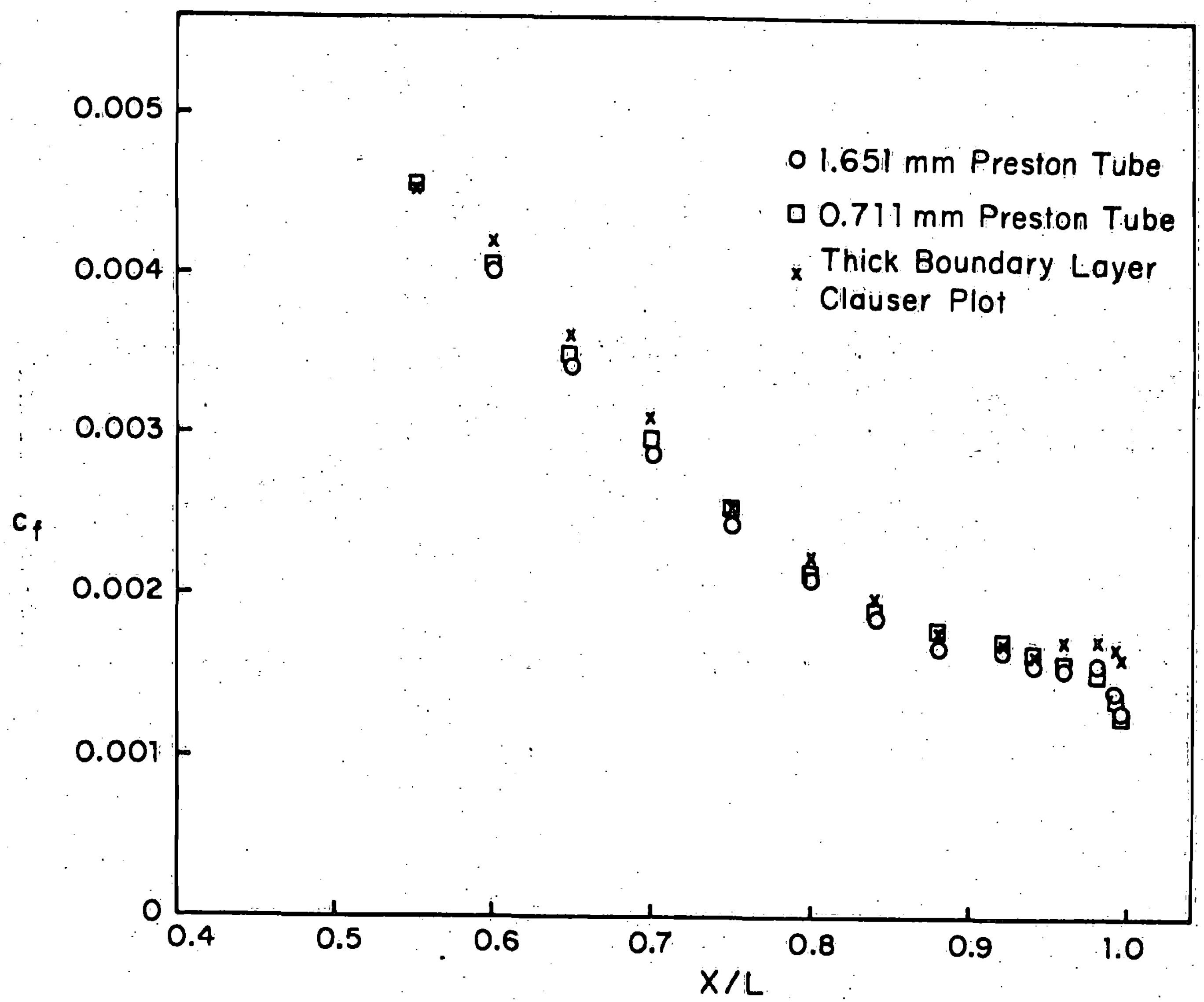

FIGURE 10 WALL SHEAR STRESS

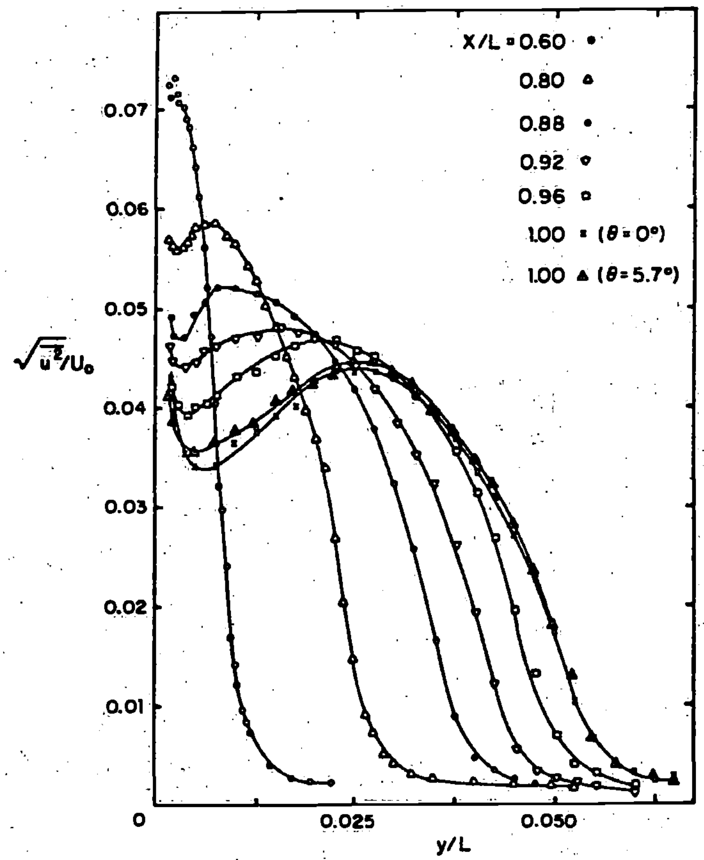

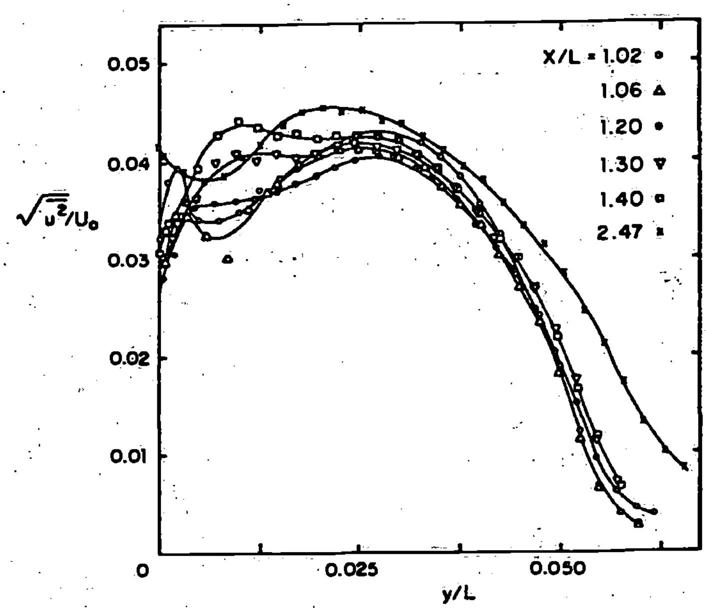

FIGURE 11 DISTRIBUTIONS OF REYNOLDS STRESS $\sqrt{\overline{u^2}}/U_o$

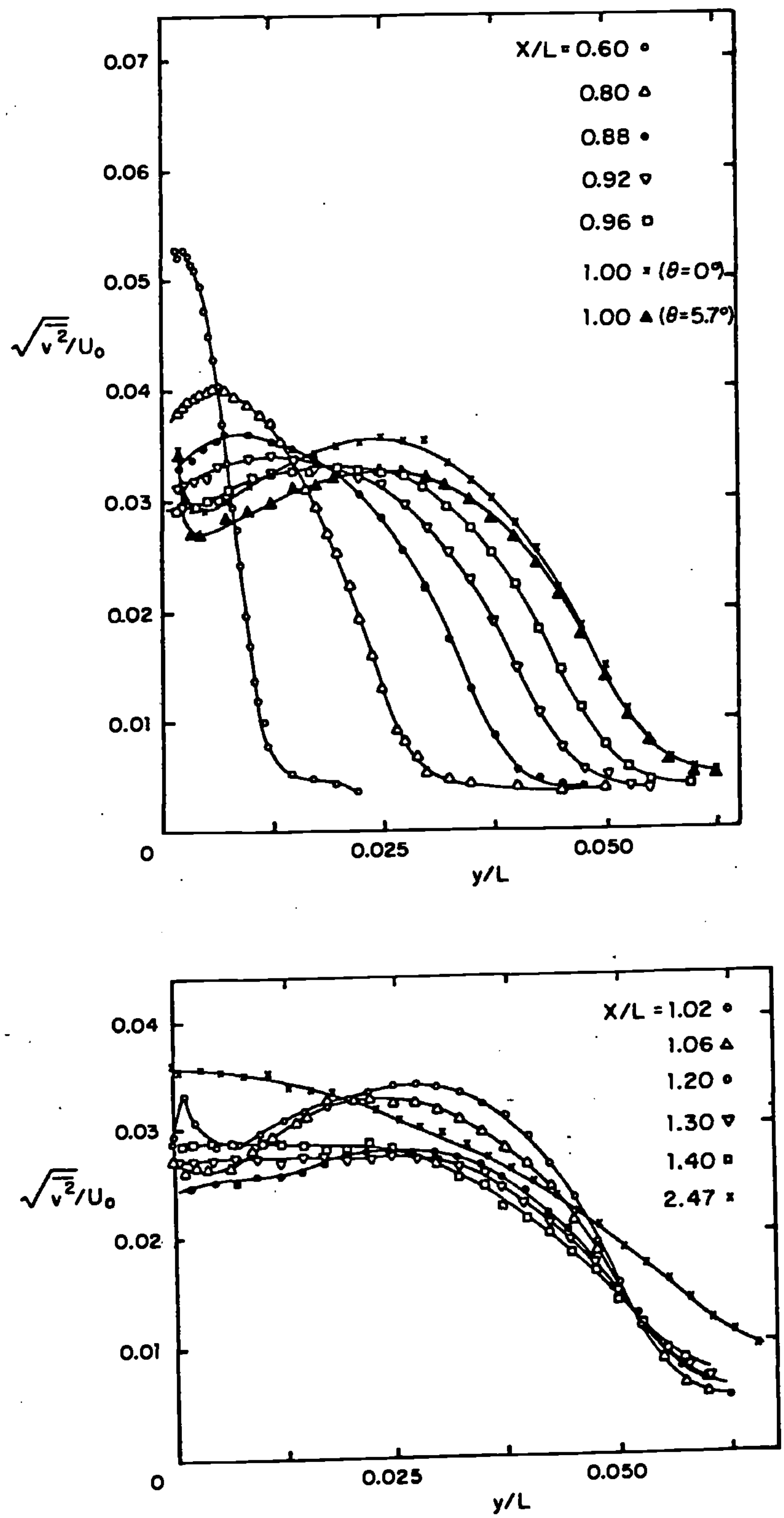

FIGURE 12 DISTRIBUTIONS OF REYNOLDS STRESS $\sqrt{v^2}/U_o$

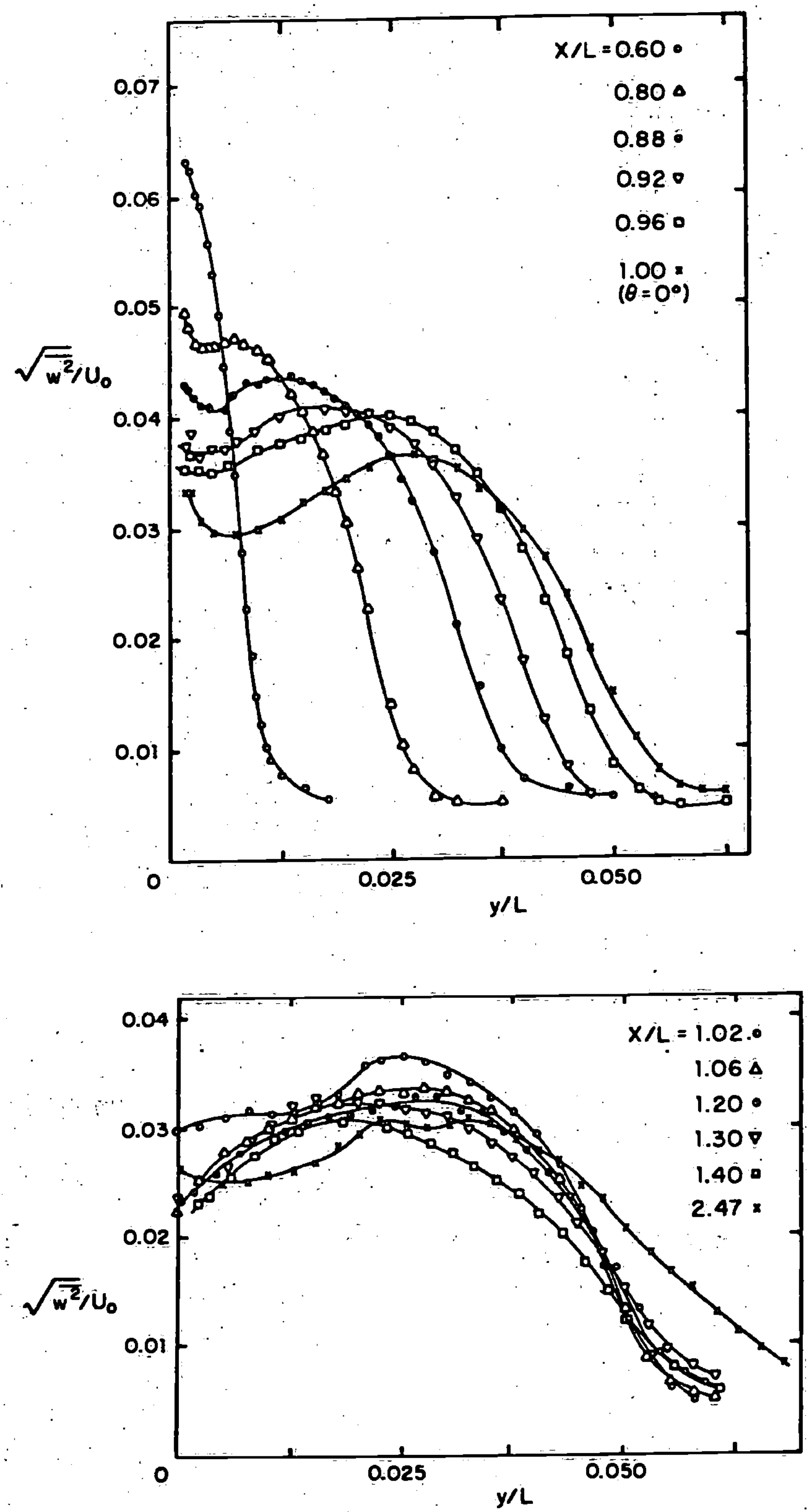

FIGURE 13 DISTRIBUTIONS OF REYNOLDS STRESS $\sqrt{\overline{w^2}}/U_o$

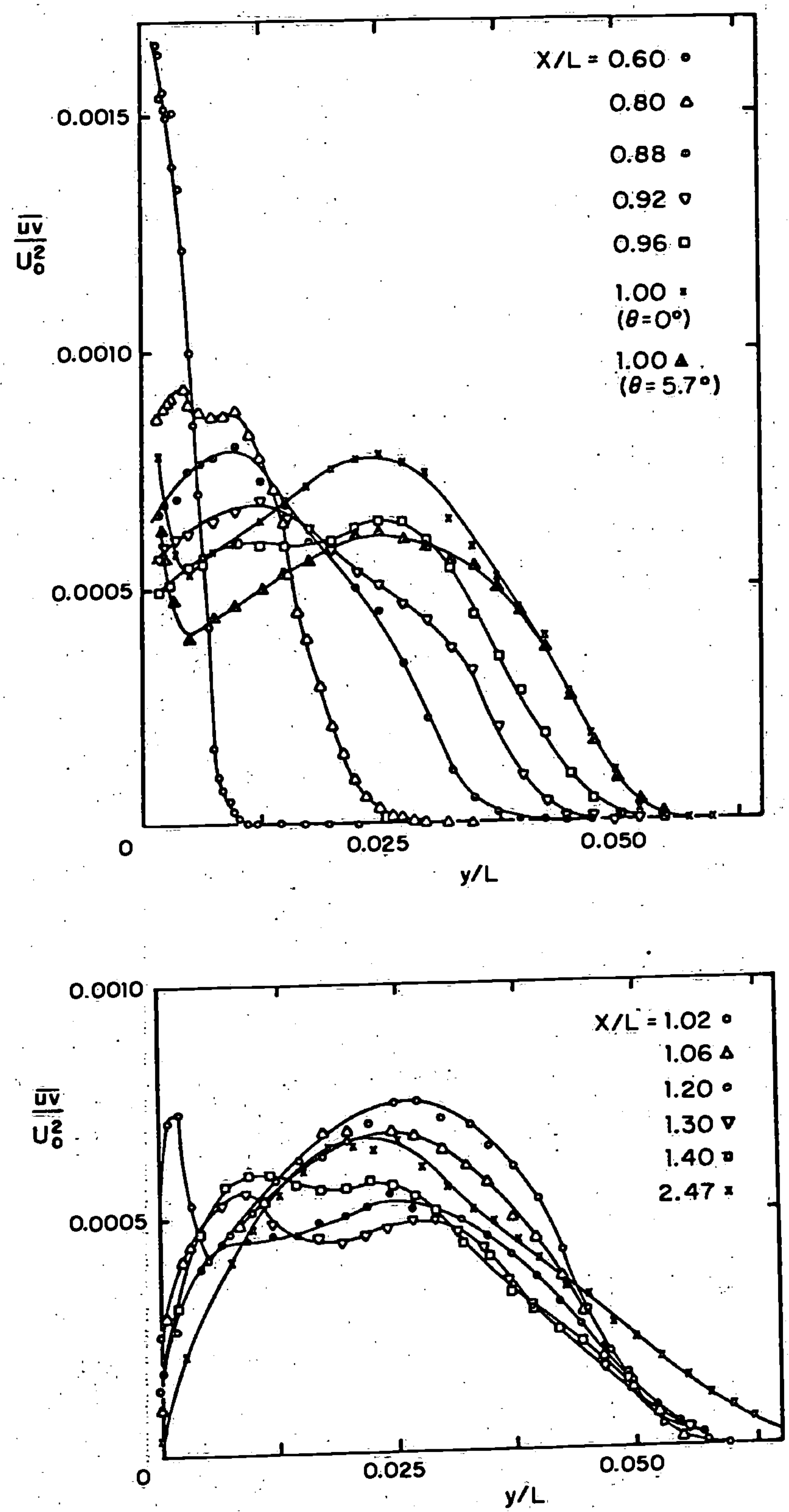

FIGURE 14 DISTRIBUTIONS OF REYNOLDS SHEAR STRESS $-\overline{uv}/U_o^2$

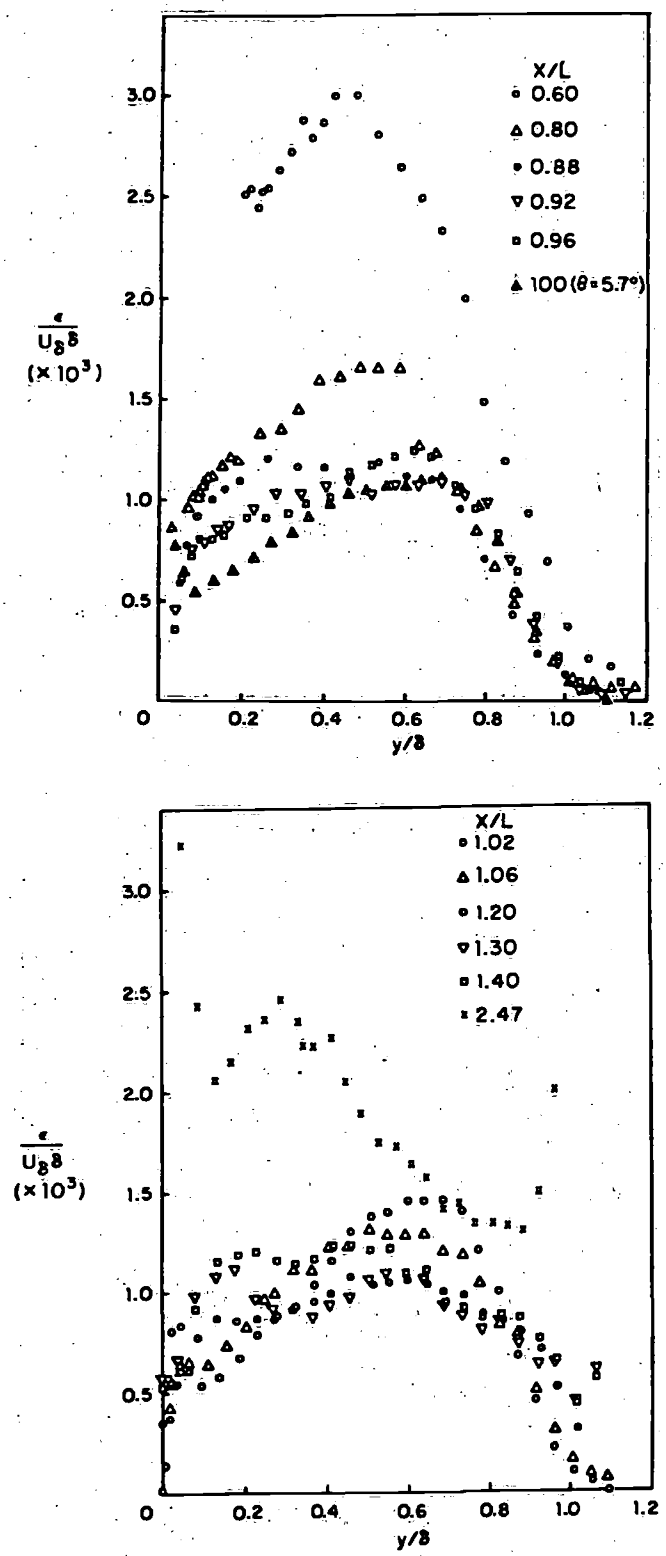

FIGURE 15 EDDY VISCOSITY PROFILES, LOW-DRAG BODY

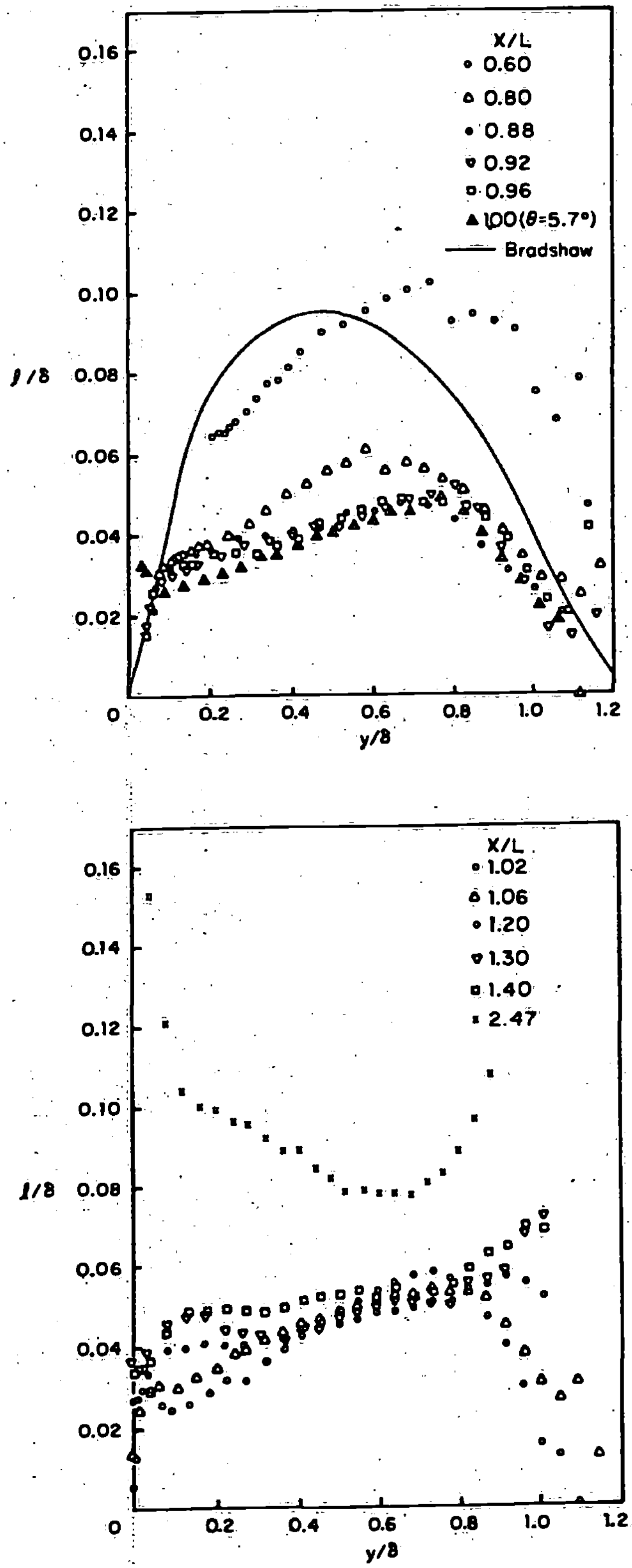

FIGURE 16 MIXING LENGTH PROFILES, LOW-DRAG BODY

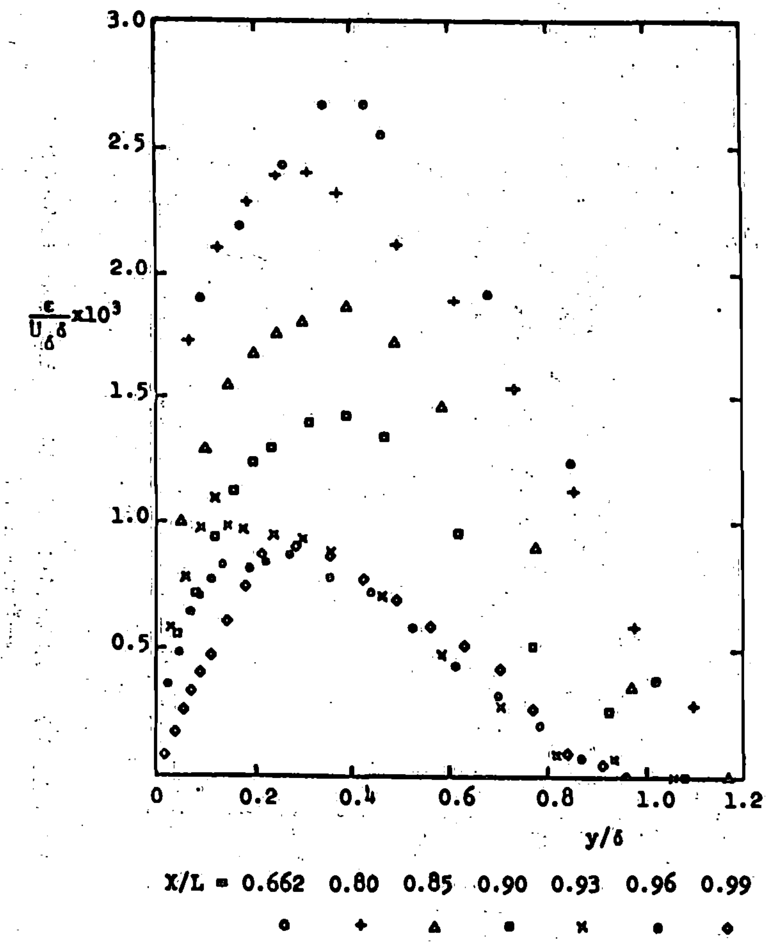

FIGURE 17 EDDY VISCOSITY PROFILES, MODIFIED SPHEROID

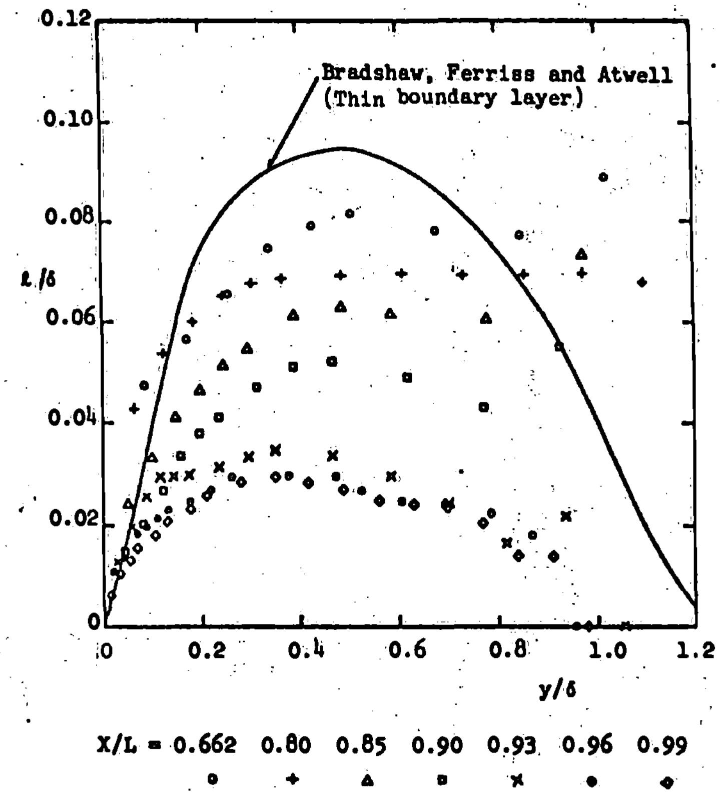

FIGURE 18 MIXING LENGTH PROFILES, MODIFIED SPHEROID

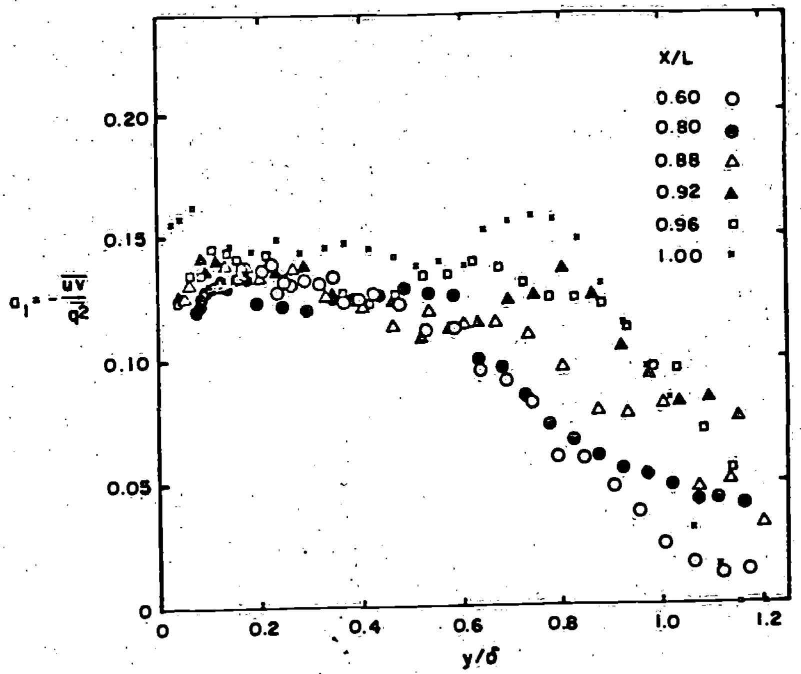

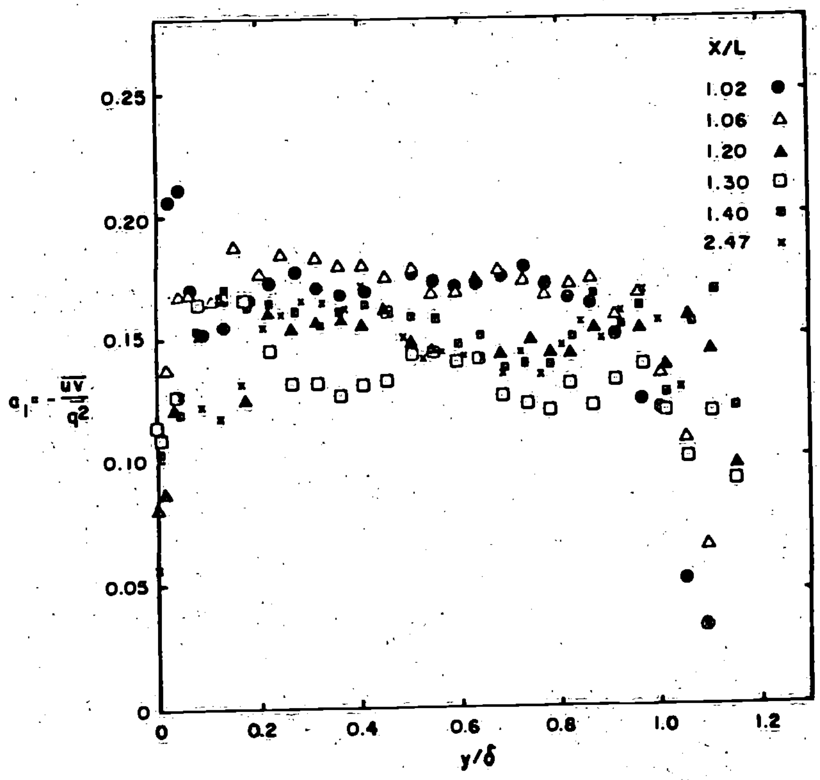

FIGURE 19 VARIATION OF THE STRUCTURE PARAMETER a_1, LOW-DRAG BODY

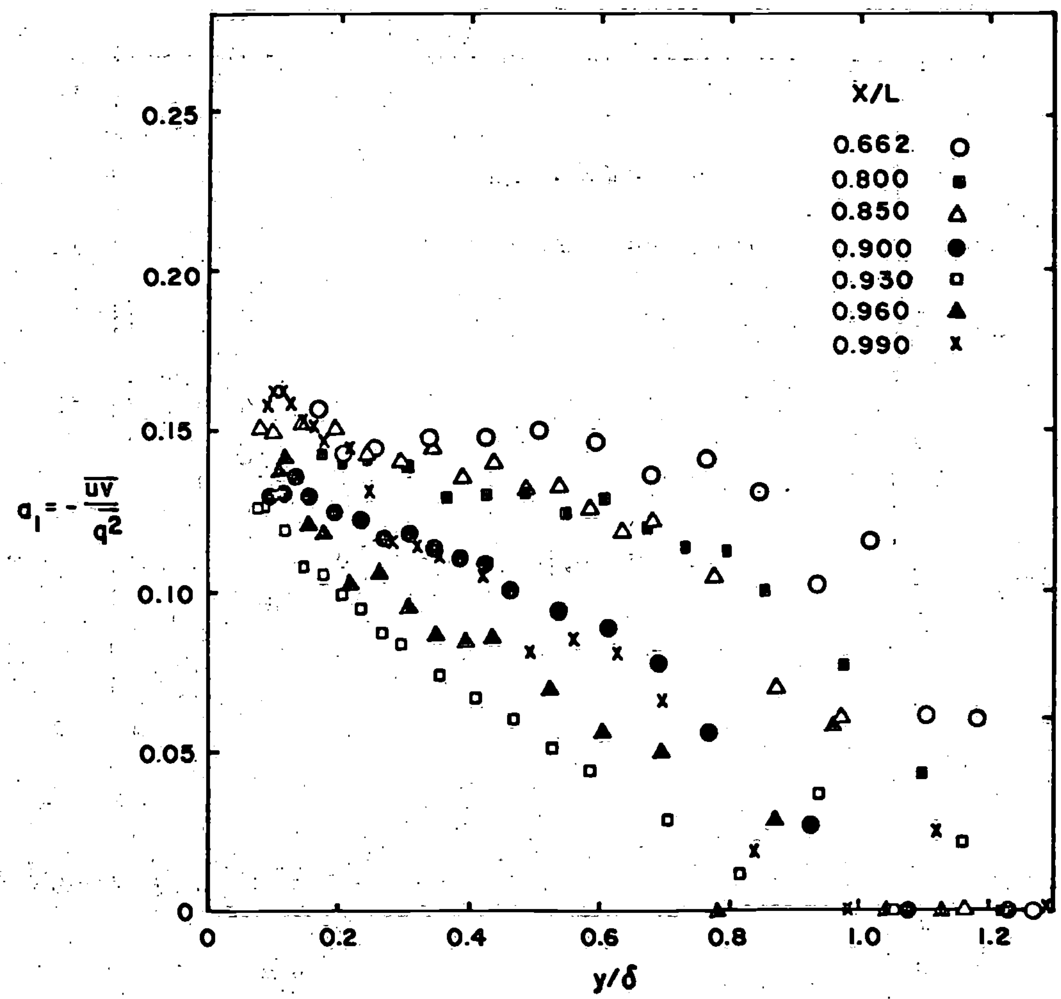

FIGURE 20 VARIATION OF STRUCTURE PARAMETER a_1, MODIFIED SPHEROID

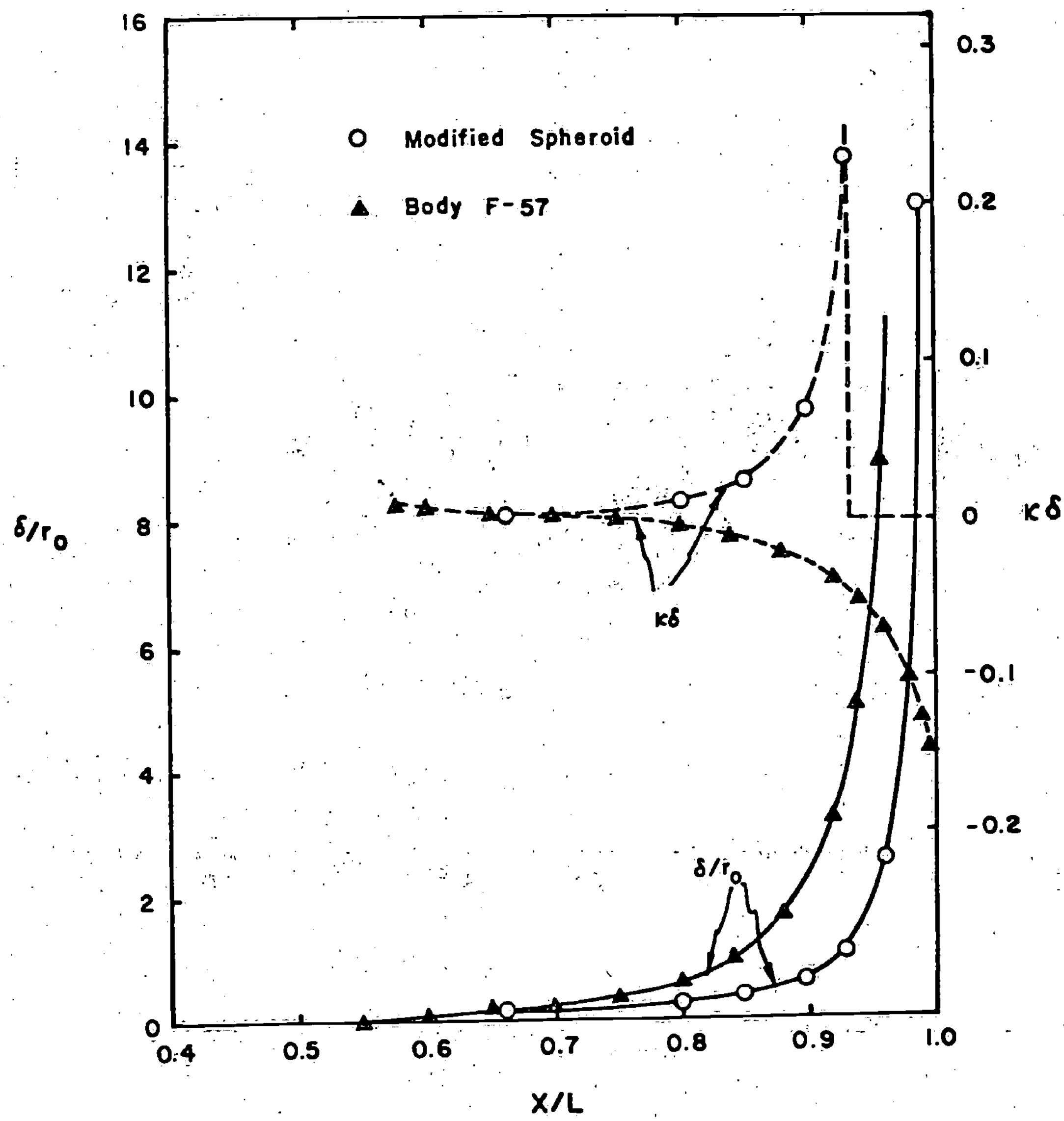

FIGURE 21 RATIOS OF BOUNDARY-LAYER THICKNESS TO THE LONGITUDINAL AND TRANSVERSE RADII OF SURFACE CURVATURE

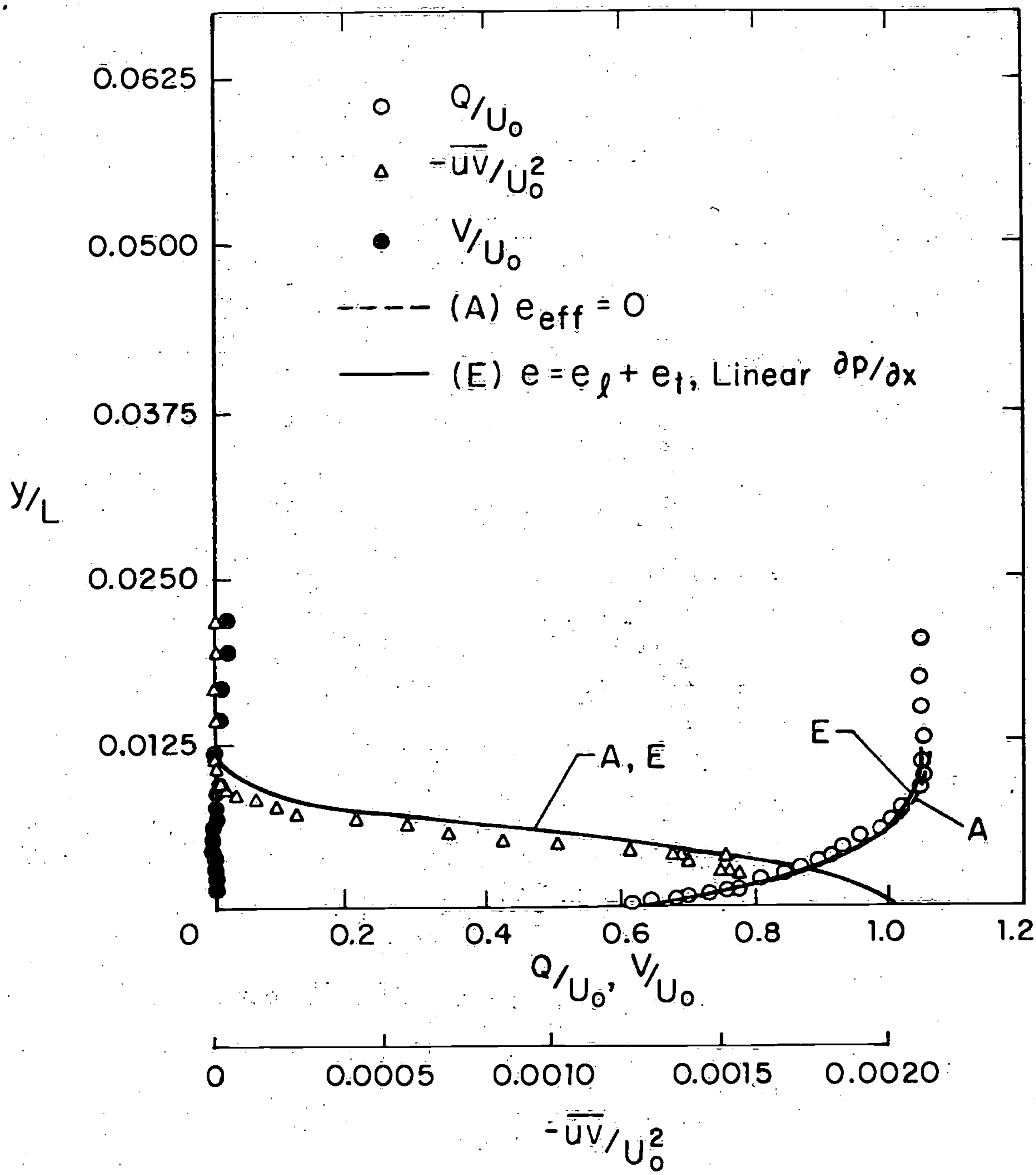

FIGURE 22 COMPARISON OF MEASUREMENTS WITH THE SOLUTION OF THE DIFFERENTIAL EQUATIONS, LOW-DRAG BODY
(a) INITIAL PROFILES AT X/L = 0.601

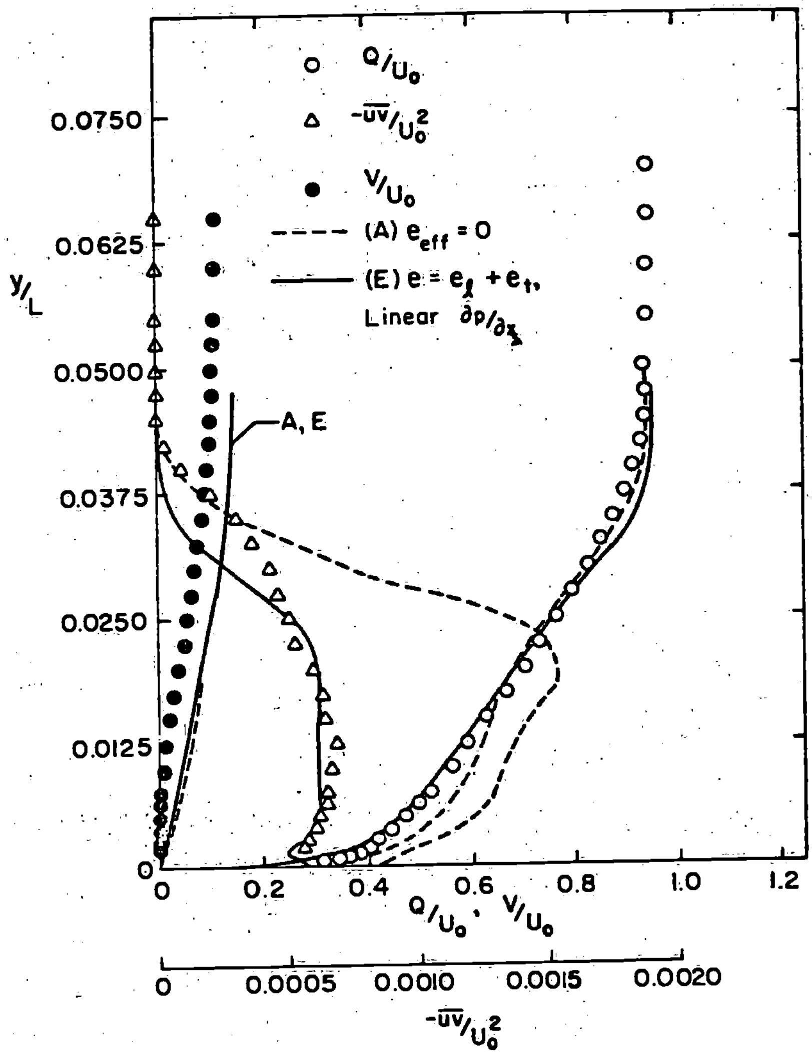

FIGURE 22 (continued)
(b) VELOCITY AND SHEAR STRESS PROFILES AT X/L = 0.920

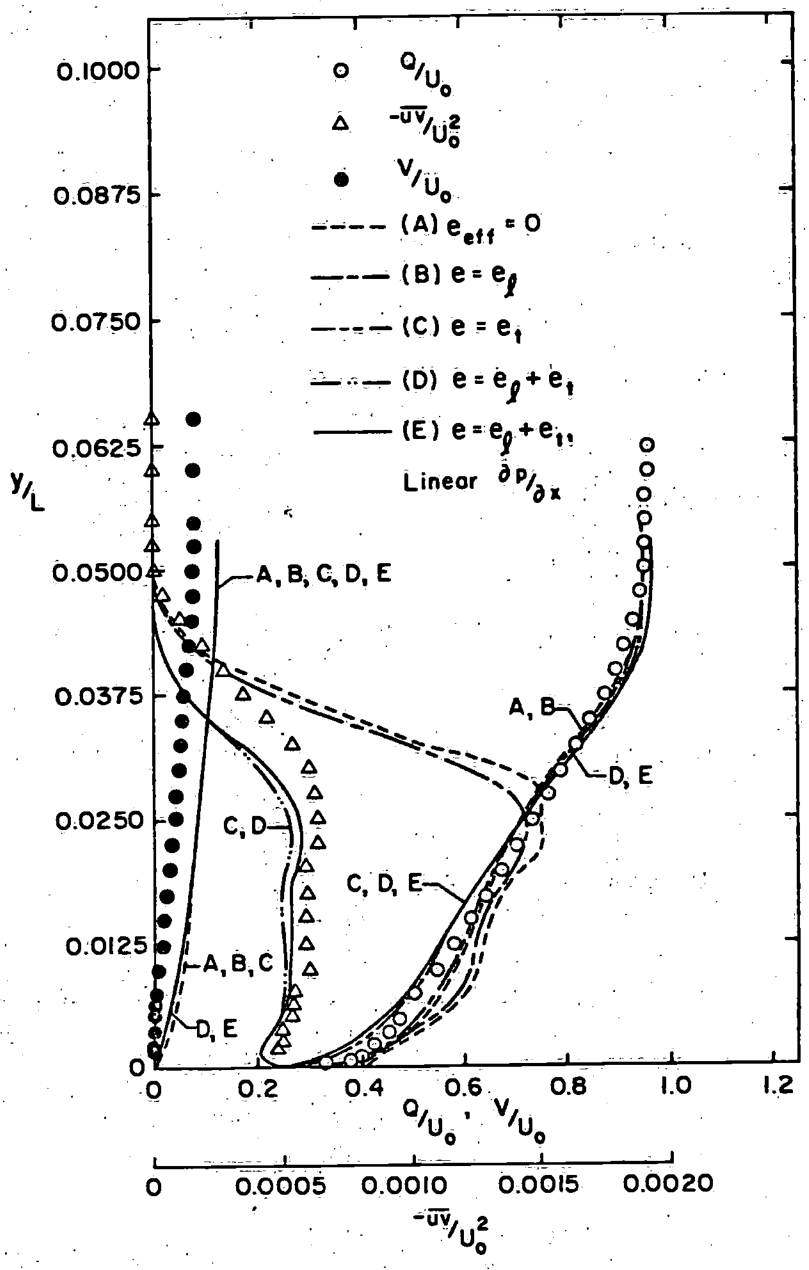

FIGURE 22 (continued)
(c) VELOCITY AND SHEAR STRESS PROFILES AT X/L = 0.960

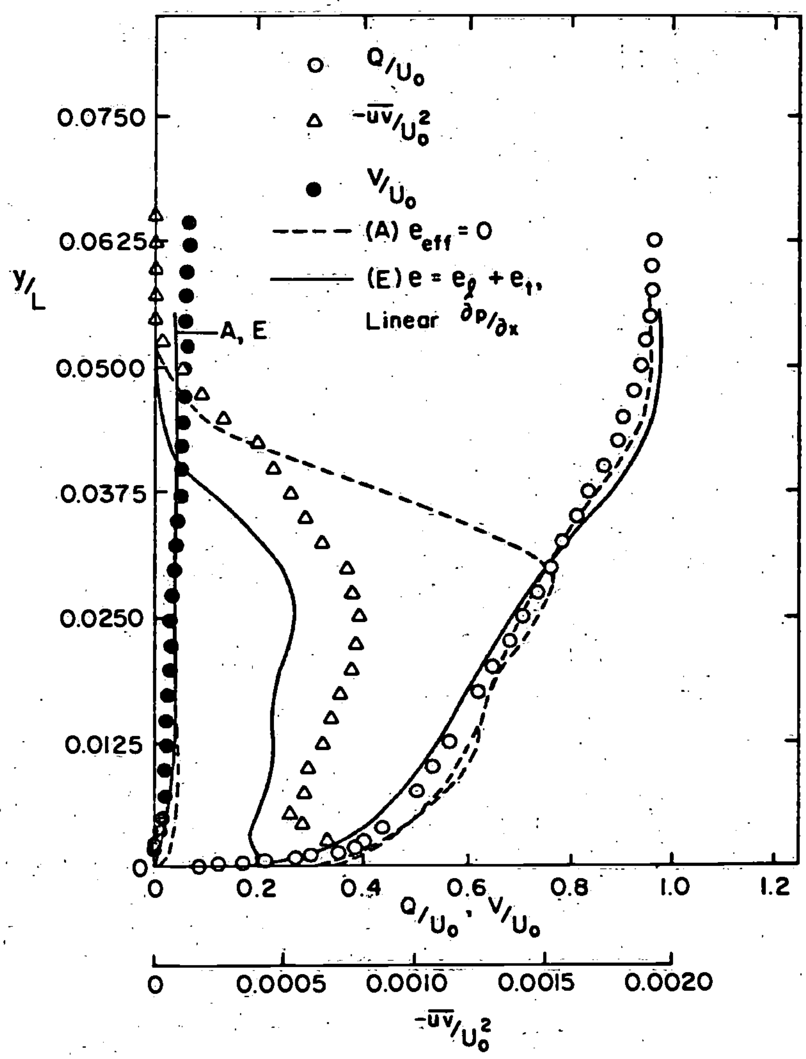

FIGURE 22 (continued)
(d) VELOCITY AND SHEAR STRESS PROFILES AT X/L = 1.000

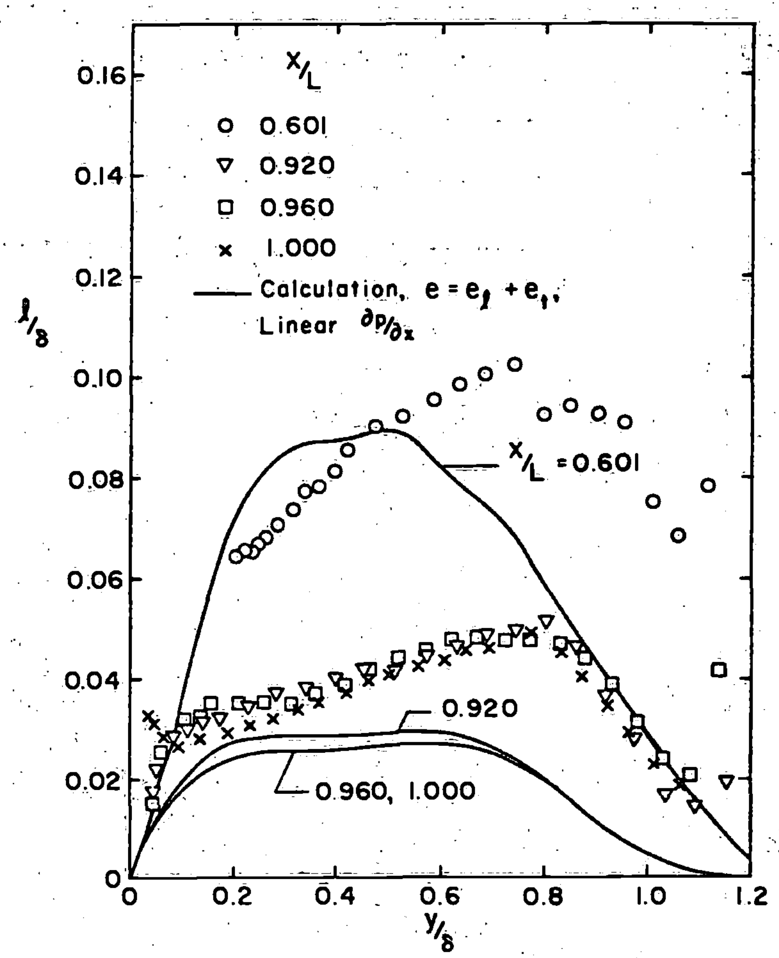

FIGURE 22 (continued)
(e) MIXING LENGTH PROFILES

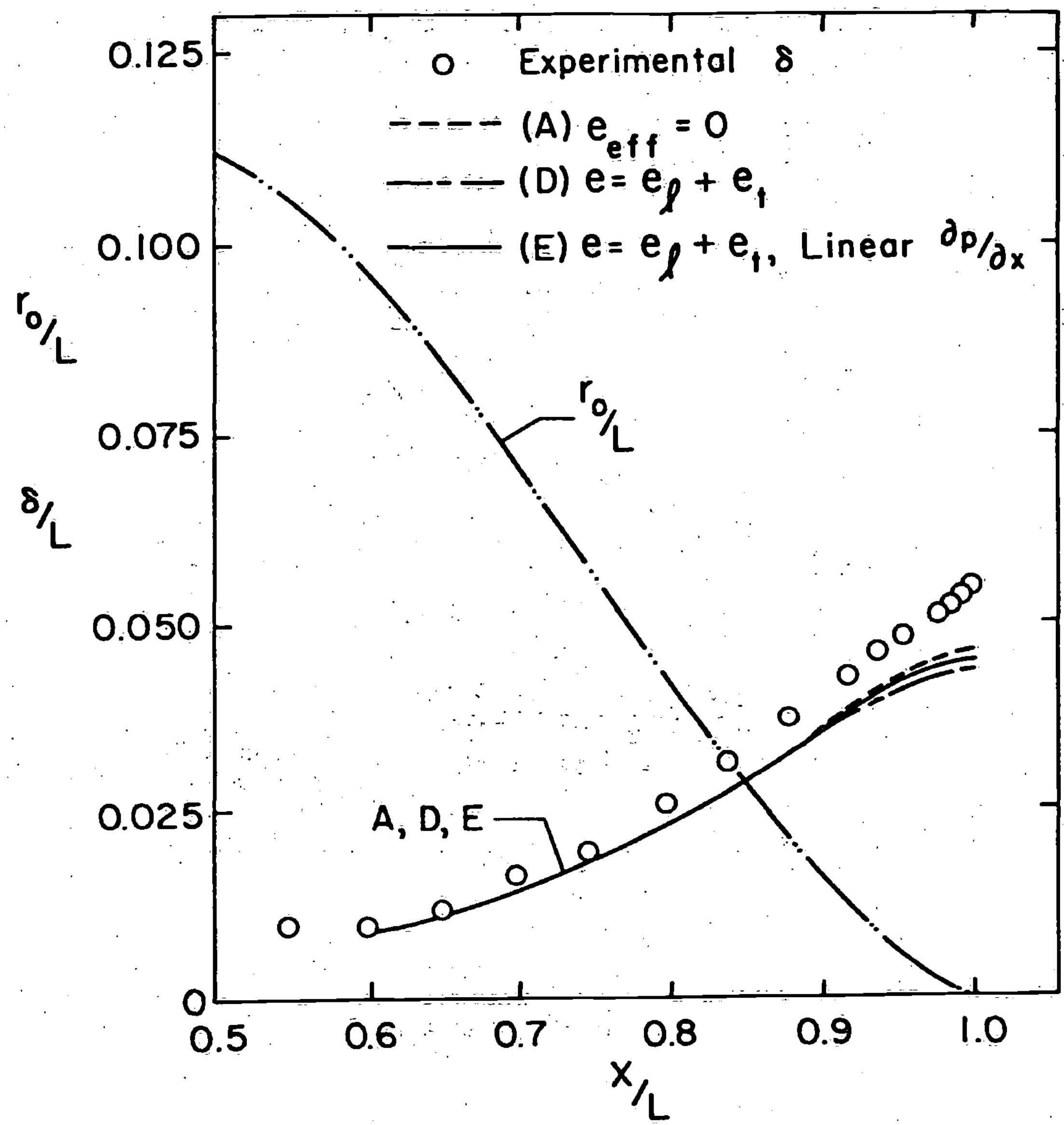

FIGURE 22 (continued)
(f) BOUNDARY LAYER THICKNESS

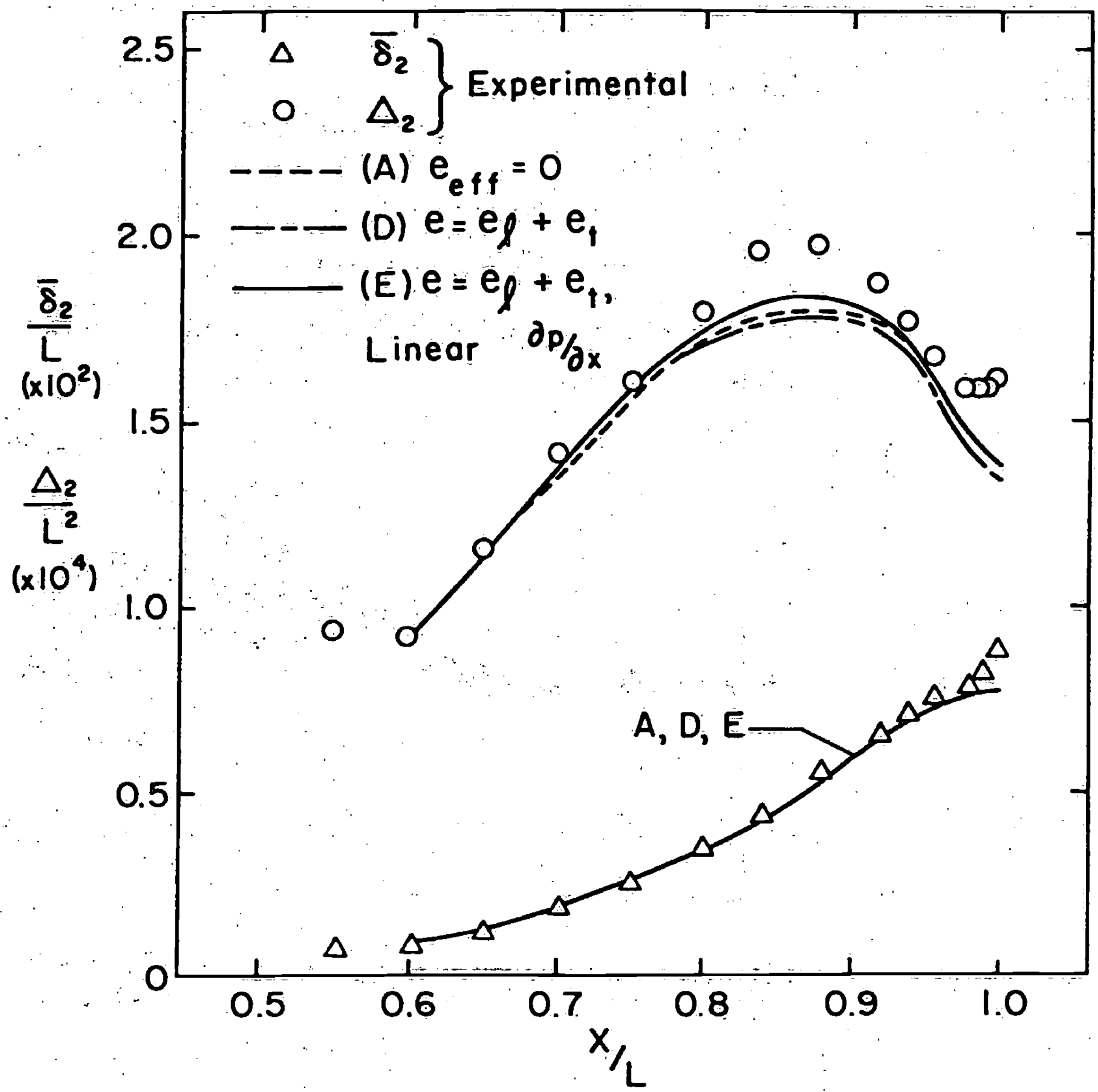

FIGURE 22 (continued)
(g) PLANAR AND AXISYMMETRIC MOMENTUM DEFICITS

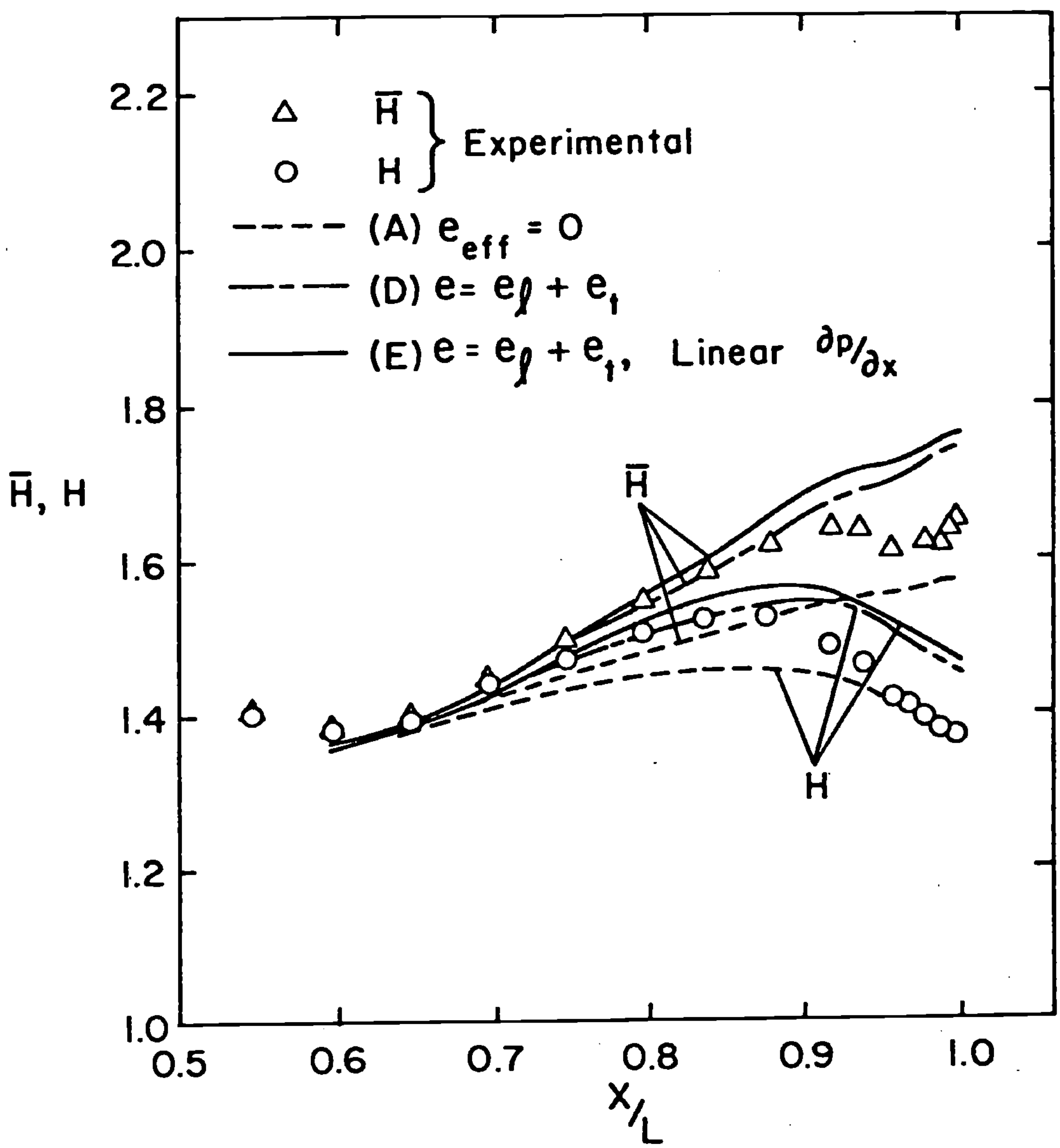

FIGURE 22 (continued)
(h) SHAPE PARAMETER

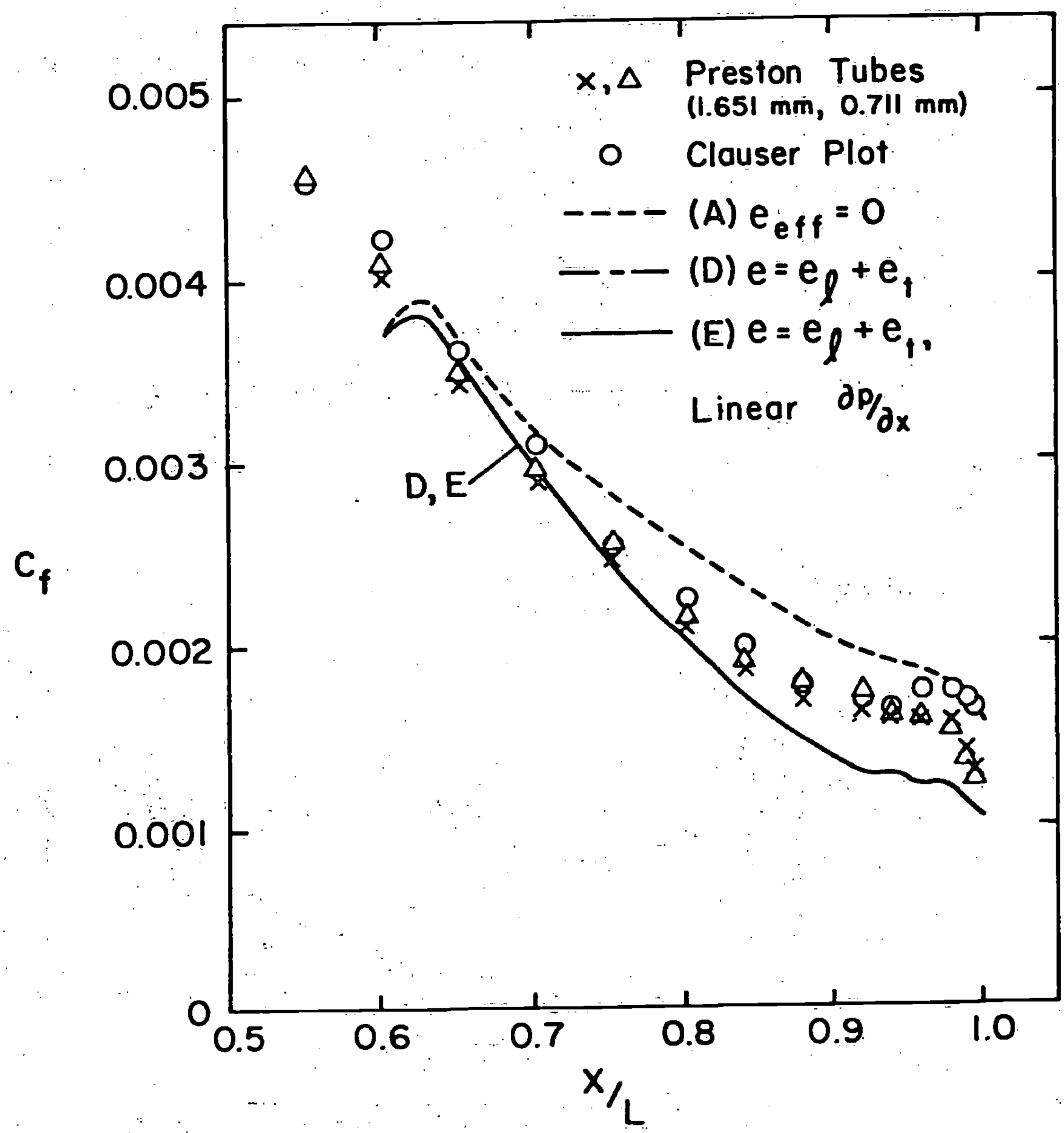

FIGURE 22 (continued)
(i) WALL SHEAR STRESS

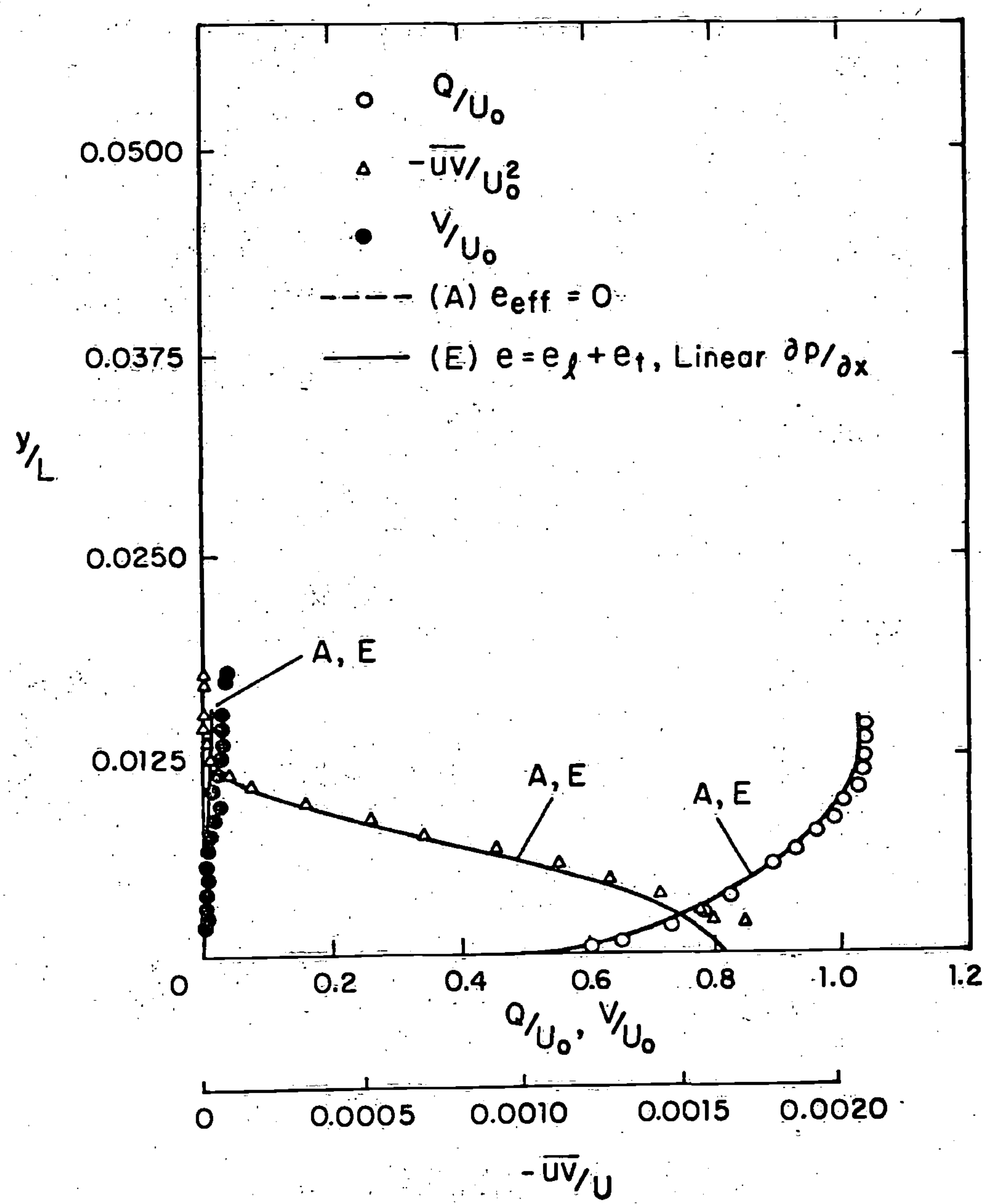

FIGURE 23 COMPARISON OF MEASUREMENTS WITH THE SOLUTION OF THE DIFFERENTIAL EQUATIONS, MODIFIED SPHEROID (a) INITIAL PROFILES AT X/L = 0.662

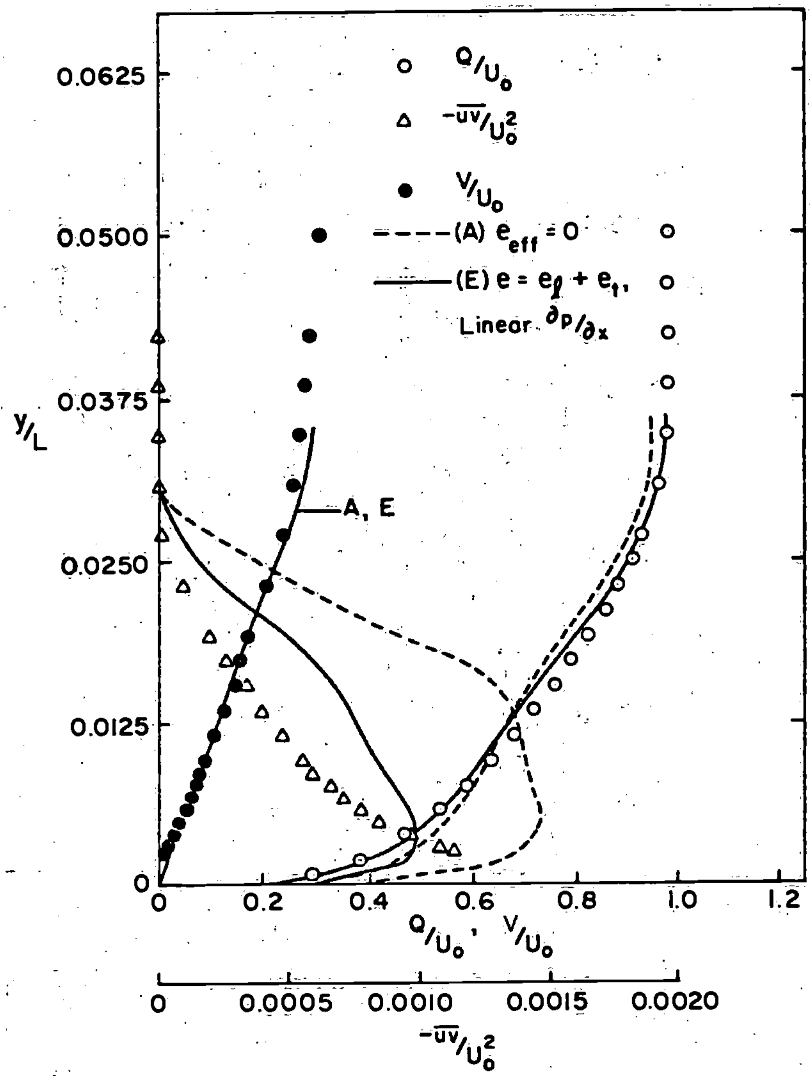

FIGURE 23 (continued)
(b) VELOCITY AND SHEAR STRESS PROFILES AT X/L = 0.930

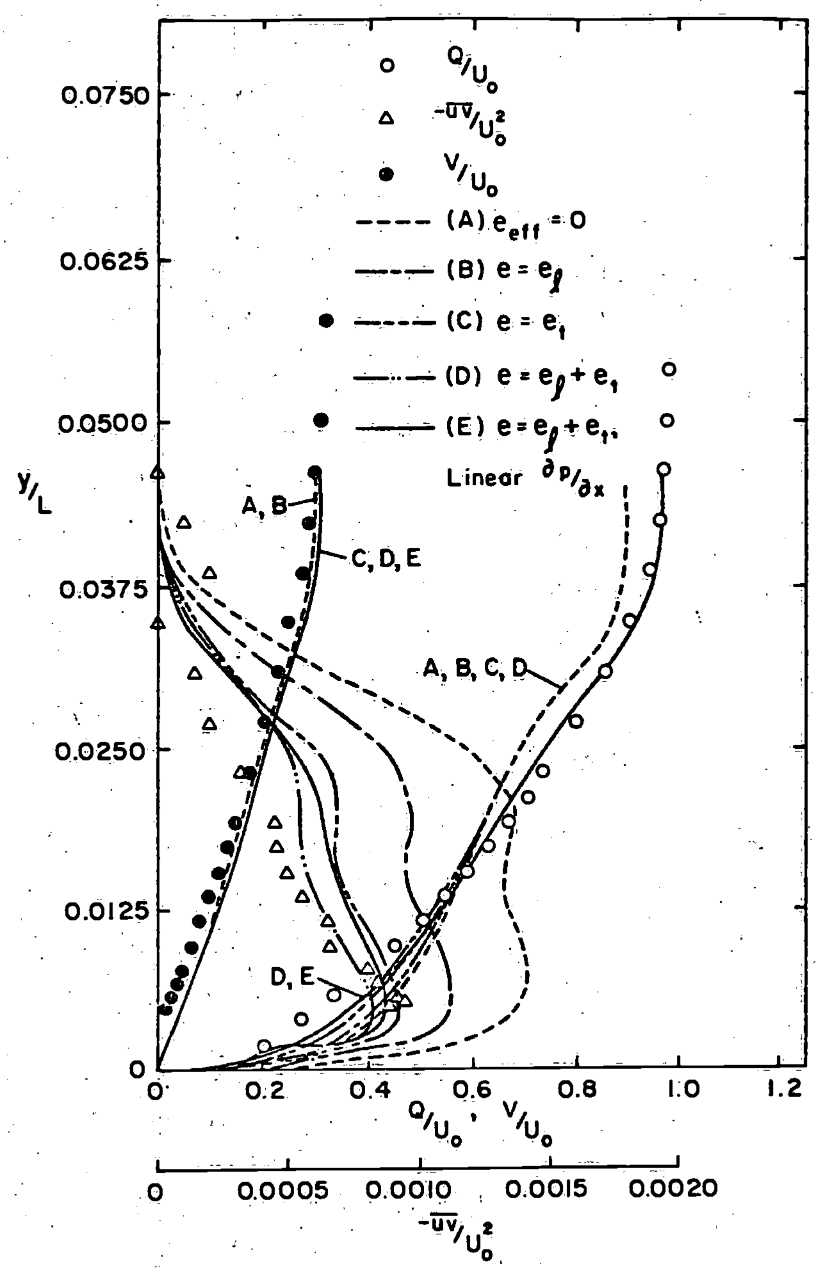

FIGURE 23 (continued)
(c) VELOCITY AND SHEAR STRESS PROFILES AT X/L = 0.960

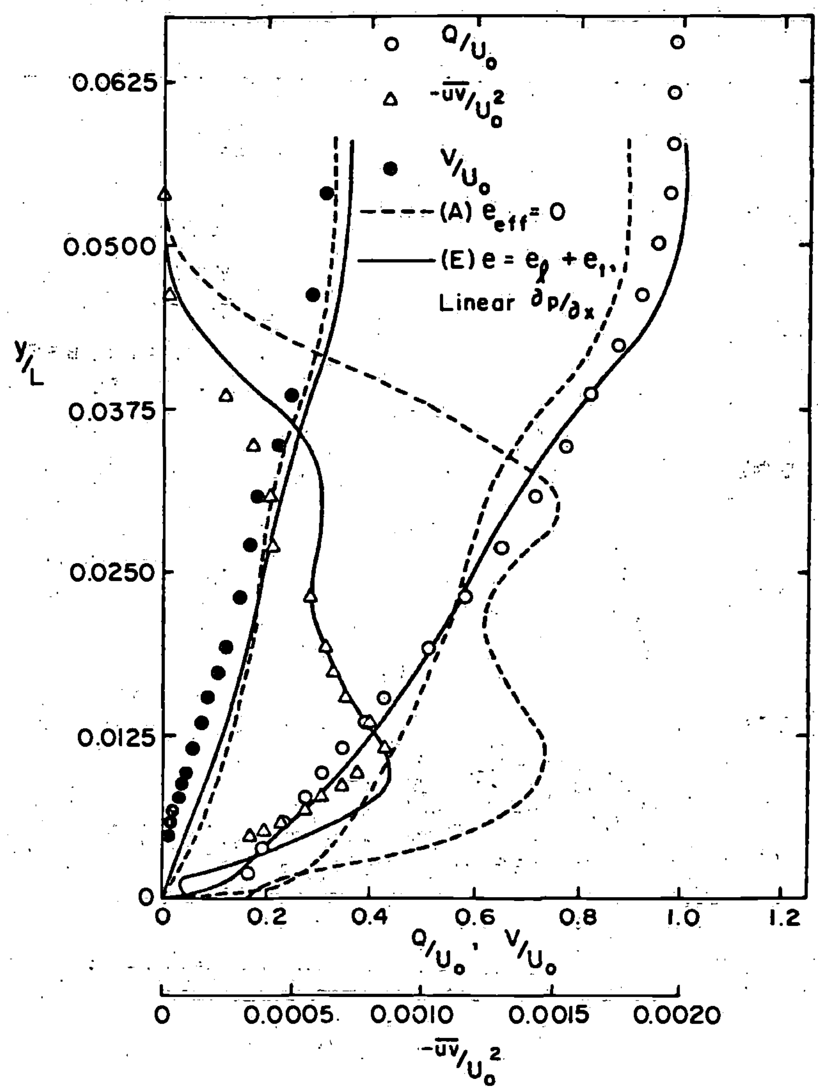

FIGURE 23 (continued)
(d) VELOCITY AND SHEAR STRESS PROFILES AT X/L = 0.990

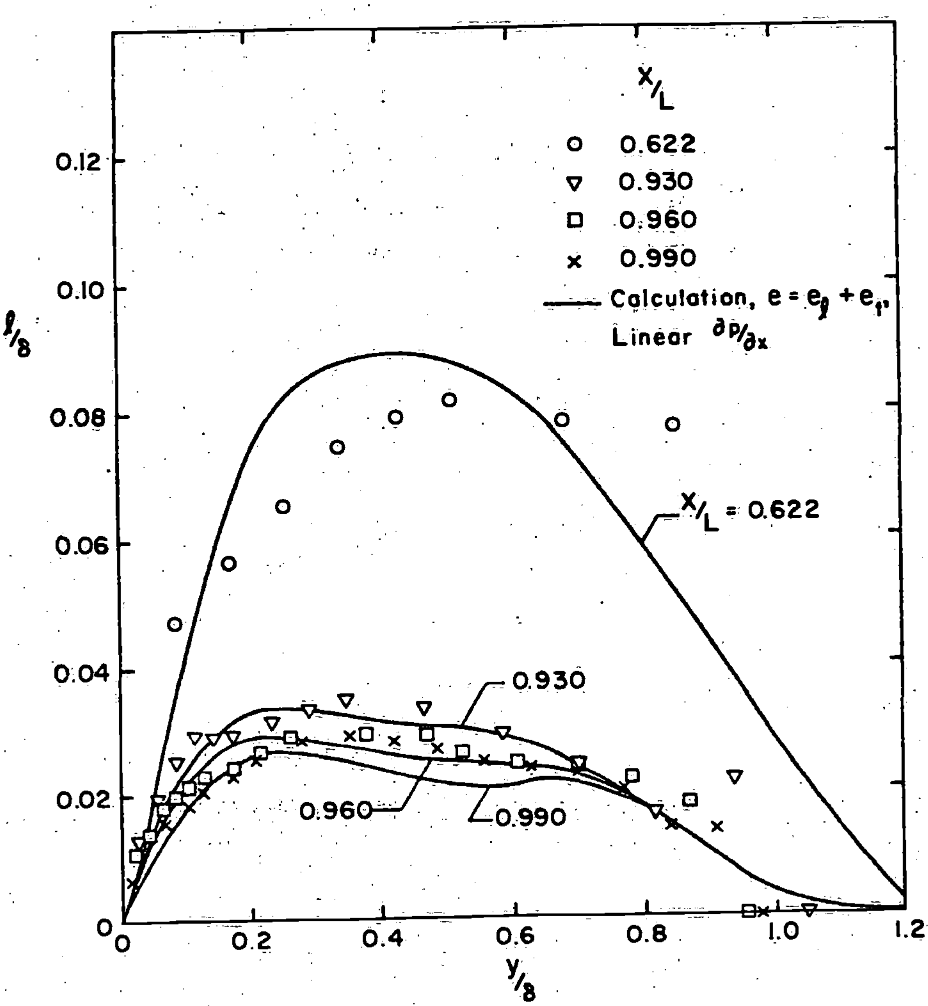

FIGURE 23 (continued)
(e) MIXING LENGTH PROFILES

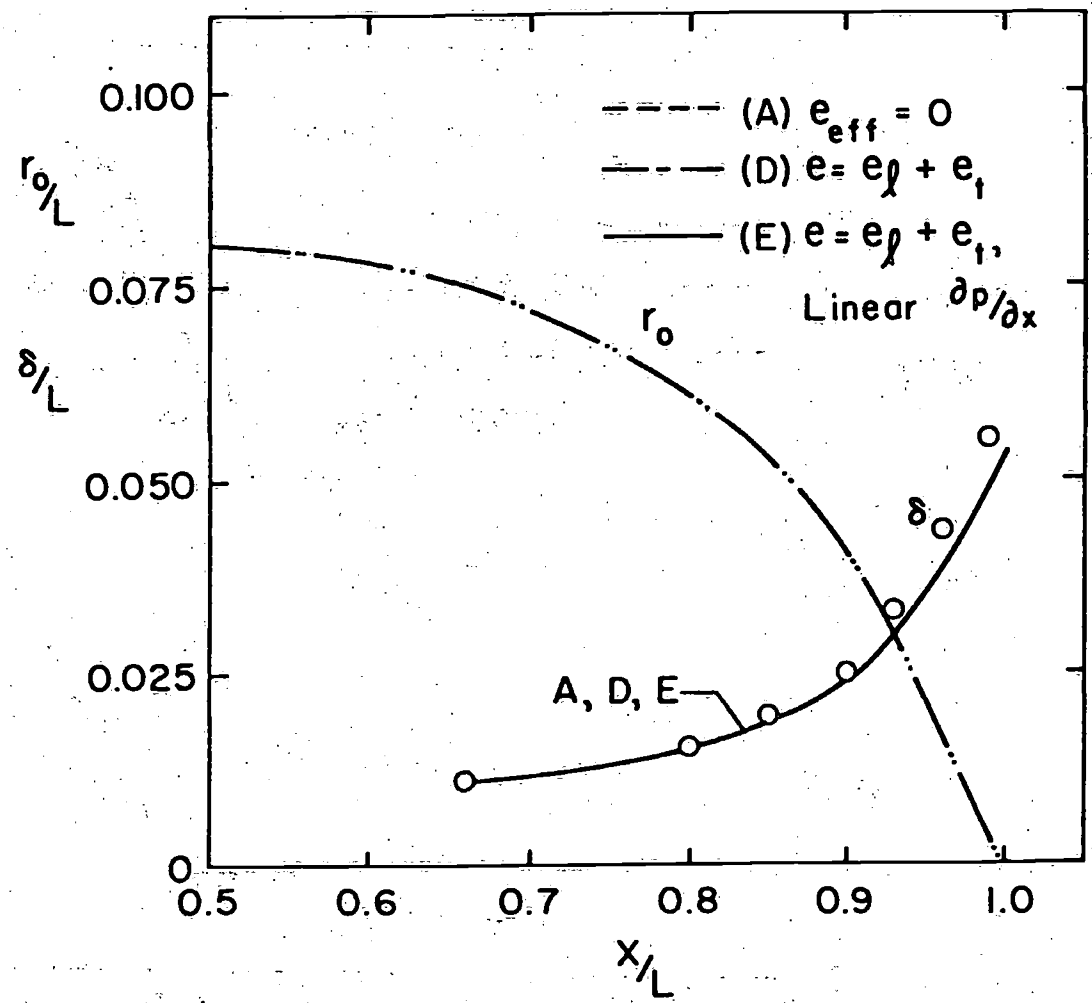

FIGURE 23 (continued)
(f) BOUNDARY LAYER THICKNESS

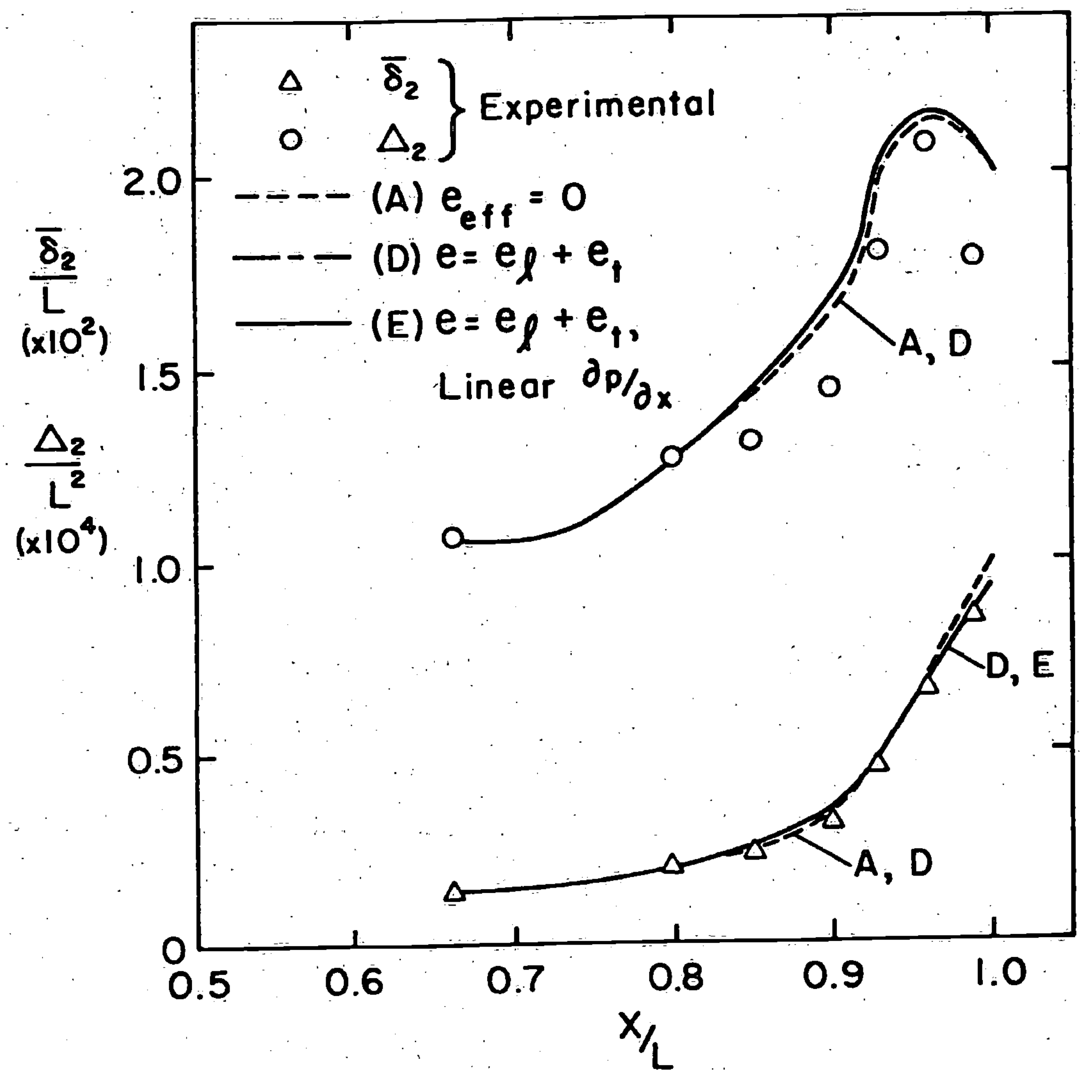

FIGURE 23 (continued)
(g) PLANAR AND AXISYMMETRIC MOMENTUM DEFICITS

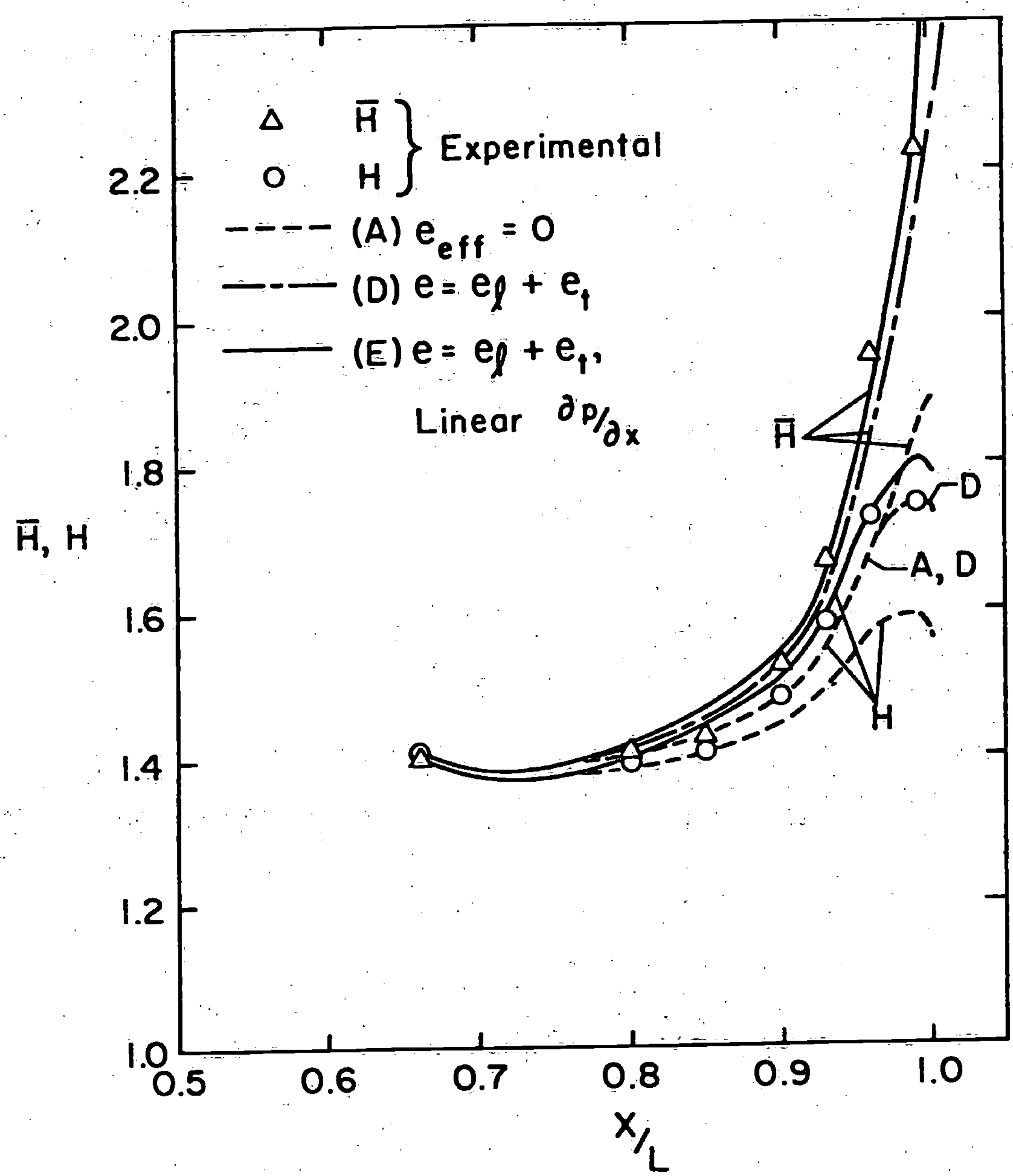

FIGURE 23 (continued)
(h) SHAPE PARAMETER

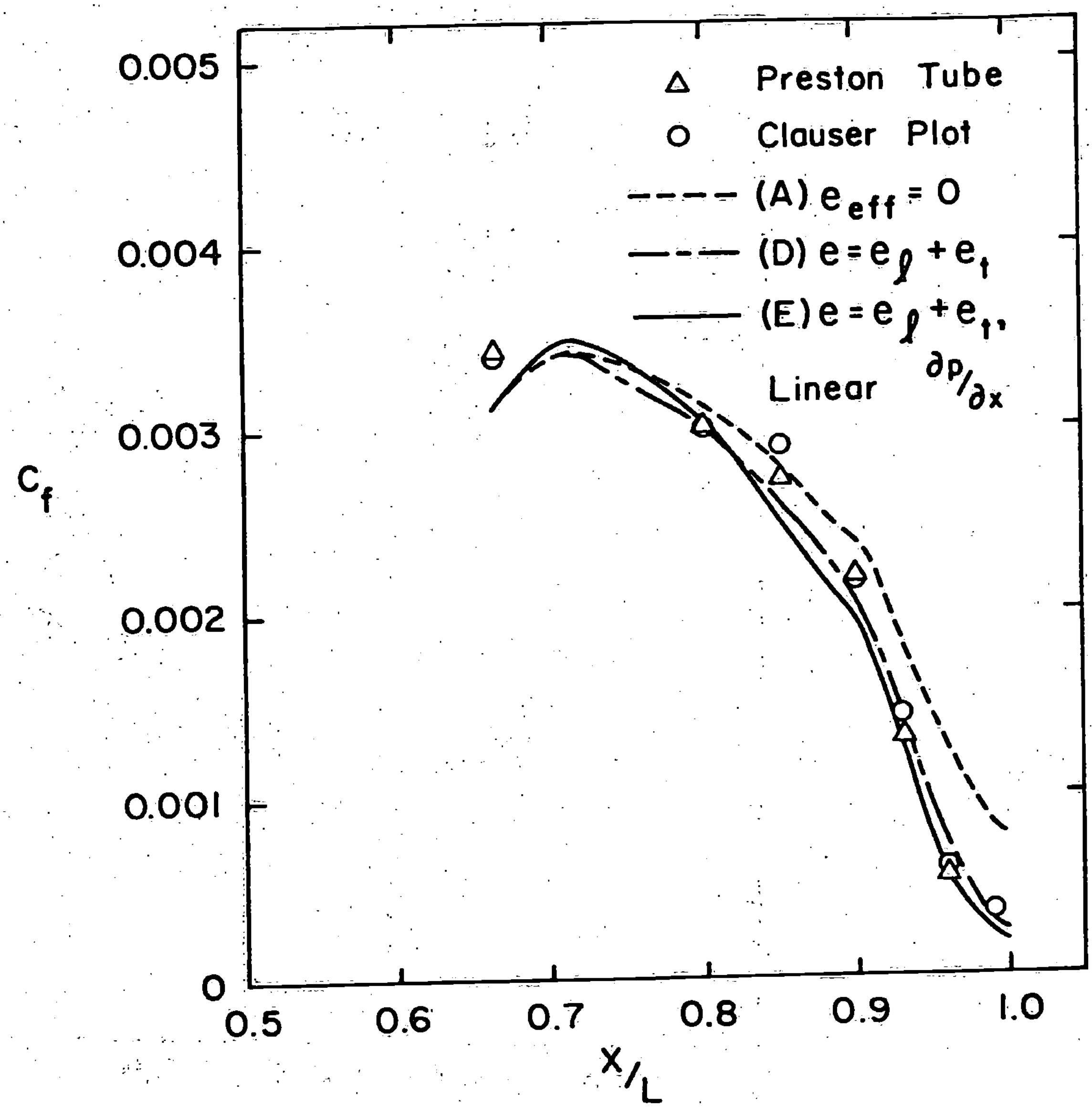

FIGURE 23 (continued)
(i) WALL SHEAR STRESS

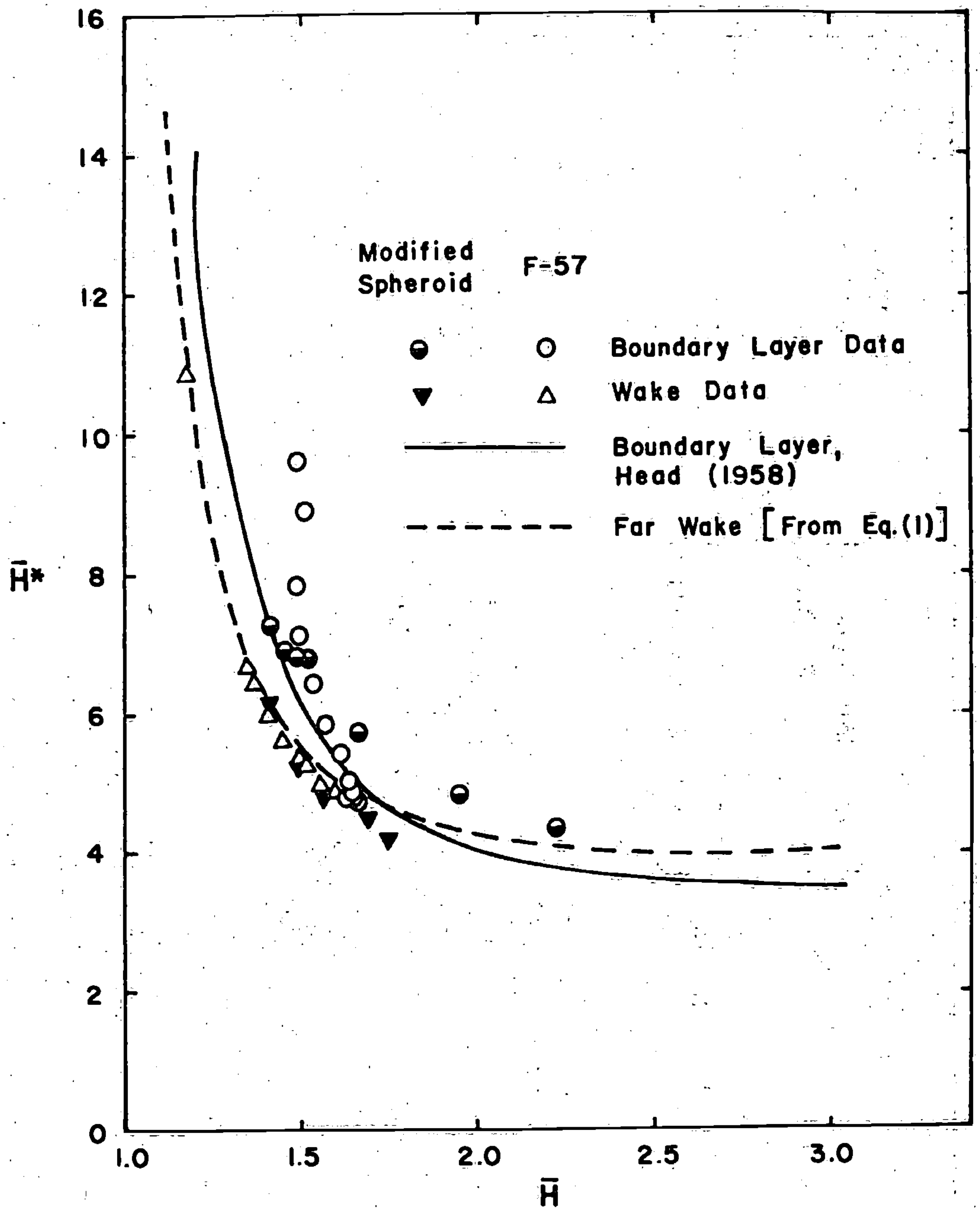

FIGURE 24 SHAPE-PARAMETER RELATIONS IN INTEGRAL METHOD

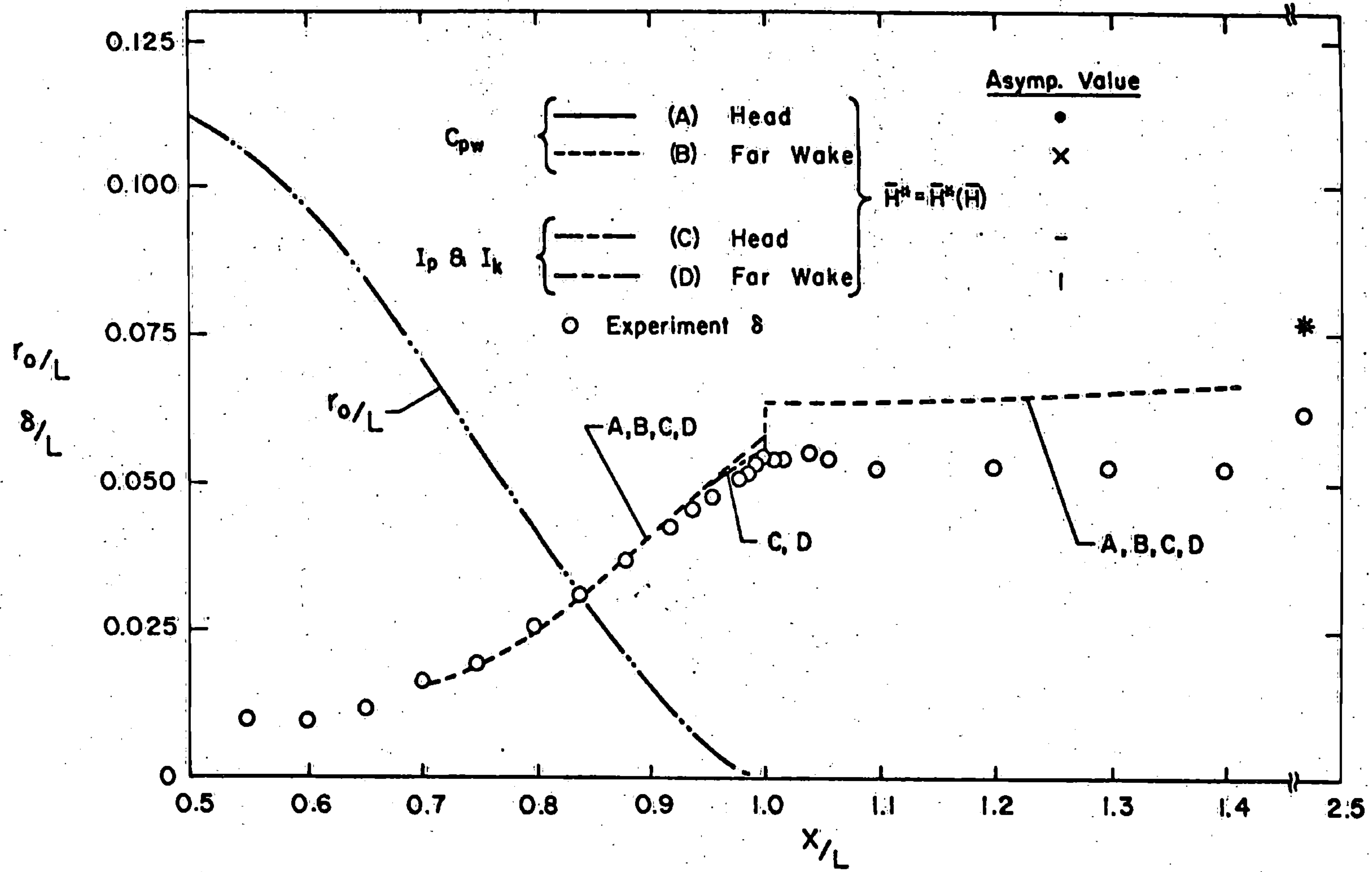

FIGURE 25 COMPARISON OF EXPERIMENTS WITH THE SOLUTION OF THE INTEGRAL EQUATIONS, LOW-DRAG BODY
(a) BOUNDARY LAYER AND WAKE THICKNESS

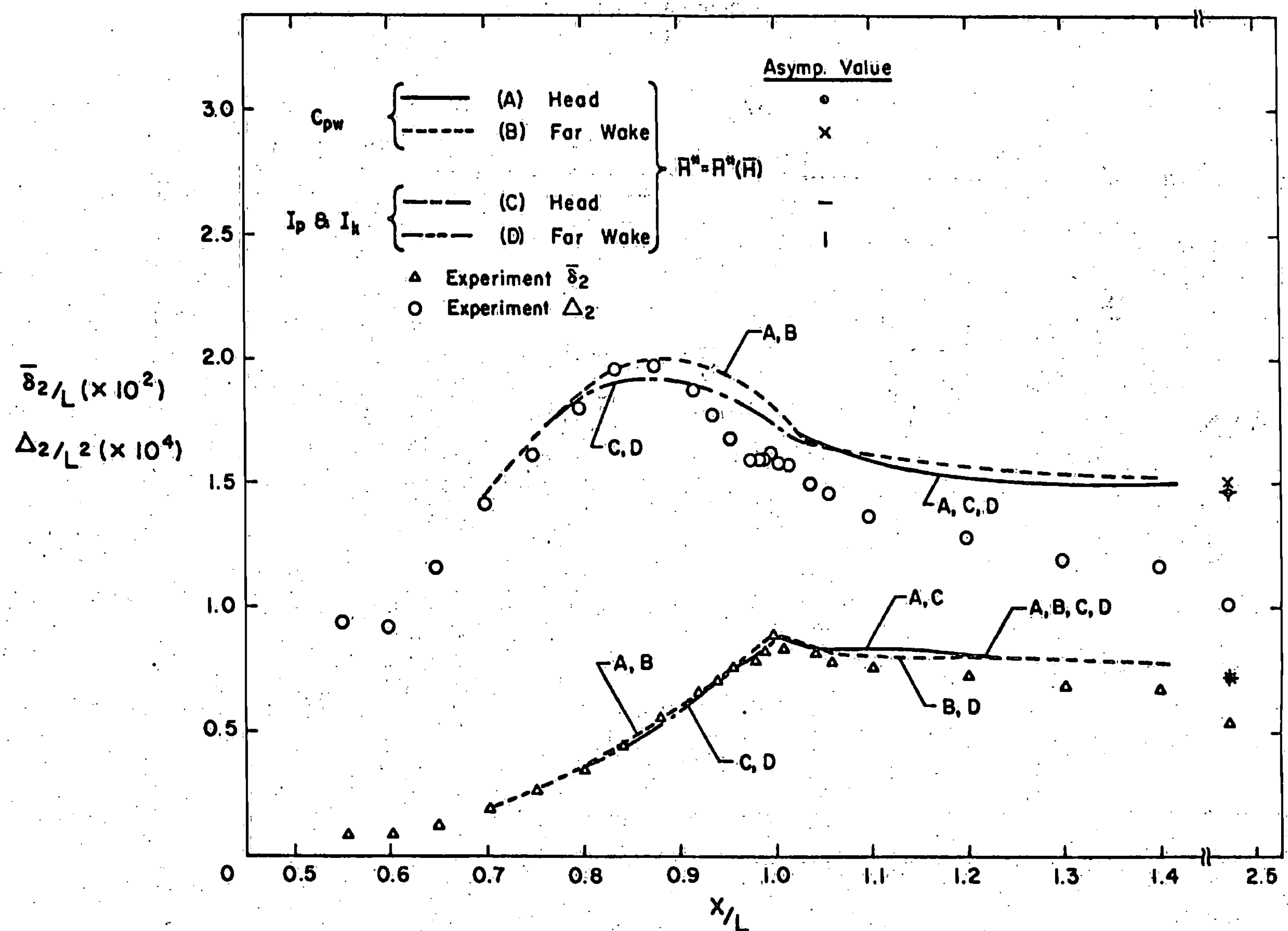

FIGURE 25 (continued)
(b) PLANAR AND AXISYMMETRIC MOMENTUM DEFICITS

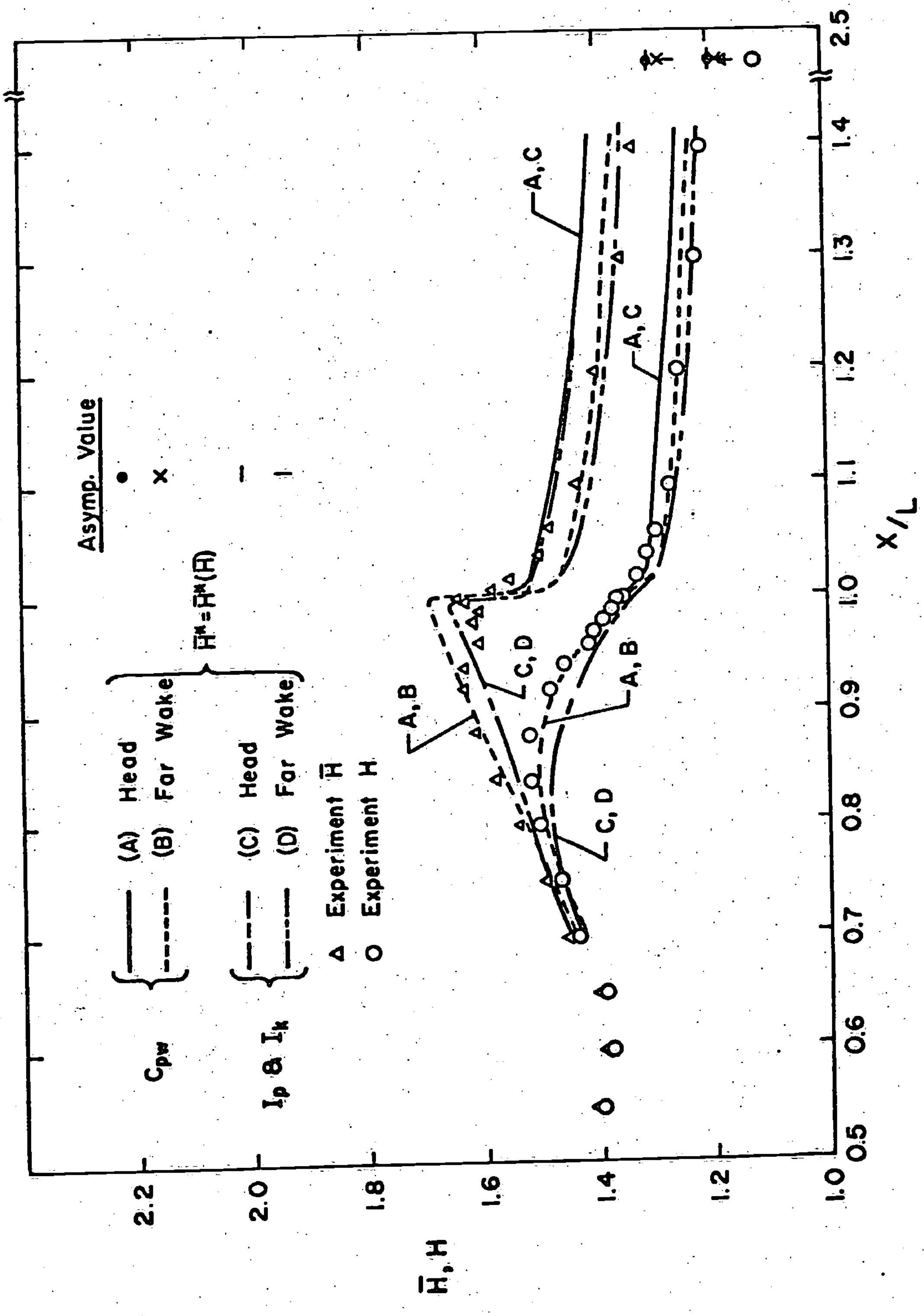

FIGURE 25 (continued)
(c) SHAPE PARAMETER

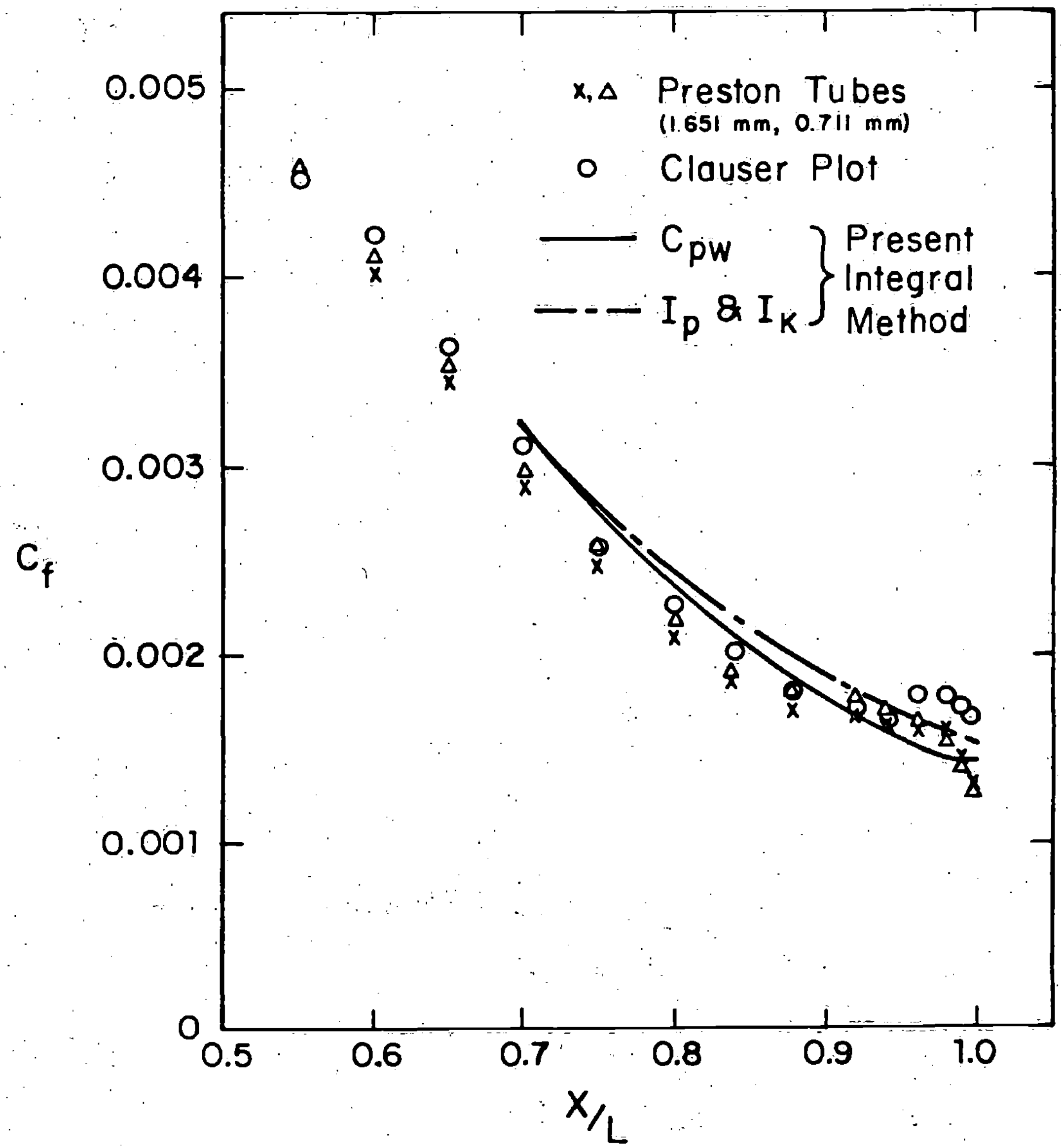

FIGURE 25 (continued)
(d) WALL SHEAR STRESS

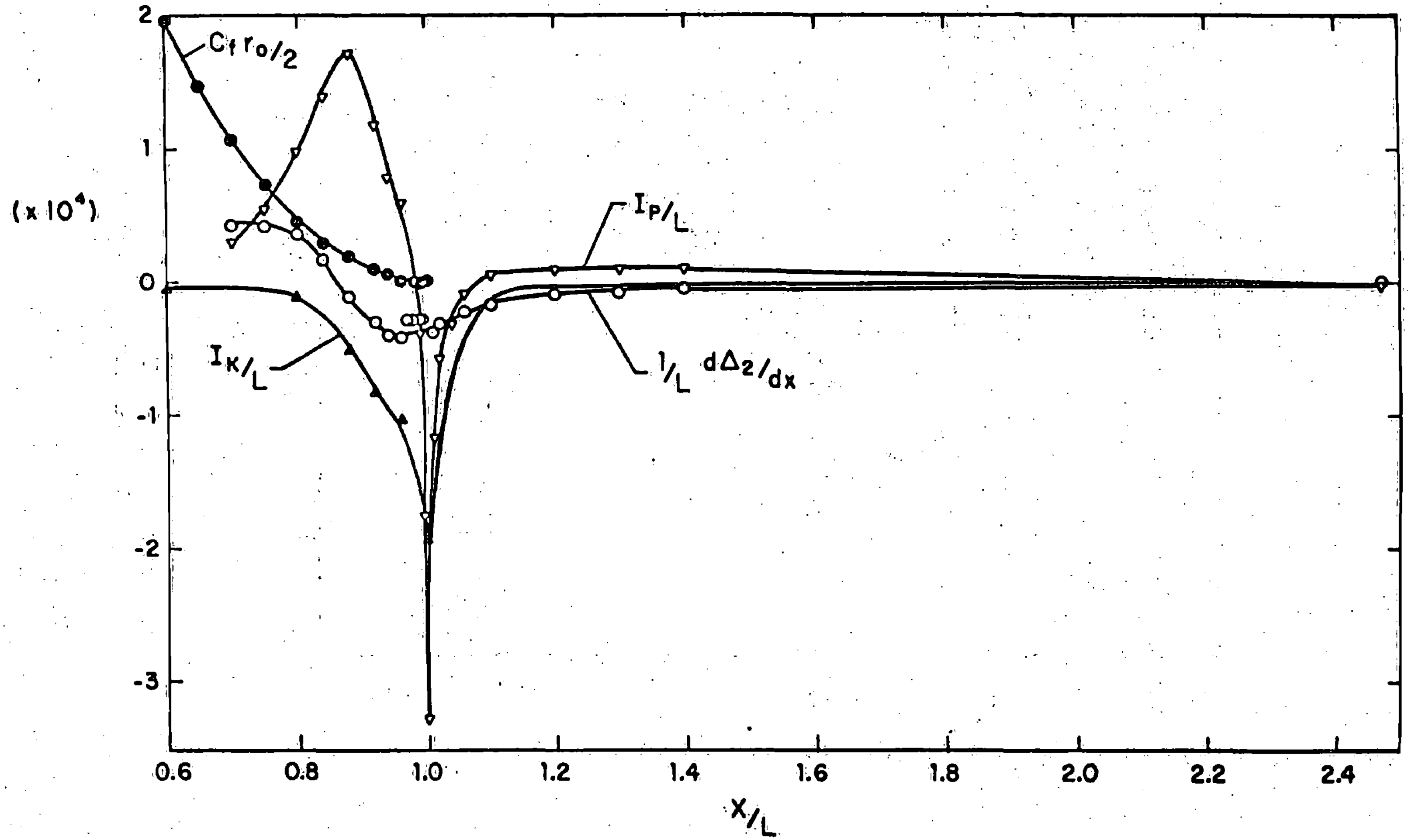

FIGURE 26 RELATIVE MAGNITUDES OF SOME TERMS IN THE MOMENTUM INTEGRAL EQUATION

TABLE 1 SUMMARY OF DATA IN THE BOUNDARY LAYER AND WAKE

Station	X/L+	r_o/L ×10	κL	δ/L ×10^2	Q_δ/U_o++	C_{pw}	$C_{p\delta}$	$\bar{\delta}_1/L$ ×10^2	$\bar{\delta}_2/L$ ×10^2	$\bar{H}$	Δ_1/L^2 ×10^4	Δ_2/L^2 ×10^4	H	δ^*/L ×10^2	C_f ×10^3 Preston	C_f ×10^3 Clauser
1	0.433	1.169	-2.080	0.158	1.145	-0.375	-0.356	0.051	0.021	2.456	0.600	0.245	2.452	0.051	--	--
2	0.551	1.068	-1.072	0.935	1.086	-0.209	-0.192	0.122	0.087	1.408	1.329	0.948	1.402	0.124	4.576	4.53
3	0.601	0.970	-0.744	0.935	1.047	-0.121	-0.070	0.130	0.093	1.392	1.290	0.930	1.387	0.132	4.110	4.22
4	0.651	0.852	-0.488	1.188	1.008	-0.041	-0.033	0.185	0.132	1.403	1.629	1.168	1.395	0.189	3.512	3.62
5	0.701	0.721	-0.268	1.575	0.975	0.031	0.037	0.270	0.186	1.451	2.052	1.428	1.438	0.279	2.978	3.10
6	0.751	0.583	-0.068	1.988	0.947	0.092	0.091	0.379	0.253	1.499	2.395	1.622	1.476	0.398	2.567	2.55
7	0.801	0.442	0.140	2.563	0.930	0.130	0.131	0.541	0.350	1.547	2.751	1.823	1.509	0.586	2.150	2.25
8	0.840	0.332	0.324	3.165	0.924	0.150	0.135	0.720	0.454	1.586	3.001	1.970	1.524	0.809	1.909	2.00
9	0.880	0.229	0.552	3.725	0.925	0.160	0.134	0.910	0.562	1.620	3.022	1.983	1.524	1.077	1.789	1.80
10	0.920	0.134	0.868	4.333	0.932	0.156	0.120	1.090	0.668	1.632	2.802	1.882	1.489	1.389	1.750	1.70
11	0.940	0.092	1.000	4.605	0.935	0.151	0.112	1.168	0.715	1.634	2.614	1.787	1.463	1.557	1.692	1.65
12	0.960	0.054	1.424	4.838	0.942	0.135	0.099	1.220	0.757	1.612	2.391	1.683	1.420	1.720	1.622	1.76
13	0.980	0.023	1.956	5.138	0.947	0.122	0.090	1.293	0.799	1.618	2.240	1.609	1.392	1.906	1.493	1.75
14	0.990	0.010	2.400	5.288	0.949	0.117	0.084	1.336	0.824	1.622	2.206	1.602	1.377	2.007	1.354	1.70
15	0.995	0.005	2.716	5.313	0.951	0.113	0.081	1.362	0.834	1.633	2.199	1.602	1.372	2.055	1.238	1.65

TABLE 1 (continued)

Station	X/L	δ/L $\times 10^2$	Q_c/U_o	Q_δ/U_o	C_{pc}	$C_{p\delta}$	$\bar{\delta}_1/L$ $\times 10^2$	$\bar{\delta}_2/L$ $\times 10^2$	$\bar{H}$	Δ_1/L^2 $\times 10^4$	Δ_2/L^2 $\times 10^4$	H	δ^*/L $\times 10^2$	C_D+++ $\times 10^2$
16	1.000	5.400	-	0.955	-	0.068	1.397	0.844	1.656	2.219	1.621	1.369	2.107	1.292
17	1.010	5.425	0.302	0.958	0.089	0.073	1.343	0.842	1.595	2.156	1.593	1.353	2.077	1.292
18	1.020	5.475	0.370	0.958	0.077	0.072	1.305	0.849	1.559	2.117	1.580	1.340	2.058	1.311
19	1.040	5.525	0.430	0.963	0.061	0.060	1.232	0.814	1.514	1.990	1.509	1.319	1.995	1.299
20	1.060	5.438	0.455	0.965	0.054	0.056	1.188	0.797	1.490	1.910	1.464	1.305	1.955	1.302
21	1.100	5.375	0.500	0.971	0.039	0.045	1.096	0.760	1.442	1.742	1.361	1.279	1.867	1.248
22	1.200	5.375	0.559	0.985	0.020	0.024	1.028	0.732	1.405	1.629	1.291	1.262	1.805	1.187
23	1.300	5.388	0.596	0.990	0.017	0.016	0.939	0.690	1.362	1.478	1.197	1.235	1.719	1.114
24	1.400	5.393	0.612	0.992	0.007	0.012	0.902	0.671	1.344	1.414	1.158	1.222	1.682	1.089
25	2.472	6.275	0.795	0.999	0.000	0.005	0.614	0.523	1.174	1.131	1.007	1.124	1.504	0.920

+ L = 1.219 m (4 ft)

++ U_o = 15.24 m/sec (50 ft/sec)

+++ drag coefficient based on the frontal area which is 0.693 m^2 (0.688 ft^2)

I measured Preston tube data extrapolated to zero-diameter

TABLE 2 PROFILES AT X/L = 0.433

Y (FT.)	Y (CM.)	CP (TOTAL)	CP (STATIC)	Q/UO +++
0.0016	0.0497	-0.0530	-0.3547	0.5493
0.0018	0.0549	-0.0474	-0.3547	0.5543
0.0021	0.0640	0.0381	-0.3547	0.6267
0.0023	0.0701	0.1165	-0.3547	0.6864
0.0025	0.0762	0.2076	-0.3547	0.7899
0.0028	0.0853	0.2912	-0.3547	0.8037
0.0032	0.0975	0.4250	-0.3547	0.8830
0.0035	0.1067	0.5634	-0.3547	0.9582
0.0038	0.1158	0.6026	-0.3547	0.9784
0.0040	0.1219	0.6921	-0.3547	1.0231
0.0043	0.1311	0.7572	-0.3547	1.0545
0.0045	0.1372	0.7760	-0.3547	1.0633
0.0047	0.1433	0.8033	-0.3547	1.0761
0.0049	0.1494	0.8332	-0.3547	1.0899
0.0050	0.1524	0.8644	-0.3547	1.1041
0.0053	0.1615	0.8884	-0.3547	1.1149
0.0055	0.1676	0.8911	-0.3547	1.1242
0.0058	0.1768	0.9236	-0.3547	1.1306
0.0060	0.1829	0.9284	-0.3547	1.1327
0.0062	0.1890	0.9471	-0.3547	1.1410
0.0064	0.1951	0.9611	-0.3547	1.1471
0.0068	0.2073	0.9687	-0.3547	1.1530
0.0070	0.2134	0.9767	-0.3547	1.1563
0.0073	0.2225	0.9823	-0.3547	1.1563

\+ CROSS WIRE PROBE
++ SINGLE WIRE PROBE
+++ PITOT-STATIC

TABLE 3 PROFILES AT X/L = 0.551

Y (FT.)	Y (CM.)	CP (TOTAL)	CP (STATIC)	Q/UO +++
0.0016	0.0497	0.2634	-0.2090	0.6873
0.0018	0.0549	0.2820	-0.2090	0.7007
0.0020	0.0610	0.3072	-0.2090	0.7185
0.0025	0.0762	0.3540	-0.2090	0.7503
0.0030	0.0914	0.3807	-0.2090	0.7679
0.0035	0.1067	0.4036	-0.2090	0.7827
0.0040	0.1219	0.4207	-0.2090	0.7935
0.0045	0.1372	0.4365	-0.2090	0.8034
0.0050	0.1524	0.4527	-0.2090	0.8134
0.0060	0.1829	0.4832	-0.2090	0.8320
0.0070	0.2134	0.5151	-0.2090	0.8509
0.0080	0.2438	0.5380	-0.2090	0.8643
0.0090	0.2743	0.5623	-0.2090	0.8782
0.0100	0.3048	0.5891	-0.2090	0.8934
0.0120	0.3658	0.6334	-0.2090	0.9178
0.0140	0.4267	0.6782	-0.2090	0.9419
0.0160	0.4877	0.7149	-0.2082	0.9608
0.0180	0.5486	0.7414	-0.2058	0.9732
0.0200	0.6096	0.7874	-0.2040	0.9957
0.0220	0.6706	0.8222	-0.2020	1.0120
0.0240	0.7315	0.8532	-0.2001	1.0263
0.0250	0.7620	0.8685	-0.1992	1.0333
0.0260	0.7925	0.8842	-0.1982	1.0404
0.0280	0.8534	0.9114	-0.1960	1.0523
0.0300	0.9144	0.9367	-0.1945	1.0636
0.0320	0.9754	0.9434	-0.1937	1.0663
0.0340	1.0363	0.9710	-0.1929	1.0788
0.0360	1.0973	0.9815	-0.1921	1.0833
0.0380	1.1582	0.9907	-0.1913	1.0872
0.0400	1.2192	0.9948	-0.1905	1.0887
0.0420	1.2802	0.9972	-0.1891	1.0892
0.0440	1.3411	1.0006	-0.1877	1.0901
0.0460	1.4021	1.0006	-0.1863	1.0894
0.0480	1.4630	1.0006	-0.1849	1.0888

+ CROSS WIRE PROBE
++ SINGLE WIRE PROBE
+++ PITOT-STATIC

TABLE 4 PROFILES AT X/L = 0.601

Y (FT.)	Y (CM.)	CP (TOATL)	CP (STATIC)	Q/UO +++	Q/UO ++	Q/UO +	U/UO +	V/UO +	URMS/UO +	VRMS/UO +	WRMS/UO +	-2UV/UO**2 +
0.0016	0.0497	0.2587	-0.1220	0.6170								
0.0018	0.0549	0.2700	-0.1220	0.6261								
0.0020	0.0610	0.2924	-0.1220	0.6437								
0.0025	0.0762	0.3405	-0.1220	0.6801								
0.0030	0.0914	0.3672	-0.1220	0.6994								
0.0035	0.1067	0.3924	-0.1220	0.7172								
0.0040	0.1219	0.4139	-0.1220	0.7321								
0.0045	0.1372	0.4320	-0.1220	0.7443								
0.0050	0.1524	0.4490	-0.1220	0.7556								
0.0052	0.1585				0.7003							
0.0060	0.1829	0.4811	-0.1220	0.7766								
0.0062	0.1890				0.7417							
0.0070	0.2134	0.5092	-0.1220	0.7945								
0.0072	0.2195				0.7724							
0.0078	0.2377										0.0630	
0.0078	0.2377					0.7811	0.7811	-0.0035	0.0726	0.0531		0.0331
0.0080	0.2438	0.5339	-0.1220	0.8099								
0.0082	0.2499				0.7846							
0.0083	0.2530					0.7902	0.7902	-0.0043	0.0710	0.0523		0.0327
0.0088	0.2682					0.8009	0.8009	-0.0047	0.0732	0.0527		0.0308
0.0090	0.2743	0.5592	-0.1220	0.8253								
0.0092	0.2804				0.7968							
0.0093	0.2835					0.8159	0.8159	-0.0044	0.0714	0.0527		0.0311
0.0098	0.2987										0.0623	
0.0098	0.2987					0.8250	0.8250	-0.0044	0.0710	0.0525		0.0307
0.0100	0.3048	0.5844	-0.1220	0.8405								
0.0108	0.3292					0.8394	0.8394	-0.0061	0.0706	0.0522		0.0304
0.0112	0.3414				0.8369							
0.0118	0.3597					0.8617	0.8617	-0.0088	0.0709	0.0523		0.0300
0.0120	0.3658	0.6326	-0.1220	0.8687								
0.0128	0.3901										0.0600	
0.0128	0.3901					0.8767	0.8766	-0.0098	0.0704	0.0525		0.0302
0.0132	0.4023				0.8664							
0.0138	0.4206					0.8897	0.8896	-0.0103	0.0703	0.0521		0.0279
0.0140	0.4267	0.6740	-0.1215	0.8919								
0.0148	0.4511										0.0591	
0.0148	0.4511					0.9078	0.9077	-0.0106	0.0691	0.0514		0.0273
0.0152	0.4633				0.8833							
0.0158	0.4816					0.9156	0.9155	-0.0123	0.0684	0.0510		0.0271
0.0160	0.4877	0.7126	-0.1206	0.9128								
0.0172	0.5243				0.9079							
0.0178	0.5425										0.0557	
0.0178	0.5425					0.9389	0.9388	-0.0108	0.0663	0.0497		0.0244
0.0180	0.5486	0.7493	-0.1197	0.9322								
0.0192	0.5852				0.9243							
0.0198	0.6035										0.0528	
0.0198	0.6035					0.9616	0.9615	-0.0117	0.0637	0.0473		0.0203
0.0200	0.6096	0.7855	-0.1187	0.9509								
0.0212	0.6462				0.9479							
0.0218	0.6645					0.9814	0.9813	-0.0116	0.0605	0.0454		0.0170

\+ CROSS WIRE PROBE
++ SINGLE WIRE PROBE
+++ PITOT-STATIC

TABLE 4 (continued)

Y (FT.)	Y (CM.)	CP (TOTAL)	CP (STATIC)	Q/UO +++	Q/UO ++	Q/UO +	U/UO +	V/UO +	URMS/UO +	VRMS/UO +	WRMS/UO +	-2UV/UO**2 +
0.0225	0.6706	0.8207	-0.1181	0.9889								
0.0228	0.6949										0.0490	
0.0232	0.7071				0.9677							
0.0238	0.7254					1.0020	1.0020	-0.0091	0.0563	0.0425		0.0140
0.0240	0.7315	0.8536	-0.1175	0.9854								
0.0248	0.7559										0.0446	
0.0252	0.7681				0.9830							
0.0258	0.7864					1.0149	1.0148	-0.0106	0.0522	0.0404		0.0114
0.0260	0.7925	0.6841	-0.1170	1.0005								
0.0272	0.8291				0.9932							
0.0278	0.8473										0.0386	
0.0278	0.8473					1.0326	1.0326	-0.0073	0.0467	0.0370		0.0084
0.0280	0.8534	0.9094	-0.1150	1.0121								
0.0292	0.8900				1.0131							
0.0298	0.9083										0.0347	
0.0298	0.9083					1.0470	1.0470	-0.0057	0.0405	0.0337		0.0049
0.0300	0.9144	0.9346	-0.1135	1.0238								
0.0312	0.9510				1.0267							
0.0318	0.9693					1.0587	1.0587	-0.0043	0.0326	0.0295		0.0035
0.0320	0.9754	0.9537	-0.1126	1.0326								
0.0328	0.9997										0.0278	
0.0332	1.0119				1.0357							
0.0338	1.0302					1.0613	1.0613	-0.0057	0.0258	0.0276		0.0022
0.0340	1.0363	0.9694	-0.1117	1.0398								
0.0348	1.0607										0.0227	
0.0352	1.0729				1.0418							
0.0358	1.0912					1.0716	1.0716	-0.0018	0.0240	0.0243		0.0012
0.0360	1.0973	0.9789	-0.1108	1.0439								
0.0372	1.1339				1.0469							
0.0378	1.1521										0.0185	
0.0378	1.1521					1.0793	1.0793	0.0022	0.0174	0.0198		0.0005
0.0380	1.1582	0.9870	-0.1100	1.0474								
0.0392	1.1948				1.0499							
0.0398	1.2131										0.0148	
0.0398	1.2131					1.0812	1.0812	0.0018	0.0143	0.0173		0.0002
0.0400	1.2192	0.9913	-0.1094	1.0491								
0.0412	1.2558				1.0520							
0.0418	1.2741										0.0121	
0.0418	1.2741					1.0841	1.0841	0.0029	0.0116	0.0139		0.0001
0.0420	1.2802	0.9951	-0.1083	1.0504								
0.0432	1.3167				1.0524							
0.0436	1.3350										0.0101	
0.0439	1.3350					1.0845	1.0845	0.0035	0.0058	0.0119		0.0001
0.0440	1.3411	0.9961	-0.1072	1.0504								
0.0452	1.3777				1.0514							
0.0458	1.3960										0.0089	
0.0458	1.3960					1.0845	1.0845	0.0038	0.0085	0.0102		0.0000
0.0460	1.4021	0.9961	-0.1061	1.0499								
0.0472	1.4387				1.0531							
0.0478	1.4569					1.0861	1.0861	0.0062	0.0071	0.0078		0.0000

\+ CROSS WIRE PROBE
\++ SINGLE WIRE PROBE
\+++ PITOT-STATIC

TABLE 4 (continued)

Y (FT.)	Y (CM.)	CP (TOATL)	CP (STATIC)	C/UO +++	Q/UO ++	Q/UO +	U/UO +	V/UO +	URMS/UO +	VRMS/UO +	WRMS/UO +	-2OUV/UO**2 +
C.C492	1.4996				1.0526							
C.C5CC	1.5240	0.9961	-0.1036	1.0487								
C.C508	1.5484										0.0076	
C.C542	1.6520				1.0513							
C.C578	1.7617					1.0846	1.0845	0.0107	0.0040	0.0054		C.0000
C.C592	1.8044				1.0505							
C.C6CO	1.8288	0.9961	-0.1004	1.0471								
C.C608	1.8532										0.0064	
0.0678	2.0665					1.0834	1.0833	0.0154	0.0028	0.0051		0.0000
C.C692	2.1092				1.0491							
C.C700	2.1336	0.9961	-0.0571	1.0456								
0.0708	2.1580										0.0054	
C.C778	2.3713					1.0821	1.0819	0.0200	0.0026	0.0046		C.0001
C.C800	2.4384	0.9961	-0.0938	1.0440								
C.C878	2.6761					1.0803	1.0800	0.0234	0.0024	0.0038		0.0001

\+ CROSS WIRE PROBE
++ SINGLE WIRE PROBE
+++ PITOT-STATIC

TABLE 5 PROFILES AT X/L = 0.651

Y (FT.)	Y (CM.)	CP (TOTAL)	CP (STATIC)	U/UO +++
0.0016	0.0497	0.2505	-0.0394	0.5384
0.0018	0.0549	0.2557	-0.0394	0.5432
0.0020	0.0610	0.2719	-0.0394	0.5579
0.0025	0.0762	0.3157	-0.0394	0.5959
0.0030	0.0914	0.3409	-0.0394	0.6167
0.0035	0.1067	0.3590	-0.0394	0.6312
0.0040	0.1219	0.3758	-0.0394	0.6444
0.0045	0.1372	0.3911	-0.0394	0.6561
0.0050	0.1524	0.4058	-0.0394	0.6672
0.0060	0.1829	0.4315	-0.0394	0.6862
0.0070	0.2134	0.4549	-0.0394	0.7031
0.0080	0.2438	0.4773	-0.0394	0.7188
0.0090	0.2743	0.4973	-0.0394	0.7326
0.0100	0.3048	0.5192	-0.0394	0.7474
0.0120	0.3658	0.5587	-0.0394	0.7734
0.0140	0.4267	0.5954	-0.0394	0.7967
0.0160	0.4877	0.6306	-0.0394	0.8185
0.0180	0.5486	0.6649	-0.0394	0.8392
0.0200	0.6096	0.6963	-0.0389	0.8574
0.0220	0.6706	0.7254	-0.0386	0.8741
0.0240	0.7315	0.7535	-0.0384	0.8899
0.0260	0.7925	0.7825	-0.0381	0.9059
0.0280	0.8534	0.8082	-0.0378	0.9198
0.0300	0.9144	0.8344	-0.0375	0.9338
0.0320	0.9754	0.8592	-0.0370	0.9467
0.0340	1.0363	0.8820	-0.0364	0.9583
0.0360	1.0973	0.9016	-0.0356	0.9681
0.0380	1.1582	0.9196	-0.0351	0.9771
0.0400	1.2192	0.9376	-0.0347	0.9861
0.0420	1.2802	0.9562	-0.0340	0.9951
0.0440	1.3411	0.9695	-0.0332	1.0013
0.0460	1.4021	0.9791	-0.0324	1.0057
0.0480	1.4630	0.9862	-0.0316	1.0089
0.0500	1.5240	0.9919	-0.0309	1.0113
0.0520	1.5850	0.9938	-0.0302	1.0119
0.0540	1.6459	0.9948	-0.0295	1.0121
0.0560	1.7069	0.9952	-0.0288	1.0119
0.0580	1.7678	0.9952	-0.0270	1.0110

\+ CROSS WIRE PROBE

\++ SINGLE WIRE PROBE

\+++ PITOT-STATIC

TABLE 6 PROFILES AT X/L = 0.701

Y (FT.)	Y (CM.)	CP (TOTAL)	CP (STATIC)	Q/UO +++
0.0016	0.0497	0.2475	0.0313	0.4650
0.0018	0.0549	0.2504	0.0313	0.4681
0.0020	0.0610	0.2637	0.0313	0.4821
0.0025	0.0762	0.2989	0.0313	0.5173
0.0030	0.0914	0.3199	0.0313	0.5372
0.0035	0.1067	0.3370	0.0313	0.5529
0.0040	0.1219	0.3498	0.0313	0.5644
0.0050	0.1524	0.3712	0.0313	0.5830
0.0060	0.1829	0.3902	0.0313	0.5991
0.0070	0.2134	0.4093	0.0313	0.6148
0.0080	0.2438	0.4279	0.0313	0.6298
0.0090	0.2743	0.4450	0.0313	0.6432
0.0100	0.3048	0.4611	0.0313	0.6556
0.0120	0.3658	0.4930	0.0313	0.6795
0.0140	0.4267	0.5234	0.0313	0.7015
0.0160	0.4877	0.5530	0.0313	0.7223
0.0180	0.5486	0.5810	0.0313	0.7714
0.0200	0.6096	0.6044	0.0313	0.7570
0.0250	0.7620	0.6709	0.0317	0.7995
0.0300	0.9144	0.7306	0.0321	0.8358
0.0350	1.0668	0.7833	0.0326	0.8664
0.0400	1.2192	0.8355	0.0331	0.8958
0.0450	1.3716	0.8829	0.0338	0.9212
0.0500	1.5240	0.9224	0.0345	0.9423
0.0550	1.6764	0.9570	0.0352	0.9601
0.0600	1.8288	0.9788	0.0359	0.9710
0.0650	1.9812	0.9902	0.0364	0.9766
0.0700	2.1336	0.9940	0.0368	0.9784
0.0750	2.2860	0.9964	0.0372	0.9794
0.0800	2.4384	0.9964	0.0373	0.9793
0.0850	2.5908	0.9964	0.0373	0.9793
0.0900	2.7432	0.9964	0.0373	0.9793
0.0950	2.8956	0.9964	0.0373	0.9793
0.1000	3.0480	0.9964	0.0373	0.9793

+ CROSS WIRE PROBE
++ SINGLE WIRE PRCEE
+++ PITOT-STATIC

TABLE 7 PROFILES AT X/L = 0.751

Y (FT.)	Y (CM.)	CP (TOTAL)	CP (STATIC)	Q/UO +++
0.0016	0.0497	0.2450	0.0920	0.3912
0.0018	0.0549	0.2480	0.0920	0.3950
0.0020	0.0610	0.2542	0.0920	0.4027
0.0025	0.0762	0.2856	0.0920	0.4400
0.0030	0.0914	0.3031	0.0920	0.4595
0.0035	0.1067	0.3183	0.0920	0.4757
0.0040	0.1219	0.3287	0.0920	0.4865
0.0050	0.1524	0.3486	0.0920	0.5066
0.0060	0.1829	0.3620	0.0920	0.5196
0.0070	0.2134	0.3752	0.0920	0.5322
0.0080	0.2438	0.3880	0.0920	0.5441
0.0090	0.2743	0.4014	0.0920	0.5562
0.0100	0.3048	0.4146	0.0920	0.5680
0.0120	0.3658	0.4422	0.0920	0.5918
0.0140	0.4267	0.4673	0.0920	0.6130
0.0160	0.4877	0.4872	0.0915	0.6290
0.0180	0.5486	0.5100	0.0915	0.6469
0.0200	0.6096	0.5338	0.0915	0.6654
0.0250	0.7620	0.5916	0.0911	0.7159
0.0300	0.9144	0.6443	0.0911	0.7438
0.0350	1.0668	0.6937	0.0911	0.7763
0.0400	1.2192	0.7373	0.0911	0.8039
0.0450	1.3716	0.7823	0.0911	0.8314
0.0500	1.5240	0.8241	0.0911	0.8562
0.0550	1.6764	0.8530	0.0911	0.8786
0.0600	1.8288	0.8958	0.0911	0.8971
0.0650	1.9812	0.9304	0.0911	0.9161
0.0700	2.1336	0.9584	0.0911	0.9316
0.0750	2.2860	0.9765	0.0906	0.9412
0.0800	2.4384	0.9874	0.0906	0.9470
0.0850	2.5908	0.9940	0.0906	0.9506
0.0900	2.7432	0.9958	0.0904	0.9517
0.0950	2.8956	0.9958	0.0901	0.9519

+ CROSS WIRE PROBE
++ SINGLE WIRE PROBE
+++ PITOT-STATIC

TABLE 8 PROFILES AT X/L = 0.801

Y (FT.)	Y (CM.)	CP (TOATL)	CP (STATIC)	Q/UO +++	Q/UO ++	Q/UO +	U/UO +	V/UO +	URMS/UO +	VRMS/UO +	WRMS/UO +	-2OUV/UC**2 +
0.0016	0.0497	0.2496	0.1303	0.3454								
0.0018	0.0549	0.2515	0.1303	0.3481								
0.0020	0.0610	0.2625	0.1303	0.3636								
0.0025	0.0762	0.2853	0.1303	0.3937								
0.0030	0.0914	0.2999	0.1303	0.4118								
0.0035	0.1067	0.3117	0.1303	0.4259								
0.0040	0.1219	0.3205	0.1303	0.4361								
0.0050	0.1524	0.3343	0.1301	0.4519								
0.0052	0.1585				0.4192							
0.0060	0.1829	0.3467	0.1301	0.4654								
0.0062	0.1890				0.4411							
0.0070	0.2134	0.3567	0.1301	0.4760								
0.0072	0.2195				0.4587							
0.0078	0.2377										0.0495	
0.0078	0.2377					0.4988	0.4988	0.0021	0.0570	0.0380		0.0172
0.0080	0.2438	0.3658	0.1301	0.4855								
0.0082	0.2499				0.4722							
0.0083	0.2530					0.5022	0.5022	0.0032	0.0565	0.0383		0.0173
0.0088	0.2682					0.5102	0.5102	0.0058	0.0563	0.0387		0.0177
0.0090	0.2743	0.3767	0.1301	0.4966								
0.0092	0.2804				0.4842							
0.0093	0.2835					0.5216	0.5216	0.0051	0.0561	0.0384		0.0177
0.0098	0.2987										0.0480	
0.0098	0.2987					0.5232	0.5232	0.0045	0.0562	0.0386		0.0175
0.0100	0.3048	0.3862	0.1301	0.5061								
0.0102	0.3109				0.4942							
0.0108	0.3292					0.5289	0.5289	0.0030	0.0559	0.0384		0.0177
0.0118	0.3597					0.5435	0.5435	0.0043	0.0559	0.0390		0.0179
0.0120	0.3658	0.4020	0.1301	0.5214								
0.0122	0.3719				0.5127							
0.0128	0.3901										0.0466	
0.0128	0.3901					0.5494	0.5494	0.0050	0.0563	0.0389		0.0182
0.0138	0.4206					0.5535	0.5535	0.0043	0.0565	0.0390		0.0179
0.0140	0.4267	0.4200	0.1301	0.5384								
0.0142	0.4328				0.5332							
0.0148	0.4511										0.0464	
0.0158	0.4816					0.5738	0.5738	0.0066	0.0565	0.0394		0.0183
0.0160	0.4877	0.4362	0.1310	0.5524								
0.0178	0.5425										0.0463	
0.0178	0.5425					0.5837	0.5837	0.0075	0.0570	0.0393		0.0184
0.0180	0.5486	0.4543	0.1310	0.5686								
0.0192	0.5852				0.5675							
0.0198	0.6035										0.0463	
0.0198	0.6035					0.5970	0.5969	0.0090	0.0584	0.0400		0.0177
0.0200	0.6096	0.4714	0.1310	0.5834								
0.0242	0.7376				0.5991							
0.0248	0.7559										0.0468	
0.0248	0.7559					0.6386	0.6385	0.0135	0.0581	0.0401		0.0175
0.0250	0.7620	0.5143	0.1310	0.6191								
0.0292	0.8900				0.6343							

\+ CROSS WIRE PROBE
\++ SINGLE WIRE PROBE
\+++ PITOT-STATIC

TABLE 8 (continued)

Y (FT.)	Y (CM.)	CP (TOTAL)	CP (STATIC)	Q/UO +++	Q/UO ++	Q/UO +	U/UO +	V/UO +	URMS/UO +	VRMS/UO +	WRMS/UO +	-2OUV/UO**2 +
0.0298	0.9083										0.0469	
0.0298	0.9083					0.6662	0.6660	0.0148	0.0584	0.0399		0.0173
0.0300	0.9144	0.5562	0.1310	0.6521								
0.0342	1.0424				0.6671							
0.0348	1.0607										0.0465	
0.0348	1.0607					0.6987	0.6984	0.0219	0.0568	0.0392		0.0173
0.0350	1.0668	0.5911	0.1307	0.6485								
0.0392	1.1948				0.6963							
0.0398	1.2131										0.0461	
0.0399	1.2131					0.7267	0.7262	0.0264	0.0562	0.0389		0.0176
0.0400	1.2192	0.6337	0.1305	0.7094								
0.0442	1.3472				0.7240							
0.0448	1.3655										0.0452	
0.0448	1.3655					0.7538	0.7532	0.0312	0.0539	0.0377		0.0164
0.0450	1.3716	0.6728	0.1295	0.7371								
0.0492	1.4996				0.7468							
0.0498	1.5179										0.0433	
0.0498	1.5179					0.7748	0.7740	0.0353	0.0527	0.0368		0.0155
0.0500	1.5240	0.7114	0.1286	0.7628								
0.0542	1.6520				0.7763							
0.0548	1.6703										0.0420	
0.0548	1.6703					0.8038	0.8027	0.0429	0.0502	0.0352		0.0141
0.0550	1.6764	0.7500	0.1280	0.7887								
0.0592	1.8044				0.7984							
0.0598	1.8227										0.0406	
0.0598	1.8227					0.8271	0.8258	0.0466	0.0481	0.0335		0.0128
0.0600	1.8288	0.7863	0.1277	0.8115								
0.0642	1.9568				0.8219							
0.0648	1.9751										0.0387	
0.0648	1.9751					0.8505	0.8489	0.0521	0.0450	0.0312		0.0090
0.0650	1.9812	0.8168	0.1263	0.8310								
0.0692	2.1092				0.8418							
0.0698	2.1275										0.0365	
0.0698	2.1275					0.8664	0.8644	0.0595	0.0429	0.0296		0.0079
0.0700	2.1336	0.8463	0.1249	0.8494								
0.0742	2.2616				0.8578							
0.0748	2.2799										0.0331	
0.0748	2.2799					0.8851	0.8828	0.0641	0.0357	0.0273		0.0059
0.0750	2.2860	0.8763	0.1244	0.8671								
0.0792	2.4140				0.8771							
0.0798	2.4323										0.0303	
0.0798	2.4323					0.9021	0.8995	0.0688	0.0365	0.0249		0.0043
0.0800	2.4384	0.9102	0.1239	0.8867								
0.0842	2.5664				0.8948							
0.0848	2.5847										0.0264	
0.0848	2.5847					0.9200	0.9170	0.0746	0.0318	0.0221		0.0030
0.0850	2.5908	0.9345	0.1239	0.9003								
0.0892	2.7188				0.9102							
0.0898	2.7371										0.0227	
0.0898	2.7371					0.9342	0.9308	0.0791	0.0266	0.0192		0.0019

\+ CROSS WIRE PROBE
\++ SINGLE WIRE PROBE
\+++ PITOT-STATIC

TABLE 8 (continued)

Y (FT.)	Y (CM.)	CP (TOATL)	CP (STATIC)	Q/UO +++	Q/UO ++	Q/UO +	U/UO +	V/UO +	URMS/UO +	VRMS/UO +	WRMS/UO +	-2OUV/UO**2 +
0.0900	2.7432	0.9535	0.1239	0.9108								
0.0942	2.8712				0.9250							
0.0948	2.8895										0.0177	
0.0948	2.8895					0.9421	0.9385	0.0825	0.0204	0.0164		0.0011
0.0950	2.8956	0.9698	0.1230	0.9202								
0.0992	3.0236				0.9322							
0.0998	3.0419										0.0139	
0.0998	3.0419					0.9508	0.9466	0.0888	0.0147	0.0132		0.0006
0.1000	3.0480	0.9812	0.1221	0.9269								
0.1042	3.1760				0.9350							
0.1048	3.1943										0.0103	
0.1048	3.1943					0.9550	0.9505	0.0927	0.0092	0.0096		0.0003
0.1050	3.2004	0.9903	0.1199	0.9330								
0.1092	3.3284				0.9399							
0.1098	3.3467										0.0080	
0.1098	3.3467					0.9575	0.9528	0.0946	0.0072	0.0083		0.0002
0.1100	3.3528	0.9931	0.1183	0.9353								
0.1142	3.4808				0.9415							
0.1148	3.4991					0.9587	0.9537	0.0982	0.0052	0.0064		0.0001
0.1150	3.5052	0.9945	0.1167	0.9369								
0.1192	3.6332				0.9443							
0.1198	3.6515										0.0055	
0.1198	3.6515					0.9586	0.9533	0.1003	0.0043	0.0050		0.0001
0.1200	3.6576	0.9945	0.1150	0.9442								
0.1292	3.9380				0.9463							
0.1298	3.9563										0.0051	
0.1298	3.9563					0.9579	0.9522	0.1041	0.0030	0.0049		0.0001
0.1300	3.9624	0.9945	0.1117	0.9396								
0.1392	4.2428				0.9445							
0.1398	4.2611					0.9606	0.9548	0.1057	0.0029	0.0043		0.0001
0.1400	4.2672	0.9945	0.1098	0.9406								
0.1498	4.5659										0.0051	
0.1592	4.8524				0.9498							
0.1598	4.8707					0.9592	0.9531	0.1081	0.0024	0.0042		0.0000
0.1600	4.8768	0.9945	0.1032	0.9441								
0.1792	5.4620				0.9508							
0.1798	5.4803					0.9614	0.9551	0.1099	0.0019	0.0037		0.0000
0.1800	5.4864	0.9945	0.0985	0.9466								
0.1992	6.0716				0.9597							
0.1998	6.0899					0.9620	0.9552	0.1145	0.0023	0.0039		0.0000
0.2000	6.0960	0.9945	0.0933	0.9493								
0.2192	6.6812				0.9598							
0.2198	6.6995					0.9636	0.9566	0.1161	0.0016	0.0036		0.0001
0.2200	6.7056	0.9945	0.0891	0.9515								

\+ CROSS WIRE PROBE
\++ SINGLE WIRE PROBE
\+++ PITOT-STATIC

TABLE 9 PROFILES AT X/L = 0.840

Y (FT.)	Y (CM.)	CP (TOTAL)	CP (STATIC)	Q/UO +++
0.0021	0.0640	0.2703	0.1493	0.3479
0.0025	0.0762	0.2845	0.1493	0.3678
0.0030	0.0914	0.2916	0.1493	0.3772
0.0040	0.1219	0.3073	0.1498	0.3975
0.0060	0.1829	0.3273	0.1502	0.4208
0.0080	0.2438	0.3430	0.1502	0.4391
0.0100	0.3048	0.3586	0.1502	0.4565
0.0150	0.4572	0.3900	0.1502	0.4897
0.0200	0.6096	0.4228	0.1498	0.5225
0.0250	0.7620	0.4570	0.1495	0.5545
0.0300	0.9144	0.4926	0.1493	0.5859
0.0400	1.2192	0.5553	0.1488	0.6376
0.0500	1.5240	0.6195	0.1479	0.6867
0.0600	1.8288	0.6836	0.1465	0.7329
0.0700	2.1336	0.7421	0.1451	0.7727
0.0800	2.4384	0.7991	0.1437	0.8096
0.0900	2.7432	0.8518	0.1423	0.8423
0.1000	3.0480	0.9031	0.1400	0.8736
0.1100	3.3528	0.9445	0.1376	0.8983
0.1200	3.6576	0.9773	0.1353	0.9176
0.1300	3.9624	0.9915	0.1330	0.9266
0.1400	4.2672	0.9958	0.1302	0.9304
0.1500	4.5720	0.9972	0.1269	0.9329
0.1600	4.8768	0.9972	0.1246	0.9341
0.1800	5.4864	0.9972	0.1194	0.9369

+ CROSS WIRE PROBE
++ SINGLE WIRE PROBE
+++ PITOT-STATIC

TABLE 10 PROFILES AT X/L = 0.880

Y (FT.)	Y (CM.)	CP (TOATL)	CP (STATIC)	Q/UO +++	Q/UO ++	Q/UO +	U/UO +	V/UO +	URMS/UO +	VRMS/UO +	WRMS/UO +	-2UV/UO**2 +
0.0021	0.0640	0.2731	0.1598	0.3366								
0.0025	0.0762	0.2803	0.1598	0.3471								
0.0030	0.0914	0.2888	0.1598	0.3592								
0.0040	0.1219	0.2988	0.1598	0.3728								
0.0052	0.1585				0.3587							
0.0060	0.1829	0.3159	0.1598	0.3951								
0.0062	0.1890				0.3875							
0.0072	0.2195				0.4068							
0.0078	0.2377										0.0428	
0.0078	0.2377					0.4352	0.4352	-0.0061	0.0488	0.0330		0.0133
0.0080	0.2438	0.3316	0.1598	0.4145								
0.0082	0.2499				0.4167							
0.0098	0.2987										0.0424	
0.0098	0.2987					0.4560	0.4560	-0.0066	0.0476	0.0334		0.0136
0.0100	0.3048	0.3416	0.1598	0.4264								
0.0102	0.3109				0.4323							
0.0128	0.3901										0.0416	
0.0148	0.4511										0.0411	
0.0148	0.4511					0.4864	0.4864	-0.0043	0.0476	0.0336		0.0139
0.0150	0.4572	0.3701	0.1608	0.4575								
0.0152	0.4633				0.4695							
0.0178	0.5425										0.0409	
0.0198	0.6035										0.0413	
0.0198	0.6035					0.5097	0.5097	-0.0031	0.0498	0.0350		0.0150
0.0200	0.6096	0.3957	0.1608	0.4847								
0.0202	0.6157				0.4974							
0.0248	0.7559										0.0407	
0.0248	0.7559					0.5355	0.5355	0.0004	0.0504	0.0357		0.0152
0.0250	0.7620	0.4200	0.1608	0.5091								
0.0252	0.7681				0.5237							
0.0298	0.9083										0.0418	
0.0298	0.9083					0.5631	0.5631	0.0040	0.0521	0.0361		0.0155
0.0300	0.9144	0.4456	0.1608	0.5337								
0.0302	0.9205				0.5449							
0.0348	1.0607										0.0430	
0.0398	1.2131										0.0429	
0.0398	1.2131					0.6072	0.6071	0.0119	0.0519	0.0362		0.0161
0.0400	1.2192	0.4955	0.1590	0.5801								
0.0402	1.2253				0.5900							
0.0448	1.3655										0.0434	
0.0498	1.5179										0.0434	
0.0498	1.5179					0.6476	0.6473	0.0210	0.0517	0.0357		0.0146
0.0500	1.5240	0.5497	0.1585	0.6255								
0.0502	1.5301				0.6331							
0.0548	1.6703										0.0436	
0.0598	1.8227										0.0431	
0.0598	1.8227					0.6881	0.6875	0.0291	0.0505	0.0347		0.0136
0.0600	1.8288	0.6024	0.1565	0.6678								
0.0602	1.8349				0.6734							
0.0648	1.9751										0.0428	

\+ CROSS WIRE PROBE
\++ SINGLE WIRE PROBE
\+++ PITOT-STATIC

TABLE 10 (continued)

Y (FT.)	Y (CM.)	CP (TOTAL)	CP (STATIC)	Q/UO +++	Q/UO ++	Q/UO +	U/UO +	V/UO +	URMS/UO +	VRMS/UO +	WRMS/UO +	-2OUV/UO**2 +
0.0698	2.1275										0.0424	
0.0698	2.1275					0.7290	0.7279	0.0400	0.0491	0.0337		0.0122
0.0700	2.1336	0.6552	0.1540	0.7080								
0.0702	2.1397				0.7126							
0.0748	2.2799										0.0415	
0.0798	2.4323										0.0408	
0.0798	2.4323					0.7612	0.7596	0.0495	0.0475	0.0327		0.0120
0.0800	2.4384	0.7079	0.1505	0.7466								
0.0802	2.4445				0.7495							
0.0848	2.5847										0.0402	
0.0898	2.7371										0.0391	
0.0898	2.7371					0.7974	0.7951	0.0599	0.0446	0.0308		0.0102
0.0900	2.7432	0.7621	0.1475	0.7840								
0.0902	2.7493				0.7834							
0.0948	2.8895										0.0381	
0.0998	3.0419										0.0365	
0.0998	3.0419					0.8225	0.8199	0.0657	0.0417	0.0286		0.0090
0.1000	3.0480	0.8105	0.1450	0.8158								
0.1002	3.0541				0.8155							
0.1048	3.1943										0.0343	
0.1098	3.3467										0.0324	
0.1098	3.3467					0.8548	0.8515	0.0749	0.0376	0.0257		0.0069
0.1100	3.3528	0.8561	0.1427	0.8446								
0.1102	3.3589				0.8452							
0.1198	3.6515										0.0276	
0.1198	3.6515					0.8815	0.8776	0.0826	0.0324	0.0219		0.0044
0.1200	3.6576	0.8989	0.1405	0.8709								
0.1202	3.6637				0.8747							
0.1298	3.9563										0.0211	
0.1298	3.9563					0.9053	0.9007	0.0915	0.0256	0.0175		0.0022
0.1300	3.9624	0.9360	0.1380	0.8933								
0.1302	3.9685				0.8974							
0.1398	4.2611										0.0155	
0.1398	4.2611					0.9212	0.9159	0.0983	0.0163	0.0127		0.0010
0.1400	4.2672	0.9702	0.1357	0.9135								
0.1402	4.2733				0.9182							
0.1498	4.5659										0.0098	
0.1498	4.5659					0.9314	0.9256	0.1042	0.0087	0.0086		0.0004
0.1500	4.5720	0.9991	0.1335	0.9255								
0.1502	4.5781				0.9297							
0.1598	4.8707										0.0072	
0.1598	4.8707					0.9327	0.9264	0.1084	0.0046	0.0057		0.0001
0.1600	4.8768	0.9944	0.1308	0.9293								
0.1602	4.8829				0.9356							
0.1698	5.1755					0.9368	0.9300	0.1127	0.0035	0.0046		0.0001
0.1700	5.1816	0.9973	0.1285	0.9321								
0.1702	5.1877				0.9379							
0.1798	5.4803										0.0062	
0.1798	5.4803					0.9374	0.9302	0.1158	0.0024	0.0041		0.0000
0.1800	5.4864	0.9973	0.1260	0.9334								

+ CROSS WIRE PROBE
++ SINGLE WIRE PROBE
+++ PITOT-STATIC

TABLE 10 (continued)

Y (FT.)	Y (CM.)	CP (TOTAL)	CP (STATIC)	Q/UO +++	Q/UO ++	Q/UO +	U/UO +	V/UO +	URMS/UO +	VRMS/UO +	WRMS/UO +	-2OUV/UO**2 +
0.1802	5.4925				0.9402							
0.1898	5.7851					0.9403	0.9328	0.1182	0.0020	0.0040		0.0001
0.1900	5.7912	0.9973	0.1235	0.9348								
0.1998	6.0899										0.0053	
0.2002	6.1021				0.9447							
0.2202	6.7117				0.9486							
0.2402	7.3213				0.9488							
0.2602	7.9309				0.9497							

\+ CROSS WIRE PROBE
\++ SINGLE WIRE PROBE
\+++ PITOT-STATIC

TABLE 11 PROFILES AT X/L = 0.920

Y (FT.)	Y (CM.)	CP (TOATL)	CP (STATIC)	Q/UO +++	C/UO ++	Q/UC +	U/UO +	V/UO +	URMS/UO +	VRMS/UC +	WRMS/UC +	-2CUV/UC**2 +
0.0021	0.0640	0.2550	0.1556	0.3153								
0.0025	0.0762	0.2635	0.1556	0.3285								
0.0030	0.0914	0.2763	0.1556	0.3474								
0.0040	0.1219	0.2905	0.1556	0.3673								
0.0052	0.1585				0.2835							
0.0060	0.1829	0.3047	0.1556	0.3861								
0.0062	0.1890				0.3587							
0.0078	0.2377										0.0374	
0.0078	0.2377					0.4248	0.4248	-0.0029	0.0462	0.0312		0.0114
0.0080	0.2438	0.3189	0.1556	0.4041								
0.0082	0.2499				0.4108							
0.0098	0.2987										0.0385	
0.0098	0.2987					0.4381	0.4381	-0.0040	0.0446	0.0311		0.0115
0.0100	0.3048	0.3303	0.1556	0.4180								
0.0102	0.3109				0.4219							
0.0148	0.4511										0.0363	
0.0148	0.4511					0.4679	0.4679	-0.0017	0.0441	0.0316		0.0121
0.0150	0.4572	0.3516	0.1556	0.4427								
0.0152	0.4633				0.4535							
0.0198	0.6035										0.0370	
0.0198	0.6035					0.4923	0.4923	-0.0003	0.0445	0.0322		0.0123
0.0200	0.6096	0.3744	0.1556	0.4678								
0.0202	0.6157				0.4788							
0.0248	0.7559										0.0371	
0.0248	0.7559					0.5150	0.5150	0.0030	0.0454	0.0332		0.0129
0.0252	0.7681				0.4997							
0.0298	0.9083										0.0378	
0.0298	0.9083					0.5366	0.5366	0.0057	0.0460	0.0336		0.0129
0.0300	0.9144	0.4156	0.1538	0.5117								
0.0302	0.9205				0.5193							
0.0398	1.2131										0.0388	
0.0398	1.2131					0.5782	0.5781	0.0129	0.0472	0.0339		0.0133
0.0400	1.2192	0.4554	0.1518	0.5510								
0.0402	1.2253				0.5544							
0.0498	1.5179										0.0398	
0.0498	1.5179					0.6128	0.6125	0.0188	0.0472	0.0341		0.0137
0.0500	1.5240	0.4980	0.1492	0.5906								
0.0502	1.5301				0.5892							
0.0598	1.8227										0.0405	
0.0598	1.8227					0.6517	0.6512	0.0259	0.0477	0.0340		0.0128
0.0600	1.8288	0.5393	0.1470	0.6263								
0.0602	1.8349				0.6339							
0.0698	2.1275										0.0407	
0.0698	2.1275					0.6894	0.6886	0.0325	0.0473	0.0330		0.0125
0.0700	2.1336	0.5848	0.1445	0.6636								
0.0702	2.1397				0.6676							
0.0798	2.4323										0.0403	
0.0798	2.4323					0.7210	0.7199	0.0394	0.0466	0.0325		0.0120
0.0800	2.4384	0.6317	0.1423	0.6996								
0.0802	2.4445				0.7015							

+ CROSS WIRE PROBE
++ SINGLE WIRE PROBE
+++ PITOT-STATIC

TABLE 11 (continued)

Y (FT.)	Y (CM.)	CP (TOATL)	CP (STATIC)	Q/UO +++	Q/UO ++	Q/UO +	U/UO +	V/UO +	URMS/UO +	VRMS/UO +	WRMS/UO +	-2OUV/UO**2 +
0.0898	2.7371										0.0401	
0.0898	2.7371					0.7530	0.7514	0.0487	0.0461	0.0320		0.0104
0.0900	2.7432	0.6786	0.1400	0.7323								
0.0902	2.7493				0.7369							
0.0998	3.0419										0.0388	
0.0998	3.0419					0.7807	0.7787	0.0560	0.0443	0.0310		0.0100
0.1000	3.0480	0.7227	0.1379	0.7647								
0.1002	3.0541				0.7703							
0.1098	3.3467										0.0374	
0.1098	3.3467					0.8163	0.8137	0.0650	0.0417	0.0294		0.0092
0.1100	3.3528	0.7653	0.1350	0.7939								
0.1102	3.3589				0.8008							
0.1198	3.6515										0.0354	
0.1198	3.6515					0.8436	0.8406	0.0707	0.0380	0.0275		0.0085
0.1200	3.6576	0.8108	0.1328	0.8234								
0.1202	3.6637				0.8324							
0.1298	3.9563										0.0325	
0.1298	3.9563					0.8694	0.8659	0.0783	0.0351	0.0250		0.0073
0.1300	3.9624	0.8520	0.1295	0.8500								
0.1302	3.9685				0.8574							
0.1398	4.2611										0.0287	
0.1398	4.2611					0.8945	0.8903	0.0861	0.0317	0.0226		0.0064
0.1400	4.2672	0.8947	0.1272	0.8761								
0.1402	4.2733				0.8847							
0.1498	4.5659										0.0233	
0.1498	4.5659					0.9135	0.9091	0.0899	0.0265	0.0187		0.0040
0.1500	4.5720	0.9302	0.1248	0.8974								
0.1502	4.5781				0.9059							
0.1598	4.8707										0.0176	
0.1598	4.8707					0.9294	0.9247	0.0933	0.0195	0.0146		0.0019
0.1600	4.8768	0.9586	0.1225	0.9144								
0.1602	4.8829				0.9267							
0.1698	5.1755										0.0123	
0.1698	5.1755					0.9406	0.9354	0.0989	0.0125	0.0104		0.0008
0.1700	5.1816	0.9828	0.1206	0.9285								
0.1702	5.1877				0.9413							
0.1798	5.4803										0.0081	
0.1798	5.4803					0.9462	0.9407	0.1017	0.0056	0.0069		0.0002
0.1800	5.4864	0.9956	0.1178	0.9369								
0.1802	5.4925				0.9503							
0.1898	5.7851										0.0056	
0.1898	5.7851					0.9498	0.9440	0.1045	0.0032	0.0054		0.0001
0.1900	5.7912	0.9970	0.1250	0.9338								
0.1902	5.7973				0.9537							
0.1998	6.0899										0.0049	
0.1998	6.0899					0.9509	0.9448	0.1078	0.0027	0.0046		0.0001
0.2000	6.0960	0.9970	0.1222	0.9353								
0.2002	6.1021				0.9579							
0.2098	6.3947										0.0043	
0.2098	6.3947					0.9532	0.9469	0.1091	0.0025	0.0038		0.0000

\+ CROSS WIRE PROBE
++ SINGLE WIRE PROBE
+++ PITOT-STATIC

TABLE 11 (continued)

Y (FT.)	Y (CM.)	CP (TOATL)	CP (STATIC)	Q/UO +++	Q/UO ++	Q/UC +	U/UO +	V/UO +	URMS/UC +	VRMS/UC +	WRMS/UC +	-2OLV/UC**2 +
0.2102	6.4069				0.9576							
0.2198	6.6995					0.9554	0.9491	0.1099	0.0018	C.C038		C.CC01
0.2200	6.7056	0.9970	0.1170	0.9381								
0.2202	6.7117				0.9601							
0.2298	7.0043										0.C045	
0.2398	7.3091					0.9583	0.9515	0.1139	0.0012	C.CC39		0.C001
0.2400	7.3152	0.9970	0.1123	0.9406								
0.2402	7.3213				0.9629							
0.2498	7.6139										C.C052	
0.2598	7.9187					0.9608	0.9536	0.1170	0.0014	C.C042		C.CC01
0.2600	7.9248	0.9970	0.1068	0.9435								
0.2602	7.9309				0.9640							
0.2800	8.5344	0.9970	0.1025	0.9458								

+ CROSS WIRE PRCBE
++ SINGLE WIRE PRCBE
+++ PITOT-STATIC

TABLE 12 PROFILES AT X/L = 0.940

Y (FT.)	Y (CM.)	CP (TOTAL)	CP (STATIC)	Q/UO +++
0.0021	0.0640	0.2507	0.1511	0.3156
0.0025	0.0762	0.2606	0.1511	0.3309
0.0030	0.0914	0.2706	0.1511	0.3457
0.0040	0.1219	0.2848	0.1511	0.3657
0.0060	0.1829	0.2990	0.1511	0.3846
0.0080	0.2438	0.3104	0.1511	0.3991
0.0100	0.3048	0.3232	0.1511	0.4148
0.0150	0.4572	0.3431	0.1506	0.4387
0.0200	0.6096	0.3630	0.1500	0.4615
0.0300	0.9144	0.4000	0.1477	0.5023
0.0400	1.2192	0.4369	0.1459	0.5394
0.0500	1.5240	0.4753	0.1426	0.5768
0.0600	1.8288	0.5137	0.1393	0.6119
0.0700	2.1336	0.5549	0.1360	0.6472
0.0800	2.4384	0.5976	0.1332	0.6815
0.0900	2.7432	0.6416	0.1308	0.7147
0.1000	3.0480	0.6829	0.1290	0.7442
0.1100	3.3528	0.7298	0.1266	0.7767
0.1200	3.6576	0.7710	0.1247	0.8039
0.1300	3.9624	0.8136	0.1224	0.8314
0.1400	4.2672	0.8556	0.1204	0.8574
0.1500	4.5720	0.8918	0.1181	0.8796
0.1600	4.8768	0.9274	0.1162	0.9007
0.1700	5.1816	0.9558	0.1139	0.9176
0.1800	5.4864	0.9771	0.1110	0.9306
0.1900	5.7912	0.9942	0.1092	0.9407
0.2000	6.0960	0.9956	0.1062	0.9431
0.2100	6.4008	0.9956	0.1045	0.9440
0.2200	6.7056	0.9956	0.1021	0.9453
0.2300	7.0104	0.9956	0.0997	0.9465
0.2400	7.3152	0.9956	0.0979	0.9475
0.2500	7.6200	0.9956	0.0955	0.9487

\+ CROSS WIRE PROBE
++ SINGLE WIRE PROBE
+++ PITOT-STATIC

TABLE 13 PROFILES AT X/L = 0.960

Y (FT.)	Y (CM.)	CP (TOATL)	CP (STATIC)	Q/UO +++	Q/UO ++	Q/UO +	U/UO +	V/UO +	URMS/UO +	VRMS/UO +	WRMS/UO +	-2OUV/UO**2 +
0.0021	0.0640	0.2465	0.1345	0.3347								
0.0025	0.0762	0.2579	0.1345	0.3513								
0.0030	0.0914	0.2679	0.1345	0.3652								
0.0040	0.1219	0.2806	0.1345	0.3822								
0.0052	0.1585				0.3397							
0.0060	0.1829	0.2963	0.1345	0.4022								
0.0062	0.1890				0.3719							
0.0078	0.2377										0.0355	
0.0078	0.2377					0.4404	0.4404	-0.0015	0.0425	0.0294		0.0098
0.0080	0.2438	0.3077	0.1345	0.4162								
0.0082	0.2499				0.4190							
0.0098	0.2987										0.0368	
0.0100	0.3048	0.3176	0.1345	0.4279								
0.0102	0.3109				0.4362							
0.0118	0.3597					0.4653	0.4653	0.0003	0.0400	0.0294		0.0102
0.0148	0.4511										0.0351	
0.0150	0.4572	0.3389	0.1340	0.4527								
0.0152	0.4633				0.4594							
0.0158	0.4816					0.4824	0.4824	0.0022	0.0393	0.0294		0.0101
0.0198	0.6035										0.0351	
0.0200	0.6096	0.3574	0.1336	0.4731								
0.0202	0.6157				0.4807							
0.0208	0.6340					0.5035	0.5035	0.0045	0.0399	0.0303		0.0110
0.0252	0.7681				0.4986							
0.0258	0.7864					0.5194	0.5193	0.0074	0.0405	0.0305		0.0110
0.0298	0.9083										0.0357	
0.0300	0.9144	0.3887	0.1327	0.5060								
0.0302	0.9205				0.5157							
0.0308	0.9388					0.5382	0.5381	0.0087	0.0411	0.0311		0.0111
0.0398	1.2131										0.0370	
0.0400	1.2192	0.4256	0.1303	0.5434								
0.0402	1.2253				0.5478							
0.0408	1.2436					0.5689	0.5687	0.0137	0.0428	0.0319		0.0121
0.0498	1.5179										0.0375	
0.0500	1.5240	0.4598	0.1275	0.5765								
0.0502	1.5301				0.5777							
0.0508	1.5484					0.6046	0.6043	0.0185	0.0436	0.0324		0.0118
0.0598	1.8227										0.0379	
0.0600	1.8288	0.4981	0.1251	0.6107								
0.0602	1.8349				0.6058							
0.0608	1.8532					0.6358	0.6354	0.0219	0.0449	0.0328		0.0118
0.0698	2.1275										0.0388	
0.0700	2.1336	0.5337	0.1232	0.6407								
0.0702	2.1397				0.6388							
0.0708	2.1580					0.6666	0.6661	0.0270	0.0458	0.0332		0.0120
0.0798	2.4323										0.0392	
0.0800	2.4384	0.5721	0.1223	0.6707								
0.0802	2.4445				0.6659							
0.0808	2.4628					0.6989	0.6982	0.0314	0.0465	0.0333		0.0120
0.0898	2.7371										0.0400	

+ CROSS WIRE PROBE
++ SINGLE WIRE PROBE
+++ PITOT-STATIC

TABLE 13 (continued)

Y (FT.)	Y (CM.)	CP (TOATL)	CP (STATIC)	Q/UO +++	Q/UO ++	Q/UO +	U/UO +	V/UO +	URMS/UO +	VRMS/UO +	WRMS/UO +	-2UV/UO**2 +
0.0900	2.7432	0.6133	0.1204	0.7021								
0.0902	2.7493				0.7024							
0.0908	2.7676					0.7253	0.7243	0.0376	0.0462	0.0332		0.0127
0.0998	3.0419										0.0400	
0.1000	3.0480	0.6545	0.1185	0.7321								
0.1002	3.0541				0.7298							
0.1008	3.0724					0.7578	0.7568	0.0395	0.0458	0.0328		0.0128
0.1098	3.3467										0.0396	
0.1100	3.3528	0.6972	0.1162	0.7622								
0.1102	3.3589				0.7627							
0.1108	3.3772					0.7834	0.7822	0.0432	0.0451	0.0321		0.0125
0.1198	3.6515										0.0386	
0.1200	3.6576	0.7384	0.1143	0.7900								
0.1202	3.6637				0.7938							
0.1208	3.6820					0.8132	0.8117	0.0493	0.0429	0.0314		0.0121
0.1298	3.9563										0.0369	
0.1300	3.9624	0.7810	0.1129	0.8174								
0.1302	3.9685				0.8236							
0.1308	3.9868					0.8395	0.8378	0.0535	0.0409	0.0297		0.0107
0.1398	4.2611										0.0347	
0.1400	4.2672	0.8223	0.1110	0.8434								
0.1402	4.2733				0.8502							
0.1408	4.2916					0.8641	0.8622	0.0566	0.0376	0.0277		0.0088
0.1498	4.5659										0.0314	
0.1500	4.5720	0.8621	0.1091	0.8678								
0.1502	4.5781				0.8758							
0.1508	4.5964					0.8896	0.8875	0.0617	0.0354	0.0254		0.0072
0.1598	4.8707										0.0279	
0.1600	4.8768	0.8962	0.1072	0.8883								
0.1602	4.8829				0.8983							
0.1608	4.9012					0.9082	0.9059	0.0651	0.0315	0.0222		0.0056
0.1698	5.1755										0.0233	
0.1700	5.1816	0.9303	0.1058	0.9080								
0.1702	5.1877				0.9166							
0.1708	5.2060					0.9300	0.9275	0.0681	0.0264	0.0183		0.0038
0.1798	5.4803										0.0182	
0.1800	5.4864	0.9616	0.1035	0.9263								
0.1802	5.4925				0.9377							
0.1808	5.5108					0.9457	0.9431	0.0699	0.0197	0.0145		0.0021
0.1898	5.7851										0.0132	
0.1900	5.7912	0.9843	0.1016	0.9395								
0.1902	5.7973				0.9506							
0.1908	5.8156					0.9566	0.9537	0.0739	0.0129	0.0113		0.0009
0.1998	6.0899										0.0085	
0.2000	6.0960	0.9929	0.0997	0.9451								
0.2002	6.1021				0.9567							
0.2008	6.1204					0.9618	0.9589	0.0746	0.0065	0.0075		0.0003
0.2098	6.3947										0.0061	
0.2100	6.4008	0.9957	0.0978	0.9476								
0.2102	6.4069				0.9648							

\+ CROSS WIRE PROBE
\++ SINGLE WIRE PROBE
\+++ PITOT-STATIC

TABLE 13 (continued)

Y (FT.)	Y (CM.)	CP (TOATL)	CP (STATIC)	Q/UO +++	Q/UO ++	Q/UO +	U/UO +	V/UO +	URMS/UO +	VRMS/UO +	WRMS/UO +	-2OUV/UO**2 +
0.2108	6.4252					0.9654	0.9625	0.0754	0.0040	0.0057		0.0001
0.2198	6.6395										0.0050	
0.2200	6.7056	0.9957	0.0959	0.9486								
0.2202	6.7117				0.9640							
0.2208	6.7300					0.9657	0.9626	0.0772	0.0031	0.0045		0.0001
0.2298	7.0043										0.0046	
0.2300	7.0104	0.9957	0.0936	0.9498								
0.2400	7.3152	0.9957	0.0917	0.9508								
0.2402	7.3213				0.9670							
0.2406	7.3396					0.9682	0.9650	0.0784	0.0019	0.0041		0.0001
0.2498	7.6139										0.0047	
0.2500	7.6200	0.9957	0.0893	0.9521								
0.2602	7.9309				0.9702							
0.2608	7.9492					0.9697	0.9664	0.0803	0.0015	0.0041		0.0001
0.2802	8.5405				0.9697							

\+ CROSS WIRE PROBE
++ SINGLE WIRE PROBE
+++ PITOT-STATIC

TABLE 14 PROFILES AT X/L = 0.980

Y (FT.)	Y (CM.)	CP (TOTAL)	CP (STATIC)	Q/UO +++
0.0016	0.0488	0.2094	0.1223	0.2951
0.0020	0.0610	0.2250	0.1223	0.3205
0.0025	0.0762	0.2392	0.1223	0.3419
0.0030	0.0914	0.2506	0.1223	0.3582
0.0040	0.1219	0.2619	0.1223	0.3736
0.0060	0.1829	0.2804	0.1223	0.3976
0.0080	0.2438	0.2932	0.1223	0.4134
0.0100	0.3048	0.3031	0.1223	0.4252
0.0150	0.4572	0.3216	0.1214	0.4474
0.0200	0.6096	0.3414	0.1205	0.4700
0.0300	0.9144	0.3755	0.1181	0.5073
0.0400	1.2192	0.4039	0.1162	0.5364
0.0500	1.5240	0.4365	0.1143	0.5676
0.0600	1.8288	0.4692	0.1124	0.5973
0.0700	2.1336	0.5061	0.1104	0.6290
0.0800	2.4384	0.5430	0.1086	0.6591
0.0900	2.7432	0.5785	0.1068	0.6868
0.1000	3.0480	0.6211	0.1049	0.7185
0.1100	3.3528	0.6609	0.1035	0.7466
0.1200	3.6576	0.7063	0.1020	0.7774
0.1300	3.9624	0.7475	0.1002	0.8045
0.1400	4.2672	0.7886	0.0988	0.8305
0.1500	4.5720	0.8255	0.0979	0.8600
0.1600	4.8768	0.8625	0.0964	0.8753
0.1700	5.1816	0.8979	0.0950	0.8960
0.1800	5.4864	0.9278	0.0940	0.9126
0.1900	5.7912	0.9604	0.0927	0.9315
0.2000	6.0960	0.9789	0.0908	0.9424
0.2100	6.4008	0.9916	0.0893	0.9499
0.2200	6.7056	0.9945	0.0880	0.9521
0.2300	7.0104	0.9959	0.0865	0.9536
0.2400	7.3152	0.9959	0.0852	0.9543
0.2500	7.6200	0.9959	0.0832	0.9554

\+ CROSS WIRE PROBE
++ SINGLE WIRE PROBE
+++ PITOT-STATIC

TABLE 15 PROFILES AT X/L = 0.990

Y (FT.)	Y (CM.)	CP (TOTAL)	CP (STATIC)	Q/UO +++
0.0012	0.0357	0.1755	0.1163	0.2650
0.0016	0.0488	0.1996	0.1163	0.2886
0.0020	0.0610	0.2138	0.1163	0.3124
0.0025	0.0762	0.2251	0.1163	0.3298
0.0030	0.0914	0.2322	0.1163	0.3404
0.0040	0.1219	0.2478	0.1163	0.3626
0.0060	0.1829	0.2677	0.1158	0.3897
0.0080	0.2438	0.2805	0.1158	0.4058
0.0100	0.3048	0.2904	0.1154	0.4183
0.0150	0.4572	0.3131	0.1140	0.4462
0.0200	0.6096	0.3288	0.1130	0.4645
0.0300	0.9144	0.3628	0.1107	0.5021
0.0400	1.2192	0.3926	0.1084	0.5331
0.0500	1.5240	0.4239	0.1050	0.5647
0.0600	1.8288	0.4579	0.1037	0.5951
0.0700	2.1336	0.4920	0.1018	0.6247
0.0800	2.4384	0.5261	0.0999	0.6528
0.0900	2.7432	0.5630	0.0986	0.6815
0.1000	3.0480	0.6042	0.0976	0.7118
0.1100	3.3528	0.6439	0.0962	0.7401
0.1200	3.6576	0.6823	0.0948	0.7665
0.1300	3.9624	0.7277	0.0939	0.7961
0.1400	4.2672	0.7660	0.0925	0.8207
0.1500	4.5720	0.8029	0.0912	0.8436
0.1600	4.8768	0.8441	0.0901	0.8683
0.1700	5.1816	0.8796	0.0893	0.8890
0.1800	5.4864	0.9137	0.0883	0.9085
0.1900	5.7912	0.9435	0.0874	0.9253
0.2000	6.0960	0.9676	0.0860	0.9389
0.2100	6.4008	0.9832	0.0846	0.9479
0.2200	6.7056	0.9932	0.0832	0.9540
0.2300	7.0104	0.9946	0.0818	0.9554
0.2400	7.3152	0.9946	0.0804	0.9561
0.2600	7.9248	0.9946	0.0778	0.9575
0.2800	8.5344	0.9946	0.0752	0.9589

+ CROSS WIRE PROBE
++ SINGLE WIRE PROBE
+++ PITOT-STATIC

TABLE 16 PROFILES AT X/L = 0.995

Y (FT.)	Y (CM.)	CP (TOTAL)	CP (STATIC)	Q/UO +++
0.0016	0.0497	0.1796	0.1129	0.2583
0.0020	0.0610	0.1966	0.1129	0.2893
0.0025	0.0762	0.2080	0.1129	0.3084
0.0030	0.0914	0.2193	0.1129	0.3262
0.0040	0.1219	0.2335	0.1129	0.3473
0.0060	0.1829	0.2548	0.1129	0.3767
0.0080	0.2438	0.2690	0.1124	0.3957
0.0100	0.3048	0.2832	0.1119	0.4139
0.0150	0.4572	0.3045	0.1100	0.4410
0.0200	0.6096	0.3230	0.1081	0.4636
0.0300	0.9144	0.3570	0.1044	0.5026
0.0400	1.2192	0.3883	0.1016	0.5354
0.0500	1.5240	0.4195	0.0992	0.5660
0.0600	1.8288	0.4507	0.0983	0.5936
0.0700	2.1336	0.4820	0.0968	0.6206
0.0800	2.4384	0.5175	0.0954	0.6497
0.0900	2.7432	0.5544	0.0945	0.6782
0.1000	3.0480	0.5927	0.0931	0.7068
0.1100	3.3528	0.6325	0.0921	0.7351
0.1200	3.6576	0.6736	0.0911	0.7632
0.1300	3.9624	0.7148	0.0898	0.7906
0.1400	4.2672	0.7560	0.0888	0.8168
0.1500	4.5720	0.7957	0.0875	0.8415
0.1600	4.8768	0.8341	0.0860	0.8618
0.1700	5.1816	0.8738	0.0851	0.8881
0.1800	5.4864	0.9050	0.0841	0.9060
0.1900	5.7912	0.9334	0.0832	0.9221
0.2000	6.0960	0.9632	0.0827	0.9383
0.2100	6.4008	0.9831	0.0818	0.9494
0.2200	6.7056	0.9916	0.0804	0.9546
0.2300	7.0104	0.9945	0.0794	0.9566
0.2400	7.3152	0.9945	0.0785	0.9571
0.2500	7.6200	0.9945	0.0775	0.9576

+ CROSS WIRE PROBE
++ SINGLE WIRE PROBE
+++ PITOT-STATIC

TABLE 17(a) PROFILES AT X/L = 1.000 (θ = 0°)

Y (FT.)	Y (CM.)	CP (TOATL)	CP (STATIC)	Q/UO +++	Q/UO ++	Q/UO +	U/UO +	V/UO +	URMS/UO +	VRMS/UO +	WRMS/UO +	-2UV/UO**2 +
0.0000	0.0000	0.1141	0.1141	0.0000								
0.0005	0.0152	0.1184	0.1108	0.0872								
0.0010	0.0305	0.1255	0.1105	0.1225								
0.0015	0.0457	0.1397	0.1103	0.1715								
0.0020	0.0610	0.1581	0.1100	0.2193								
0.0030	0.0914	0.1836	0.1095	0.2722								
0.0040	0.1219	0.2029	0.1090	0.3050								
0.0052	0.1585				0.2388							
0.0060	0.1829	0.2332	0.1085	0.3531								
0.0062	0.1890				0.2907							
0.0072	0.2195				0.3338							
0.0078	0.2377										0.0333	
0.0078	0.2377					0.4235	0.4211	-0.0452	0.0430	0.0346		0.0156
0.0080	0.2438	0.2559	0.1081	0.3844								
0.0092	0.2804				0.3778							
0.0098	0.2987										0.0332	
0.0098	0.2987					0.4443	0.4421	-0.0446	0.0391	0.0312		0.0134
0.0100	0.3048	0.2673	0.1071	0.4002								
0.0102	0.3109				0.3860							
0.0148	0.4511										0.0305	
0.0148	0.4511					0.4805	0.4783	-0.0461	0.0353	0.0291		0.0115
0.0150	0.4572	0.2956	0.1043	0.4374								
0.0152	0.4633				0.4495							
0.0198	0.6035										0.0294	
0.0198	0.6035					0.4990	0.4967	-0.0479	0.0339	0.0290		0.0106
0.0200	0.6096	0.3183	0.1020	0.4651								
0.0202	0.6157				0.4733							
0.0252	0.7681				0.4944							
0.0298	0.9083										0.0295	
0.0298	0.9083					0.5351	0.5326	-0.0521	0.0341	0.0300		0.0116
0.0300	0.9144	0.3523	0.0997	0.5026								
0.0302	0.9205				0.5135							
0.0398	1.2131										0.0299	
0.0398	1.2131					0.5679	0.5654	-0.0534	0.0364	0.0313		0.0119
0.0400	1.2192	0.3807	0.0978	0.5319								
0.0402	1.2253				0.5303							
0.0498	1.5179										0.0308	
0.0498	1.5179					0.5959	0.5930	-0.0583	0.0376	0.0323		0.0129
0.0500	1.5240	0.4119	0.0959	0.5621								
0.0502	1.5301				0.5572							
0.0598	1.8227										0.0323	
0.0598	1.8227					0.6264	0.6233	-0.0620	0.0393	0.0333		0.0136
0.0600	1.8288	0.4445	0.0950	0.5912								
0.0602	1.8349				0.5824							
0.0698	2.1275										0.0333	
0.0698	2.1275					0.6520	0.6484	-0.0687	0.0406	0.0340		0.0143
0.0700	2.1336	0.4785	0.0936	0.6204								
0.0702	2.1397				0.6122							
0.0798	2.4323										0.0343	
0.0798	2.4323					0.6776	0.6739	-0.0703	0.0428	0.0348		0.0150

\+ CROSS WIRE PROBE
\++ SINGLE WIRE PROBE
\+++ PITOT-STATIC

TABLE 17(a) (continued)

Y (FT.)	Y (CM.)	CP (TOTAL)	CP (STATIC)	Q/UO +++	Q/UO ++	Q/UO +	U/UO +	V/UO +	URMS/UO +	VRMS/UO +	WRMS/UO +	-2OUV/UO**2 +
0.0800	2.4384	0.5125	0.0927	0.6479								
0.0802	2.4445				0.6403							
0.0898	2.7371										0.0354	
0.0898	2.7371					0.7059	0.7023	-0.0716	0.0436	0.0352		0.0154
0.0900	2.7432	0.5480	0.0917	0.6755								
0.0902	2.7493				0.6678							
0.0998	3.0419										0.0362	
0.0998	3.0419					0.7305	0.7261	-0.0799	0.0438	0.0357		0.0156
0.1000	3.0480	0.5877	0.0908	0.7049								
0.1002	3.0541				0.6960							
0.1098	3.3467										0.0364	
0.1098	3.3467					0.7617	0.7574	-0.0807	0.0438	0.0352		0.0152
0.1100	3.3528	0.6260	0.0899	0.7319								
0.1102	3.3589				0.7251							
0.1198	3.6515										0.0360	
0.1198	3.6515					0.7847	0.7803	-0.0827	0.0429	0.0350		0.0148
0.1200	3.6576	0.6671	0.0890	0.7603								
0.1202	3.6637				0.7529							
0.1298	3.9563										0.0354	
0.1298	3.9563					0.8124	0.8077	-0.0871	0.0409	0.0331		0.0129
0.1300	3.9624	0.7068	0.0875	0.7870								
0.1302	3.9685				0.7842							
0.1398	4.2611										0.0333	
0.1398	4.2611					0.8409	0.8369	-0.0819	0.0352	0.0316		0.0117
0.1400	4.2672	0.7465	0.0861	0.8126								
0.1402	4.2733				0.8089							
0.1498	4.5659										0.0316	
0.1498	4.5659					0.8691	0.8651	-0.0830	0.0368	0.0299		0.0104
0.1500	4.5720	0.7862	0.0847	0.8376								
0.1502	4.5781				0.8352							
0.1598	4.8707										0.0297	
0.1598	4.8707					0.8925	0.8892	-0.0767	0.0333	0.0276		0.0091
0.1600	4.8768	0.8244	0.0833	0.8609								
0.1602	4.8829				0.8588							
0.1698	5.1755										0.0270	
0.1696	5.1755					0.9138	0.9101	-0.0827	0.0308	0.0255		0.0079
0.1700	5.1816	0.8641	0.0819	0.8844								
0.1702	5.1877				0.8802							
0.1798	5.4803										0.0238	
0.1798	5.4803					0.9285	0.9249	-0.0816	0.0271	0.0220		0.0055
0.1800	5.4864	0.8992	0.0810	0.9048								
0.1802	5.4925				0.8995							
0.1898	5.7851										0.0190	
0.1898	5.7851					0.9473	0.9439	-0.0806	0.0227	0.0184		0.0037
0.1900	5.7912	0.9308	0.0801	0.9223								
0.1902	5.7973				0.9191							
0.1998	6.0899										0.0150	
0.1998	6.0899					0.9633	0.9601	-0.0787	0.0175	0.0148		0.0021
0.2000	6.0960	0.9606	0.0791	0.9389								
0.2002	6.1021				0.9391							

+ CROSS WIRE PROBE
++ SINGLE WIRE PROBE
+++ PITOT-STATIC

TABLE 17(a) (continued)

Y (FT.)	Y (CM.)	CP (TOATL)	CP (STATIC)	Q/UO +++	Q/UO ++	Q/UO +	U/UO +	V/UO +	URMS/UO +	VRMS/UO +	WRMS/UO +	-2OUV/UO**2 +
0.2098	6.3947										0.0108	
0.2098	6.3947					0.9738	0.9707	-0.0779	0.0104	0.0108		0.0005
0.2100	6.4008	0.9804	0.0783	0.9498								
0.2102	6.4069				0.9556							
0.2198	6.6995										0.0079	
0.2198	6.6995					0.9804	0.9774	-0.0762	0.0065	0.0077		0.0002
0.2200	6.7056	0.9932	0.0775	0.9569								
0.2202	6.7117				0.9637							
0.2298	7.0043										0.0063	
0.2298	7.0043					0.9831	0.9801	-0.0770	0.0038	0.0063		0.0001
0.2300	7.0104	0.9974	0.0765	0.9596								
0.2302	7.0165				0.9684							
0.2398	7.3091										0.0060	
0.2398	7.3091					0.9826	0.9795	-0.0782	0.0032	0.0055		0.0001
0.2400	7.3152	0.9988	0.0756	0.9608								
0.2402	7.3213				0.9718							
0.2498	7.6139										0.0057	
0.2498	7.6139					0.9852	0.9821	-0.0777	0.0024	0.0051		0.0000
0.2500	7.6200	0.9988	0.0746	0.9614								
0.2502	7.6261				0.9714							
0.2598	7.9187					0.9880	0.9853	-0.0733	0.0029	0.0056		0.0000
0.2600	7.9248	0.9988	0.0737	0.9618								

+ CROSS WIRE PROBE
++ SINGLE WIRE PROBE
+++ PITOT-STATIC

TABLE 17(b) PROFILES AT X/L = 1.00 (θ = 5.7°)

Y (FT.)	Y (CM.)	CP (TOATL)	CP (STATIC)	Q/UO +++	Q/UO ++	Q/UC +	U/UO +	V/UO +	URMS/UC +	VRMS/UC +	WRMS/UC +	-2UV/UC**2 +
0.0000	0.0000	0.1141	0.1141	0.0000								
0.0005	0.0152	0.1184	0.1108	0.0872								
0.0010	0.0305	0.1255	0.1105	0.1225								
0.0015	0.0457	0.1397	0.1103	0.1715								
0.0020	0.0610	0.1581	0.1100	0.2193								
0.0030	0.0914	0.1836	0.1095	0.2722								
0.0040	0.1219	0.2020	0.1090	0.3050								
0.0052	0.1585				0.2388							
0.0060	0.1829	0.2332	0.1085	0.3531								
0.0062	0.1890				0.2907							
0.0072	0.2195				0.3338							
0.0078	0.2377										0.0333	
0.0078	0.2377					0.4091	0.4091	0.0047	0.0413	0.0344		0.0125
0.0080	0.2438	0.2559	0.1081	0.3844								
0.0092	0.2804				0.3778							
0.0098	0.2987										0.0332	
0.0098	0.2987					0.4322	0.4321	0.0085	0.0388	0.0304		0.0112
0.0100	0.3048	0.2673	0.1071	0.4002								
0.0102	0.3109				0.3860							
0.0148	0.4511										0.0305	
0.0148	0.4511					0.4653	0.4651	0.0126	0.0354	0.0270		0.0094
0.0150	0.4572	0.2956	0.1043	0.4374								
0.0152	0.4633				0.4495							
0.0198	0.6035										0.0294	
0.0198	0.6035					0.4916	0.4914	0.0151	0.0358	0.0270		0.0078
0.0200	0.6096	0.3183	0.1020	0.4651								
0.0202	0.6157				0.4733							
0.0252	0.7681				0.4944							
0.0298	0.9083										0.0295	
0.0298	0.9083					0.5294	0.5291	0.0185	0.0367	0.0284		0.0087
0.0300	0.9144	0.3523	0.0997	0.5026								
0.0302	0.9205				0.5135							
0.0398	1.2131										0.0299	
0.0398	1.2131					0.5601	0.5597	0.0198	0.0379	0.0290		0.0092
0.0400	1.2192	0.3807	0.0978	0.5319								
0.0402	1.2253				0.5303							
0.0498	1.5179										0.0308	
0.0498	1.5179					0.5880	0.5876	0.0207	0.0387	0.0299		0.0100
0.0500	1.5240	0.4119	0.0959	0.5621								
0.0502	1.5301				0.5572							
0.0598	1.8227										0.0323	
0.0598	1.8227					0.6143	0.6138	0.0239	0.0408	0.0310		0.0106
0.0600	1.8288	0.4445	0.0950	0.5912								
0.0602	1.8349				0.5824							
0.0698	2.1275										0.0333	
0.0698	2.1275					0.6447	0.6442	0.0245	0.0419	0.0313		0.0111
0.0700	2.1336	0.4785	0.0936	0.6204								
0.0702	2.1397				0.6122							
0.0798	2.4323										0.0343	
0.0798	2.4323					0.6754	0.6749	0.0254	0.0425	0.0319		0.0118

\+ CROSS WIRE PROBE
++ SINGLE WIRE PROBE } (θ=0°)
+++ PITOT-STATIC

TABLE 17(b) (continued)

Y (FT.)	Y (CM.)	CP (TOATL)	CP (STATIC)	Q/UO +++	Q/UO ++	Q/UO +	U/UO +	V/UO +	URMS/UO +	VRMS/UC +	WRMS/UC +	-2OUV/UO**2 +
0.0800	2.4384	0.5125	0.0927	0.6479								
0.0802	2.4445				0.6403							
0.0898	2.7371										0.0354	
0.0898	2.7371					0.7054	0.7048	0.0284	0.0437	C.C323		C.C122
0.0900	2.7432	0.5480	0.0917	0.6755								
0.0902	2.7493				0.6678							
0.0998	3.0419										C.0362	
0.0998	3.0419					0.7342	0.7337	0.0282	0.0446	C.C324		C.C123
0.1000	3.0480	0.5877	0.0908	0.7049								
0.1002	3.0541				0.6960							
0.1093	3.3467										C.0364	
0.1098	3.3467					0.7627	0.7619	C.0349	0.0446	C.C323		C.C120
0.1100	3.3528	0.6260	0.0899	0.7319								
0.1102	3.3589				0.7251							
0.1193	3.6515										0.C360	
0.1198	3.6515					0.7883	0.7875	C.0356	0.0434	C.C317		C.C117
0.1200	3.6576	0.6671	0.0890	0.7603								
0.1202	3.6637				0.7529							
0.1293	3.9563										0.0354	
0.1296	3.9563					0.8145	0.8135	0.0402	0.0424	C.C313		C.C111
0.1300	3.9624	0.7068	0.0875	0.7870								
0.1302	3.9685				0.7842							
0.1398	4.2611										C.0333	
0.1398	4.2611					0.8423	0.8412	C.C426	0.0355	C.C259		C.C108
0.1400	4.2672	0.7465	0.0861	0.8126								
0.1402	4.2733				0.8089							
0.1498	4.5659										0.0316	
0.1498	4.5659					0.8636	0.8625	C.C441	0.0377	C.C28C		C.C10C
0.1500	4.5720	0.7862	0.0847	0.8376								
0.1502	4.5781				0.8352							
0.1598	4.8707										C.C297	
0.1598	4.8707					0.8881	0.8869	C.C467	C.0347	C.C266		C.C088
0.1600	4.8768	0.8244	0.0833	0.8609								
0.1602	4.8829				0.8588							
0.1698	5.1755										C.C270	
0.1698	5.1755					0.9095	0.9082	C.C479	0.0323	C.C242		C.C074
0.1700	5.1816	0.8641	0.0819	0.8844								
0.1702	5.1877				0.8802							
0.1798	5.4803										0.0238	
0.1798	5.4803					0.9277	0.9263	0.0518	0.0282	C.C213		C.C054
0.1800	5.4864	0.8992	0.0810	0.9048								
0.1802	5.4925				0.8995							
0.1898	5.7851										0.C190	
0.1898	5.7851					0.9500	0.9484	C.0547	0.0239	C.C177		C.C032
0.1900	5.7912	0.9308	0.0801	0.9223								
0.1902	5.7973				0.9191							
0.1998	6.0899										C.C15C	
0.1998	6.0899					0.9654	0.9638	C.0548	0.0181	C.C140		C.C017
0.2000	6.0960	0.9606	0.0791	0.9389								
0.2002	6.1021				0.9391							

\+ CROSS WIRE PROBF

++ SINGLE WIRE PRCBE } $(\theta=0°)$

+++ PITOT-STATIC

TABLE 17(b) (continued)

Y (FT.)	Y (CM.)	CP (TOATL)	CP (STATIC)	Q/UO +++	Q/UO ++	Q/UO +	U/UO +	V/UO +	URMS/UO +	VRMS/UO +	WRMS/UO +	-2OUV/UO**2 +
0.2098	6.3947										0.0108	
0.2098	6.3947					0.9761	0.9744	0.0579	0.0132	0.0107		0.0008
0.2100	6.4308	0.9804	0.0783	0.9498								
0.2102	6.4367				0.9556							
0.2198	6.6995										0.0079	
0.2198	6.6995					0.9814	0.9796	0.0588	0.0065	0.0078		0.0003
0.2200	6.7056	0.9932	0.0775	0.9569								
0.2202	6.7117				0.9637							
0.2298	7.0043										0.0063	
0.2298	7.0043					0.9832	0.9815	0.0586	0.0041	0.0063		0.0001
0.2300	7.0104	0.9974	0.0765	0.9596								
0.2302	7.0165				0.9684							
0.2398	7.3091										0.0060	
0.2398	7.3091					0.9846	0.9826	0.0620	0.0029	0.0052		0.0000
0.2400	7.3152	0.9988	0.0756	0.9608								
0.2402	7.3213				0.9718							
0.2498	7.6139										0.0057	
0.2498	7.6139					0.9860	0.9841	0.0617	0.0030	0.0045		0.0000
0.2500	7.6200	0.9988	0.0746	0.9614								
0.2502	7.6261				0.9714							
0.2598	7.9187					0.9865	0.9845	0.0625	0.0024	0.0046		0.0001
0.2600	7.9248	0.9988	0.0737	0.9618								

\+ CROSS WIRE PROBE
++ SINGLE WIRE PROBE } ($\theta=0°$)
+++ PITOT-STATIC

TABLE 18 PROFILES AT X/L = 1.010

Y (FT.)	Y (CM.)	CP (TOTAL)	CP (STATIC)	Q/UO +++
0.0000	0.0000	0.1795	0.0885	0.3017
0.0005	0.0152	0.1795	0.0885	0.3017
0.0010	0.0305	0.1837	0.0885	0.3085
0.0015	0.0457	0.1880	0.0884	0.3156
0.0020	0.0610	0.1951	0.0883	0.3268
0.0030	0.0914	0.2050	0.0881	0.3419
0.0040	0.1219	0.2163	0.0881	0.3581
0.0060	0.1829	0.2376	0.0877	0.3872
0.0080	0.2438	0.2546	0.0877	0.4085
0.0100	0.3048	0.2674	0.0877	0.4239
0.0150	0.4572	0.2929	0.0872	0.4535
0.0200	0.6096	0.3184	0.0867	0.4814
0.0300	0.9144	0.3553	0.0863	0.5187
0.0400	1.2192	0.3851	0.0853	0.5475
0.0500	1.5240	0.4163	0.0843	0.5762
0.0600	1.8288	0.4489	0.0833	0.6046
0.0700	2.1336	0.4829	0.0830	0.6324
0.0800	2.4384	0.5169	0.0825	0.6591
0.0900	2.7432	0.5524	0.0825	0.6855
0.1000	3.0480	0.5878	0.0825	0.7108
0.1100	3.3528	0.6318	0.0825	0.7411
0.1200	3.6576	0.6715	0.0821	0.7677
0.1300	3.9624	0.7112	0.0811	0.7938
0.1400	4.2672	0.7495	0.0802	0.8181
0.1500	4.5720	0.7906	0.0794	0.8433
0.1600	4.8768	0.8289	0.0784	0.8663
0.1700	5.1816	0.8686	0.0776	0.8894
0.1800	5.4864	0.9012	0.0766	0.9081
0.1900	5.7912	0.9296	0.0757	0.9241
0.2000	6.0960	0.9636	0.0747	0.9428
0.2100	6.4008	0.9821	0.0739	0.9530
0.2200	6.7056	0.9920	0.0732	0.9585
0.2300	7.0104	0.9962	0.0723	0.9612
0.2400	7.3152	0.9977	0.0714	0.9624
0.2500	7.6200	0.9977	0.0705	0.9629
0.2600	7.9248	0.9977	0.0696	0.9634
0.2800	8.5344	0.9977	0.0677	0.9644
0.3000	9.1440	0.9977	0.0659	0.9653

\+ CROSS WIRE PROBE
++ SINGLE WIRE PROBE
+++ PITOT-STATIC

TABLE 19 PROFILES AT X/L = 1.020

Y (FT.)	Y (CM.)	CP (TOATL)	CP (STATIC)	Q/UO +++	Q/UO ++	Q/UO +	U/UO +	V/UO +	URMS/UO +	VRMS/UO +	WRMS/UO +	-2OUV/UO**2 +
0.0000	0.0000										0.0298	
0.0000	0.0000					0.3803	0.3799	-0.0170	0.0309	0.0307		0.0005
0.0000	0.0000				0.3897							
0.0000	0.0000	0.2141	0.0769	0.3704								
0.0005	0.0152	0.2155	0.0769	0.3723								
0.0010	0.0305					0.3796	0.3792	-0.0178	0.0314	0.0312		0.0026
0.0010	0.0305				0.3911							
0.0010	0.0305	0.2169	0.0769	0.3742								
0.0015	0.0457	0.2183	0.0769	0.3760								
0.0020	0.0610										0.0296	
0.0020	0.0610				0.3958							
0.0020	0.0610	0.2211	0.0769	0.3797								
0.0030	0.0914				0.4007							
0.0030	0.0914	0.2268	0.0769	0.3872								
0.0040	0.1219										0.0290	
0.0040	0.1219				0.4071							
0.0040	0.1219	0.2339	0.0769	0.3962								
0.0050	0.1524					0.4041	0.4033	-0.0260	0.0381	0.0330		0.0141
0.0050	0.1524				0.4126							
0.0060	0.1829										0.0291	
0.0060	0.1829				0.4190							
0.0060	0.1829	0.2481	0.0769	0.4138								
0.0070	0.2134				0.4284							
0.0080	0.2438										0.0297	
0.0080	0.2438				0.4357							
0.0080	0.2438	0.2609	0.0769	0.4290								
0.0090	0.2743				0.4405							
0.0100	0.3048										0.0302	
0.0100	0.3048					0.4495	0.4483	-0.0334	0.0393	0.0307		0.0144
0.0100	0.3048	0.2736	0.0769	0.4435								
0.0120	0.3658										0.0306	
0.0140	0.4267				0.4752							
0.0150	0.4572					0.4849	0.4835	-0.0362	0.0357	0.0283		0.0102
0.0150	0.4572	0.2991	0.0769	0.4714								
0.0170	0.5791				0.4964							
0.0230	0.6096					0.5111	0.5096	-0.0388	0.0342	0.0285		0.0089
0.0200	0.6096	0.3218	0.0769	0.4949								
0.0220	0.6706										0.0310	
0.0240	0.7315				0.5156							
0.0300	0.9144					0.5413	0.5397	-0.0413	0.0340	0.0287		0.0092
0.0300	0.9144	0.3587	0.0769	0.5308								
0.0320	0.9754										0.0316	
0.0340	1.0363				0.5449							
0.0400	1.2192					0.5698	0.5680	-0.0453	0.0349	0.0299		0.0103
0.0400	1.2192	0.3899	0.0774	0.5590								
0.0420	1.2802										0.0312	
0.0440	1.3411				0.5739							
0.0500	1.5240					0.5976	0.5957	-0.0475	0.0370	0.0310		0.0115
0.0500	1.5240	0.4197	0.0774	0.5851								
0.0520	1.5850										0.0313	

\+ CROSS WIRE PROBE
++ SINGLE WIRE PROBE
+++ PITOT-STATIC

TABLE 19 (continued)

Y (FT.)	Y (CM.)	CP (TOTAL)	CP (STATIC)	Q/UO +++	Q/UO ++	Q/UO +	U/UO +	V/UO +	URMS/UO +	VRMS/UO +	WRMS/UO +	-2OUV/UO**2 +
0.0540	1.6459				0.5984							
0.0600	1.8288					0.6238	0.6218	-0.0502	0.0382	0.0316		0.0123
0.0600	1.8288	0.4537	0.0774	0.6134								
0.0620	1.8898										0.0321	
0.0640	1.9507				0.6258							
0.0700	2.1336					0.6521	0.6500	-0.0519	0.0355	0.0322		0.0125
0.0700	2.1336	0.4877	0.0774	0.6405								
0.0720	2.1946										0.0329	
0.0740	2.2555				0.6521							
0.0800	2.4384					0.6789	0.6767	-0.0547	0.0403	0.0329		0.0132
0.0800	2.4384	0.5189	0.0774	0.6645								
0.0820	2.4994										0.0356	
0.0840	2.5603				0.6789							
0.0900	2.7432					0.7064	0.7042	-0.0557	0.0414	0.0334		0.0139
0.0900	2.7432	0.5572	0.0774	0.6927								
0.0920	2.8042										0.0359	
0.0940	2.8651				0.7052							
0.1000	3.0480					0.7322	0.7299	-0.0580	0.0420	0.0339		0.0148
0.1000	3.0480	0.5941	0.0774	0.7188								
0.1020	3.1090										0.0363	
0.1040	3.1699				0.7347							
0.1100	3.3528					0.7561	0.7537	-0.0607	0.0422	0.0338		0.0148
0.1100	3.3528	0.6338	0.0774	0.7459								
0.1120	3.4138										0.0358	
0.1140	3.4747				0.7556							
0.1200	3.6576					0.7845	0.7821	-0.0616	0.0420	0.0336		0.0141
0.1200	3.6576	0.6721	0.0774	0.7712								
0.1220	3.7186										0.0346	
0.1240	3.7795				0.7819							
0.1300	3.9624					0.8107	0.8083	-0.0625	0.0418	0.0333		0.0138
0.1300	3.9624	0.7118	0.0769	0.7968								
0.1320	4.0234										0.0339	
0.1340	4.0843				0.8050							
0.1400	4.2672					0.8321	0.8297	-0.0626	0.0404	0.0321		0.0129
0.1400	4.2672	0.7472	0.0765	0.8190								
0.1420	4.3282										0.0326	
0.1440	4.3891				0.8293							
0.1500	4.5720					0.8592	0.8567	-0.0653	0.0385	0.0310		0.0120
0.1500	4.5720	0.7884	0.0761	0.8440								
0.1520	4.6330										0.0312	
0.1540	4.6939				0.8560							
0.1600	4.8768					0.8797	0.8773	-0.0645	0.0355	0.0289		0.0106
0.1600	4.8768	0.8295	0.0756	0.8683								
0.1620	4.9378										0.0293	
0.1640	4.9987				0.8731							
0.1700	5.1816					0.8999	0.8975	-0.0656	0.0323	0.0263		0.0084
0.1700	5.1816	0.8621	0.0751	0.8868								
0.1720	5.2426										0.0262	
0.1740	5.3035				0.8904							
0.1800	5.4864					0.9183	0.9159	-0.0658	0.0250	0.0233		0.0064

\+ CROSS WIRE PROBE
++ SINGLE WIRE PROBE
+++ PITOT-STATIC

TABLE 19 (continued)

Y (FT.)	Y (CM.)	CP (TOATL)	CP (STATIC)	C/UO +++	Q/UO ++	Q/UC +	U/UC +	V/UO +	URMS/UC +	VRMS/UC +	WRMS/UC +	-20UV/UC**2 +
0.1800	5.4864	0.8990	0.0742	0.9082								
0.1820	5.5474										0.0224	
0.1840	5.6083				0.9108							
0.1900	5.7912					0.9398	0.9375	-0.0653	0.0244	0.0191		0.0039
0.1900	5.7912	0.9287	0.0732	0.9249								
0.1920	5.8522										0.0171	
0.1940	5.9131				0.9297							
0.2000	6.0960					0.9496	0.9476	-0.0620	0.0190	0.0153		0.0023
0.2000	6.0960	0.9585	0.0723	0.9414								
0.2020	6.1570										0.0124	
0.2040	6.2179				0.9427							
0.2100	6.4008					0.9608	0.9588	-0.0622	0.0122	0.0111		0.0010
0.2100	6.4008	0.9798	0.0716	0.9530								
0.2120	6.4618										0.0085	
0.2140	6.5227				0.9450							
0.2200	6.7056					0.9643	0.9624	-0.0600	0.0069	0.0083		0.0002
0.2200	6.7056	0.9883	0.0709	0.9578								
0.2220	6.7666										0.0059	
0.2240	6.8275				0.9484							
0.2300	7.0104					0.9672	0.9653	-0.0605	0.0039	0.0061		0.0001
0.2300	7.0104	0.9940	0.0699	0.9613								
0.2320	7.0714										0.0049	
0.2340	7.1323				0.9482							
0.2400	7.3152					0.9681	0.9663	-0.0592	0.0030	0.0053		0.0000
0.2400	7.3152	0.9940	0.0690	0.9618								
0.2420	7.3762										0.0051	
0.2440	7.4371				0.9502							
0.2500	7.6200	0.9964	0.0672	0.9640								
0.2520	7.6810										0.0044	
0.2600	7.9248	0.9964	0.0671	0.9650								

\+ CROSS WIRE PROBE
\++ SINGLE WIRE PROBE
\+++ PITOT-STATIC

TABLE 20 PROFILES AT X/L = 1.040

Y (FT.)	Y (CM.)	CP (TOTAL)	CP (STATIC)	Q/UO +++
0.0000	0.0000	0.2454	0.0613	0.4297
0.0005	0.0152	0.2468	0.0613	0.4313
0.0010	0.0305	0.2468	0.0613	0.4313
0.0015	0.0457	0.2482	0.0613	0.4329
0.0020	0.0610	0.2496	0.0613	0.4345
0.0030	0.0914	0.2525	0.0613	0.4378
0.0040	0.1219	0.2567	0.0613	0.4426
0.0060	0.1829	0.2667	0.0613	0.4538
0.0080	0.2438	0.2766	0.0613	0.4645
0.0100	0.3048	0.2865	0.0613	0.4751
0.0150	0.4572	0.3092	0.0613	0.4984
0.0200	0.6096	0.3305	0.0613	0.5193
0.0300	0.9144	0.3673	0.0615	0.5534
0.0400	1.2192	0.3971	0.0618	0.5795
0.0500	1.5240	0.4311	0.0620	0.6079
0.0600	1.8288	0.4623	0.0622	0.6329
0.0700	2.1336	0.4964	0.0622	0.6593
0.0800	2.4384	0.5304	0.0622	0.6846
0.0900	2.7432	0.5659	0.0624	0.7099
0.1000	3.0480	0.6013	0.0626	0.7343
0.1100	3.3528	0.6424	0.0626	0.7618
0.1200	3.6576	0.6821	0.0626	0.7874
0.1300	3.9624	0.7190	0.0626	0.8105
0.1400	4.2672	0.7587	0.0626	0.8346
0.1500	4.5720	0.7956	0.0626	0.8564
0.1600	4.8768	0.8339	0.0626	0.8785
0.1700	5.1816	0.8736	0.0626	0.9008
0.1800	5.4864	0.9048	0.0626	0.9180
0.1900	5.7912	0.9374	0.0626	0.9356
0.2000	6.0960	0.9643	0.0626	0.9498
0.2100	6.4008	0.9785	0.0624	0.9574
0.2200	6.7056	0.9870	0.0622	0.9619
0.2300	7.0104	0.9927	0.0618	0.9651
0.2400	7.3152	0.9941	0.0613	0.9661
0.2500	7.6200	0.9941	0.0606	0.9664
0.2600	7.9248	0.9941	0.0599	0.9668
0.2800	8.5344	0.9941	0.0585	0.9675
0.3000	9.1440	0.9941	0.0572	0.9682

\+ CROSS WIRE PROBE
++ SINGLE WIRE PROBE
+++ PITOT-STATIC

TABLE 21 PROFILES AT X/L = 1.060

Y (FT.)	Y (CM.)	CP (TOATL)	CP (STATIC)	Q/UO +++	Q/UO ++	Q/UO +	U/UO +	V/UO +	URMS/UO +	VRMS/UO +	WRMS/UO +	-2CUV/UO**2 +
0.0000	0.0000										0.0223	
0.0000	0.0000					0.4712	0.4707	-0.0212	0.0279	0.0275		0.0019
0.0000	0.0000				0.4848							
0.0000	0.0000	0.2598	0.0535	0.4548								
0.0005	0.0152	0.2612	0.0535	0.4563								
0.0010	0.0305	0.2626	0.0535	0.4578								
0.0015	0.0457	0.2626	0.0535	0.4578								
0.0020	0.0610										0.0223	
0.0020	0.0610	0.2640	0.0535	0.4593								
0.0030	0.0914	0.2669	0.0535	0.4625								
0.0040	0.1219										0.0229	
0.0040	0.1219					0.4799	0.4792	-0.0258	0.0299	0.0262		0.0057
0.0040	0.1219	0.2697	0.0535	0.4655								
0.0050	0.1524				0.4858							
0.0060	0.1829										0.0235	
0.0060	0.1629				0.4888							
0.0060	0.1829	0.2754	0.0535	0.4716								
0.0070	0.2134				0.4911							
0.0080	0.2438										0.0241	
0.0080	0.2438				0.4935							
0.0080	0.2438	0.2839	0.0535	0.4805								
0.0090	0.2743					0.4973	0.4964	-0.0295	0.0336	0.0265		0.0082
0.0090	0.2743				0.4977							
0.0100	0.3048										0.0252	
0.0100	0.3048				0.5090							
0.0100	0.3048	0.2937	0.0535	0.4906								
0.0110	0.3353				0.5061							
0.0120	0.3658										0.0257	
0.0120	0.3658				0.5099							
0.0130	0.3962				0.5151							
0.0140	0.4267					0.5192	0.5182	-0.0324	0.0345	0.0265		0.0087
0.0140	0.4267				0.5209							
0.0150	0.4572				0.5224							
0.0150	0.4572	0.3150	0.0535	0.5119								
0.0200	0.6096				0.5440							
0.0200	0.6096	0.3348	0.0535	0.5308								
0.0220	0.6706										0.0277	
0.0240	0.7315					0.5552	0.5541	-0.0344	0.0325	0.0264		0.0084
0.0250	0.7620				0.5625							
0.0300	0.9144				0.5838							
0.0300	0.9144	0.3717	0.0535	0.5645								
0.0320	0.9754										0.0287	
0.0340	1.0363					0.5821	0.5809	-0.0373	0.0302	0.0280		0.0095
0.0400	1.2192				0.6106							
0.0400	1.2192	0.4043	0.0535	0.5927								
0.0420	1.2802										0.0299	
0.0440	1.3411					0.6084	0.6071	-0.0405	0.0351	0.0292		0.0105
0.0500	1.5240				0.6333							
0.0500	1.5240	0.4383	0.0535	0.6207								
0.0520	1.5650										0.0307	

+ CROSS WIRE PROBE
++ SINGLE WIRE PROBE
+++ PITOT-STATIC

TABLE 21 (continued)

Y (FT.)	Y (CM.)	CP (TOATL)	CP (STATIC)	Q/UO +++	C/UO ++	Q/UO +	U/UO +	V/UO +	URMS/UO +	VRMS/UO +	WRMS/UO +	-2UV/UO**2 +
0.0540	1.6459					0.6347	0.6332	-0.0437	0.0369	0.0306		0.0120
0.0590	1.7983					0.6459	0.6443	-0.0454	0.0373	0.0311		0.0122
0.0600	1.8288				0.6568							
0.0600	1.8288	0.4695	0.0535	0.6454								
0.0620	1.8898										0.0317	
0.0690	2.1031					0.6718	0.6701	-0.0483	0.0398	0.0325		0.0134
0.0700	2.1336				0.6826							
0.0700	2.1336	0.5021	0.0535	0.6701								
0.0720	2.1946										0.0321	
0.0790	2.4079					0.6935	0.6918	-0.0490	0.0406	0.0328		0.0135
0.0800	2.4384				0.7093							
0.0800	2.4384	0.5390	0.0535	0.6971								
0.0820	2.4994										0.0329	
0.0890	2.7127					0.7201	0.7182	-0.0524	0.0411	0.0326		0.0138
0.0900	2.7432				0.7348							
0.0900	2.7432	0.5745	0.0535	0.7221								
0.0920	2.8042										0.0332	
0.0990	3.0175					0.7461	0.7441	-0.0543	0.0413	0.0321		0.0134
0.1000	3.0480				0.7639							
0.1000	3.0480	0.6099	0.0540	0.7459								
0.1020	3.1090										0.0329	
0.1090	3.3223					0.7674	0.7654	-0.0560	0.0410	0.0321		0.0135
0.1100	3.3528				0.7870							
0.1100	3.3528	0.6496	0.0542	0.7719								
0.1120	3.4138										0.0334	
0.1190	3.6271					0.7950	0.7929	-0.0573	0.0406	0.0315		0.0126
0.1200	3.6576				0.8110							
0.1200	3.6576	0.6879	0.0544	0.7962								
0.1220	3.7186										0.0331	
0.1290	3.9319					0.8210	0.8189	-0.0585	0.0393	0.0306		0.0119
0.1300	3.9624				0.8372							
0.1300	3.9624	0.7219	0.0547	0.8171								
0.1320	4.0234										0.0323	
0.1390	4.2367					0.8405	0.8383	-0.0602	0.0375	0.0294		0.0113
0.1400	4.2672				0.8597							
0.1400	4.2672	0.7673	0.0549	0.8443								
0.1420	4.3282										0.0313	
0.1490	4.5415					0.8681	0.8660	-0.0604	0.0354	0.0281		0.0098
0.1500	4.5720				0.8847							
0.1500	4.5720	0.8028	0.0551	0.8650								
0.1520	4.6330										0.0296	
0.1590	4.8463					0.8856	0.8835	-0.0611	0.0332	0.0264		0.0089
0.1600	4.8768				0.9048							
0.1600	4.8768	0.8354	0.0553	0.8835								
0.1620	4.9378										0.0275	
0.1690	5.1511					0.9047	0.9026	-0.0612	0.0303	0.0242		0.0072
0.1700	5.1816				0.9306							
0.1700	5.1816	0.8694	0.0553	0.9026								
0.1720	5.2426										0.0249	
0.1790	5.4559					0.9237	0.9215	-0.0637	0.0270	0.0214		0.0057

+ CROSS WIRE PROBE
++ SINGLE WIRE PROBE
+++ PITOT-STATIC

TABLE 21 (continued)

Y (FT.)	Y (CM.)	CP (TOATL)	CP (STATIC)	Q/UO +++	Q/UO ++	Q/UO +	U/UO +	V/UO +	URMS/UO +	VRMS/UO +	WRMS/UO +	-20UV/UO**2 +
0.1800	5.4864				0.9440							
0.1800	5.4864	0.9006	0.0553	0.9197								
0.1820	5.5474										0.0211	
0.1890	5.7607					0.9418	0.9397	-0.0629	0.0233	0.0184		0.0043
0.1900	5.7912				0.9620							
0.1900	5.7912	0.9346	0.0553	0.9380								
0.1920	5.8522										0.0175	
0.1990	6.0655					0.9576	0.9556	-0.0626	0.0182	0.0152		0.0024
0.2000	6.0960				0.9772							
0.2000	6.0960	0.9589	0.0553	0.9508								
0.2020	6.1570										0.0129	
0.2090	6.3703					0.9733	0.9711	-0.0655	0.0117	0.0113		0.0012
0.2100	6.4008				0.9873							
0.2100	6.4008	0.9773	0.0553	0.9605								
0.2120	6.4618										0.0088	
0.2190	6.6751					0.9773	0.9751	-0.0661	0.0070	0.0084		0.0005
0.2200	6.7056				0.9929							
0.2200	6.7056	0.9872	0.0553	0.9656								
0.2220	6.7666										0.0065	
0.2290	6.9799					0.9804	0.9782	-0.0661	0.0043	0.0065		0.0002
0.2300	7.0104				0.9963							
0.2300	7.0104	0.9915	0.0553	0.9678								
0.2320	7.0714										0.0054	
0.2390	7.2847					0.9795	0.9772	-0.0666	0.0032	0.0052		0.0001
0.2400	7.3152				0.9992							
0.2400	7.3152	0.9929	0.0553	0.9687								
0.2420	7.3762										0.0049	
0.2490	7.5895					0.9806	0.9783	-0.0673	0.0030	0.0051		0.0002
0.2500	7.6200				0.9977							
0.2500	7.6200	0.9929	0.0551	0.9687								
0.2520	7.6810										0.0045	
0.2600	7.9248				0.9964							
0.2600	7.9248	0.9929	0.0549	0.9715								

+ CROSS WIRE PROBE
++ SINGLE WIRE PROBE
+++ PITOT-STATIC

TABLE 22 PROFILES AT X/L = 1.100

Y (FT.)	Y (CM.)	CP (TOTAL)	CP (STATIC)	Q/UO +++
0.0000	0.0000	0.2886	0.0385	0.5001
0.0005	0.0152	0.2900	0.0385	0.5015
0.0010	0.0305	0.2900	0.0385	0.5015
0.0015	0.0457	0.2914	0.0385	0.5029
0.0020	0.0610	0.2928	0.0385	0.5043
0.0030	0.0914	0.2942	0.0385	0.5057
0.0040	0.1219	0.2957	0.0385	0.5071
0.0060	0.1829	0.3013	0.0385	0.5126
0.0080	0.2438	0.3070	0.0385	0.5182
0.0100	0.3048	0.3141	0.0385	0.5249
0.0150	0.4572	0.3354	0.0385	0.5448
0.0200	0.6096	0.3566	0.0385	0.5639
0.0300	0.9144	0.3921	0.0385	0.5946
0.0400	1.2192	0.4276	0.0385	0.6238
0.0500	1.5240	0.4587	0.0385	0.6480
0.0600	1.8288	0.4928	0.0385	0.6738
0.0700	2.1336	0.5254	0.0385	0.6974
0.0800	2.4384	0.5594	0.0385	0.7217
0.0900	2.7432	0.5920	0.0394	0.7434
0.1000	3.0480	0.6317	0.0403	0.7683
0.1100	3.3528	0.6672	0.0408	0.7915
0.1200	3.6576	0.7083	0.0413	0.8168
0.1300	3.9624	0.7452	0.0418	0.8387
0.1400	4.2672	0.7806	0.0423	0.8592
0.1500	4.5720	0.8161	0.0417	0.8800
0.1600	4.8768	0.8515	0.0421	0.8997
0.1700	5.1816	0.8762	0.0423	0.9132
0.1800	5.4864	0.9196	0.0426	0.9365
0.1900	5.7912	0.9437	0.0428	0.9492
0.2000	6.0960	0.9664	0.0431	0.9609
0.2100	6.4008	0.9820	0.0433	0.9689
0.2200	6.7056	0.9905	0.0435	0.9731
0.2300	7.0104	0.9933	0.0435	0.9746
0.2400	7.3152	0.9933	0.0435	0.9746
0.2500	7.6200	0.9948	0.0435	0.9753
0.2600	7.9248	0.9948	0.0431	0.9756

\+ CROSS WIRE PROBE
++ SINGLE WIRE PROBE
+++ PITOT-STATIC

TABLE 23 PROFILES AT X/L = 1.200

Y (FT.)	Y (CM.)	CP (TOATL)	CP (STATIC)	Q/UO +++	Q/UO ++	Q/UO +	U/UO +	V/UO +	URMS/UO +	VRMS/UO +	WRMS/UO +	-2OUV/UO**2 +
0.0080	0.2438					0.5680	0.5680	0.0008	0.0306	0.0246		0.0051
0.0080	0.2438				0.5879							
0.0080	0.2438	0.3419	0.0200	0.5656								
0.0080	0.2438										0.0240	
0.0080	0.2438					0.5680	0.5680	0.0008	0.0306	0.0246		0.0051
0.0080	0.2438				0.5879							
0.0080	0.2438	0.3419	0.0200	0.5656								
0.0080	0.2438										0.0240	
0.0080	0.2438					0.5680	0.5680	0.0008	0.0306	0.0246		0.0051
0.0080	0.2438				0.5879							
0.0080	0.2438	0.3419	0.0200	0.5656								
0.0080	0.2438										0.0240	
0.0080	0.2438					0.5680	0.5680	0.0008	0.0306	0.0246		0.0051
0.0080	0.2438				0.5879							
0.0080	0.2438	0.3419	0.0200	0.5656								
0.0080	0.2438										0.0240	
0.0080	0.2438					0.5680	0.5680	0.0008	0.0306	0.0246		0.0051
0.0080	0.2438				0.5879							
0.0080	0.2438	0.3419	0.0200	0.5656								
0.0100	0.3048	0.3461	0.0200	0.5693								
0.0130	0.3962				0.5947							
0.0150	0.4572	0.3588	0.0200	0.5803								
0.0180	0.5486										0.0258	
0.0180	0.5486					0.5894	0.5894	-0.0024	0.0354	0.0251		0.0077
0.0200	0.6096	0.3733	0.0200	0.5927								
0.0230	0.7010				0.6201							
0.0280	0.8534										0.0277	
0.0280	0.8534					0.6157	0.6157	-0.0042	0.0357	0.0252		0.0089
0.0300	0.9144	0.4061	0.0200	0.6198								
0.0330	1.0058				0.6455							
0.0380	1.1582										0.0408	
0.0380	1.1582					0.6433	0.6433	-0.0055	0.0360	0.0256		0.0089
0.0400	1.2192	0.4398	0.0200	0.6464								
0.0430	1.3106				0.6726							
0.0480	1.4630										0.0298	
0.0480	1.4630					0.6677	0.6676	-0.0086	0.0360	0.0257		0.0091
0.0500	1.5240	0.4759	0.0200	0.6737								
0.0530	1.6154				0.6964							
0.0580	1.7678										0.0304	
0.0580	1.7678					0.6913	0.6913	-0.0075	0.0367	0.0260		0.0091
0.0600	1.8288	0.5110	0.0200	0.6993								
0.0630	1.9202				0.7219							
0.0680	2.0726										0.0310	
0.0680	2.0726					0.7179	0.7179	-0.0081	0.0378	0.0268		0.0097
0.0700	2.1336	0.5443	0.0200	0.7227								
0.0730	2.2250				0.7408							
0.0780	2.3774										0.0310	
0.0780	2.3774					0.7387	0.7386	-0.0093	0.0383	0.0275		0.0100
0.0800	2.4384	0.5776	0.0205	0.7451								
0.0830	2.5298				0.7652							

\+ CROSS WIRE PROBE
\++ SINGLE WIRE PROBE
\+++ PITOT-STATIC

TABLE 23 (continued)

Y (FT.)	Y (CM.)	CP (TOATL)	CP (STATIC)	Q/UO +++	Q/UO ++	Q/UO +	U/UO +	V/UO +	URMS/UO +	VRMS/UO +	WRMS/UO +	-2UV/UO**2 +
0.0880	2.6822										0.0315	
0.0880	2.6822					0.7630	0.7629	-0.0091	0.0392	0.0278		0.0103
0.0900	2.7432	0.6132	0.0210	0.7682								
0.0930	2.8346				0.7835							
0.0980	2.9870										0.0320	
0.0980	2.9870					0.7858	0.7858	-0.0087	0.0399	0.0278		0.0109
0.1000	3.0480	0.6502	0.0214	0.7917								
0.1030	3.1394				0.8070							
0.1080	3.2918										0.0327	
0.1080	3.2918					0.8083	0.8083	-0.0088	0.0403	0.0276		0.0102
0.1100	3.3528	0.6872	0.0217	0.8146								
0.1130	3.4442				0.8264							
0.1180	3.5966										0.0327	
0.1180	3.5966					0.8273	0.8273	-0.0086	0.0402	0.0275		0.0100
0.1200	3.6576	0.7266	0.0219	0.8383								
0.1230	3.7490				0.8486							
0.1280	3.9014										0.0314	
0.1280	3.9014					0.8542	0.8542	-0.0092	0.0393	0.0270		0.0096
0.1300	3.9624	0.7622	0.0224	0.8590								
0.1330	4.0538				0.8707							
0.1380	4.2062										0.0313	
0.1380	4.2062					0.8751	0.8751	-0.0082	0.0382	0.0263		0.0089
0.1400	4.2672	0.8065	0.0228	0.8841								
0.1430	4.3586				0.8917							
0.1480	4.5110										0.0295	
0.1480	4.5110					0.8939	0.8938	-0.0098	0.0362	0.0251		0.0081
0.1500	4.5720	0.8343	0.0231	0.8996								
0.1530	4.6634				0.9139							
0.1580	4.8158										0.0278	
0.1580	4.8158					0.9161	0.9161	-0.0066	0.0333	0.0239		0.0073
0.1600	4.8768	0.8666	0.0233	0.9172								
0.1630	4.9682				0.9351							
0.1680	5.1206										0.0256	
0.1680	5.1206					0.9363	0.9363	-0.0076	0.0313	0.0220		0.0060
0.1700	5.1816	0.8985	0.0233	0.9345								
0.1730	5.2730				0.9497							
0.1780	5.4254										0.0235	
0.1780	5.4254					0.9531	0.9531	-0.0051	0.0288	0.0204		0.0051
0.1800	5.4864	0.9304	0.0233	0.9514								
0.1830	5.5778				0.9635							
0.1880	5.7302										0.0202	
0.1880	5.7302					0.9669	0.9669	-0.0069	0.0249	0.0178		0.0041
0.1900	5.7912	0.9580	0.0235	0.9657								
0.1930	5.8826				0.9729							
0.1980	6.0350										0.0170	
0.1980	6.0350					0.9837	0.9837	-0.0052	0.0205	0.0149		0.0030
0.2000	6.0960	0.9781	0.0238	0.9759								
0.2030	6.1874				0.9879							
0.2080	6.3398										0.0133	
0.2080	6.3398					0.9950	0.9950	-0.0044	0.0151	0.0125		0.0017

\+ CROSS WIRE PROBE
\++ SINGLE WIRE PROBE
\+++ PITOT-STATIC

TABLE 23 (continued)

Y (FT.)	Y (CM.)	CP (TOATL)	CP (STATIC)	Q/UO +++	Q/UO ++	Q/UO +	U/UO +	V/UO +	URMS/UO +	VRMS/UO +	WRMS/UO +	-2OUV/UO**2 +
0.2100	6.4008	0.9927	0.0238	0.9833								
0.2130	6.4922				0.9981							
0.2180	6.6446										0.0093	
0.2180	6.6446					0.9995	0.9995	-0.0035	0.0096	0.0096		0.0007
0.2200	6.7056	0.9992	0.0238	0.9866								
0.2230	6.7970				1.0036							
0.2280	6.9494										0.0069	
0.2280	6.9494					1.0042	1.0042	-0.0040	0.0060	0.0077		0.0005
0.2300	7.0104	1.0030	0.0236	0.9886								
0.2330	7.1018				1.0030							
0.2380	7.2542										0.0062	
0.2380	7.2542					1.0047	1.0047	-0.0036	0.0043	0.0064		0.0003
0.2400	7.3152	1.0034	0.0233	0.9890								
0.2430	7.4066				1.0049							
0.2480	7.5590										0.0064	
0.2480	7.5590					1.0060	1.0060	-0.0049	0.0038	0.0077		0.0002
0.2500	7.6200	1.0034	0.0233	0.9890								
0.2530	7.7114				1.0049							
0.2600	7.9248	1.0034	0.0233	0.9890								

\+ CROSS WIRE PROBE
\++ SINGLE WIRE PROBE
\+++ PITOT-STATIC

TABLE 24 PROFILES AT X/L = 1.300

Y (FT.)	Y (CM.)	CP (TOTAL)	CP (STATIC)	Q/UO +++	Q/UO ++	Q/UO +	U/UO +	V/UO +	URMS/UO +	VRMS/UO +	WRMS/UO +	-2UV/UO**2 +
0.0020	0.0610	0.3676	0.0116	0.5960								
0.0020	0.0610										0.0233	
0.0020	0.0610					0.5999	0.5999	-0.0003	0.0304	0.0270		0.0048
0.0020	0.0610				0.5966							
0.0020	0.0610	0.3676	0.0116	0.5960								
0.0020	0.0610										0.0233	
0.0020	0.0610					0.5999	0.5999	-0.0003	0.0304	0.0270		0.0048
0.0020	0.0610				0.5966							
0.0020	0.0610	0.3676	0.0116	0.5960								
0.0030	0.0914	0.3690	0.0116	0.5970								
0.0040	0.1219				0.5989							
0.0050	0.1524	0.3730	0.0116	0.5980								
0.0060	0.1829				0.6011							
0.0090	0.2438					0.6043	0.6043	-0.0013	0.0324	0.0271		0.0059
0.0100	0.3048	0.3799	0.0116	0.6060								
0.0120	0.3658										0.0245	
0.0150	0.4572	0.3911	0.0116	0.6150								
0.0160	0.4877				0.6115							
0.0180	0.5486					0.6238	0.6238	-0.0057	0.0365	0.0272		0.0090
0.0200	0.6096	0.4032	0.0116	0.6250								
0.0220	0.6706										0.0265	
0.0260	0.7925				0.6328							
0.0280	0.8534					0.6445	0.6445	-0.0055	0.0400	0.0274		0.0104
0.0300	0.9144	0.4351	0.0116	0.6500								
0.0320	0.9754										0.0288	
0.0360	1.0973				0.6590							
0.0380	1.1582					0.6700	0.6700	-0.0067	0.0409	0.0274		0.0109
0.0400	1.2192	0.4698	0.0116	0.6760								
0.0420	1.2802										0.0305	
0.0460	1.4021				0.6788							
0.0480	1.4630					0.6927	0.6927	-0.0081	0.0401	0.0267		0.0095
0.0500	1.5240	0.5072	0.0119	0.7030								
0.0520	1.5850										0.0318	
0.0560	1.7069				0.7015							
0.0580	1.7678					0.7176	0.7175	-0.0111	0.0411	0.0270		0.0091
0.0600	1.8288	0.5400	0.0121	0.7260								
0.0620	1.8898										0.0326	
0.0660	2.0117				0.7231							
0.0680	2.0726					0.7451	0.7450	-0.0145	0.0404	0.0269		0.0090
0.0700	2.1336	0.5738	0.0123	0.7490								
0.0720	2.1946										0.0331	
0.0760	2.3165				0.7422							
0.0780	2.3774					0.7565	0.7564	-0.0137	0.0408	0.0270		0.0087
0.0800	2.4384	0.6094	0.0125	0.7720								
0.0820	2.4994										0.0328	
0.0860	2.6213				0.7679							
0.0880	2.6822					0.7812	0.7811	-0.0119	0.0409	0.0271		0.0091
0.0900	2.7432	0.6426	0.0127	0.7930								
0.0920	2.8042										0.0326	
0.0960	2.9261				0.7896							

\+ CROSS WIRE PROBE
++ SINGLE WIRE PROBE
+++ PITOT-STATIC

TABLE 24 (continued)

Y (FT.)	Y (CM.)	CP (TOATL)	CP (STATIC)	C/UC +++	Q/UO ++	Q/UO +	U/UO +	V/UO +	URMS/UO +	VRMS/UC +	WRMS/UC +	-2CUV/UC**2 +
0.0980	2.9870					0.8011	0.8010	-0.0110	0.0417	0.0275		0.0093
0.1000	3.0480	0.6750	0.0130	0.8130								
0.1020	3.1090										0.0318	
0.1060	3.2309				0.8112							
0.1080	3.2918					0.8194	0.8194	-0.0055	0.0410	0.0275		0.0098
0.1100	3.3528	0.7125	0.0133	0.8360								
0.1120	3.4138										0.0313	
0.1160	3.5357				0.8291							
0.1180	3.5966					0.8385	0.8384	-0.0095	0.0414	0.0270		0.0097
0.1200	3.6576	0.7485	0.0136	0.8570								
0.1220	3.7186										0.0310	
0.1260	3.8405				0.8499							
0.1280	3.9014					0.8594	0.8593	-0.0109	0.0405	0.0263		0.0091
0.1300	3.9624	0.7850	0.0140	0.8770								
0.1320	4.0234										0.0299	
0.1360	4.1453				0.8720							
0.1380	4.2062					0.8812	0.8812	-0.0062	0.0391	0.0261		0.0086
0.1400	4.2672	0.8187	0.0144	0.8960								
0.1420	4.3282										0.0285	
0.1460	4.4501				0.8939							
0.1480	4.5110					0.9026	0.9026	-0.0057	0.0375	0.0246		0.0070
0.1500	4.5720	0.8469	0.0147	0.9120								
0.1520	4.6330										0.0272	
0.1560	4.7549				0.9131							
0.1580	4.8158					0.9213	0.9213	-0.0015	0.0352	0.0229		0.0060
0.1600	4.8768	0.8802	0.0149	0.9296								
0.1620	4.9378										0.0257	
0.1660	5.0597				0.9266							
0.1680	5.1206					0.9345	0.9345	-0.0015	0.0323	0.0212		0.0050
0.1700	5.1816	0.9102	0.0151	0.9455								
0.1720	5.2426										0.0234	
0.1760	5.3645				0.9449							
0.1780	5.4254					0.9498	0.9498	0.0017	0.0299	0.0195		0.0046
0.1800	5.4864	0.9364	0.0154	0.9592								
0.1820	5.5474										0.0212	
0.1860	5.6693				0.9551							
0.1880	5.7302					0.9688	0.9688	0.0010	0.0268	0.0173		0.0034
0.1900	5.7912	0.9650	0.0156	0.9738								
0.1920	5.8522										0.0182	
0.1960	5.9741				0.9688							
0.1980	6.0350					0.9847	0.9847	0.0021	0.0208	0.0148		0.0024
0.2000	6.0960	0.9809	0.0158	0.9819								
0.2020	6.1570										0.0152	
0.2060	6.2789				0.9876							
0.2080	6.3398					0.9935	0.9935	-0.0011	0.0177	0.0126		0.0018
0.2100	6.4008	0.9931	0.0159	0.9880								
0.2120	6.4618										0.0114	
0.2160	6.5837				0.9982							
0.2180	6.6446					1.0019	1.0019	0.0030	0.0116	0.0105		0.0008
0.2200	6.7056	0.9987	0.0161	0.9908								

+ CROSS WIRE PROBE
++ SINGLE WIRE PROBE
+++ PITOT-STATIC

TABLE 24 (continued)

Y (FT.)	Y (CM.)	CP (TOATL)	CP (STATIC)	Q/UO +++	Q/UO ++	Q/UC +	U/UO +	V/UO +	URMS/UC +	VRMS/UC +	WRMS/UC +	-2OUV/UC**2 +
0.2220	6.7666										0.0094	
0.2260	6.8885				1.0042							
0.2280	6.9494					1.0003	1.0002	0.0117	0.0071	0.0082		0.0004
0.2300	7.0104	1.0010	0.0162	0.9918								
0.2320	7.0714										0.0079	
0.2360	7.1933				1.0063							
0.2380	7.2542					1.0009	1.0008	0.0115	0.0046	0.0063		0.0003
0.2400	7.3152	1.0034	0.0163	0.9930								
0.2420	7.3762										0.0064	
0.2460	7.4981				1.0067							
0.2480	7.5590					0.9990	0.9989	0.0150	0.0037	0.0058		0.0001
0.2500	7.6200	1.0034	0.0163	0.9930								

\+ CROSS WIRE PROBE
\++ SINGLE WIRE PRCBE
\+++ PITOT-STATIC

TABLE 25 PROFILES AT X/L = 1.400

Y (FT.)	Y (CM.)	CP (TOTAL)	CP (STATIC)	Q/UO +++	Q/UO ++	Q/UO +	U/UO +	V/UO +	URMS/UO +	VRMS/UO +	WRMS/UO +	-2OUV/UO**2 +
0.0000	0.0000										0.0223	
0.0000	0.0000				0.6420							
0.0000	0.0000	0.3830	0.0074	0.6120								
0.0010	0.0305					0.6139	0.6138	0.0091	0.0323	0.0289		0.0049
0.0010	0.0305				0.6456							
0.0020	0.0610										0.0222	
0.0020	0.0610				0.6464							
0.0020	0.0610	0.3830	0.0074	0.6121								
0.0030	0.0914					0.6110	0.6110	0.0052	0.0330	0.0287		0.0052
0.0040	0.1219										0.0223	
0.0040	0.1219	0.3830	0.0074	0.6121								
0.0050	0.1524					0.6203	0.6203	0.0030	0.0337	0.0283		0.0052
0.0050	0.1524	0.3834	0.0074	0.6124								
0.0060	0.1829										0.0224	
0.0070	0.2134	0.3848	0.0074	0.6135								
0.0080	0.2438										0.0227	
0.0090	0.2743					0.6216	0.6216	0.0032	0.0347	0.0286		0.0061
0.0090	0.2743				0.6502							
0.0090	0.2743	0.3884	0.0074	0.6164								
0.0100	0.3048										0.0230	
0.0120	0.3658										0.0231	
0.0140	0.4267										0.0236	
0.0140	0.4267				0.6619							
0.0140	0.4267	0.3971	0.0074	0.6235								
0.0190	0.5791					0.6389	0.6389	-0.0013	0.0393	0.0286		0.0089
0.0190	0.5791	0.4085	0.0074	0.6325								
0.0240	0.7315										0.0254	
0.0240	0.7315				0.6842							
0.0290	0.8839					0.6594	0.6594	-0.0049	0.0426	0.0287		0.0113
0.0290	0.8839	0.4381	0.0074	0.6555								
0.0340	1.0363										0.0274	
0.0340	1.0363				0.7052							
0.0390	1.1887					0.6755	0.6753	-0.0147	0.0440	0.0287		0.0117
0.0390	1.1887	0.4838	0.0074	0.6895								
0.0440	1.3411										0.0292	
0.0440	1.3411				0.7300							
0.0490	1.4935					0.7123	0.7122	-0.0116	0.0434	0.0287		0.0118
0.0490	1.4935	0.5175	0.0079	0.7132								
0.0540	1.6459										0.0297	
0.0540	1.6459				0.7507							
0.0590	1.7983					0.7311	0.7311	-0.0080	0.0426	0.0284		0.0113
0.0590	1.7983	0.5558	0.0079	0.7395								
0.0640	1.9507										0.0309	
0.0640	1.9507				0.7766							
0.0690	2.1031					0.7558	0.7557	-0.0131	0.0428	0.0279		0.0110
0.0690	2.1031	0.5887	0.0081	0.7613								
0.0740	2.2555										0.0305	
0.0740	2.2555				0.8012							
0.0790	2.4079					0.7731	0.7730	-0.0141	0.0421	0.0279		0.0111
0.0790	2.4079	0.6206	0.0083	0.7819								

\+ CROSS WIRE PROBE
\++ SINGLE WIRE PROBE
\+++ PITOT-STATIC

TABLE 25 (continued)

Y (FT.)	Y (CM.)	CP (TOTAL)	CP (STATIC)	Q/UO +++	Q/UO ++	Q/UO +	U/UO +	V/UO +	URMS/UO +	VRMS/UO +	WRMS/UO +	-2UV/UO**2 +
0.0840	2.5603										0.0301	
0.0840	2.5603				0.8214							
0.0890	2.7127					0.7997	0.7996	-0.0124	0.0424	0.0286		0.0115
0.0890	2.7127	0.6567	0.0085	0.8045								
0.0940	2.8651										0.0300	
0.0940	2.8651				0.8414							
0.0990	3.0175					0.8111	0.8111	-0.0047	0.0425	0.0281		0.0112
0.1000	3.0480	0.6927	0.0088	0.8264								
0.1040	3.1699										0.0293	
0.1040	3.1699				0.8632							
0.1090	3.3223					0.8308	0.8308	-0.0051	0.0420	0.0276		0.0106
0.1100	3.3528	0.7269	0.0090	0.8467								
0.1140	3.4747										0.0285	
0.1140	3.4747				0.8747							
0.1190	3.6271					0.8546	0.8545	-0.0151	0.0420	0.0268		0.0102
0.1200	3.6576	0.7569	0.0092	0.8641								
0.1240	3.7795										0.0277	
0.1240	3.7795				0.8874							
0.1290	3.9319					0.8784	0.8783	-0.0105	0.0393	0.0254		0.0086
0.1300	3.9624	0.7902	0.0095	0.8830								
0.1340	4.0843										0.0262	
0.1340	4.0843				0.9091							
0.1390	4.2367					0.8868	0.8868	-0.0027	0.0386	0.0246		0.0083
0.1400	4.2672	0.8239	0.0097	0.9018								
0.1440	4.3891										0.0249	
0.1440	4.3891				0.9304							
0.1490	4.5415					0.9065	0.9065	-0.0028	0.0360	0.0225		0.0066
0.1500	4.5720	0.8520	0.0097	0.9172								
0.1540	4.6939										0.0238	
0.1540	4.6939				0.9490							
0.1590	4.8463					0.9277	0.9276	-0.0111	0.0332	0.0214		0.0058
0.1600	4.8768	0.8853	0.0101	0.9350								
0.1640	4.9987										0.0218	
0.1640	4.9987				0.9610							
0.1690	5.1511					0.9455	0.9454	-0.0137	0.0311	0.0202		0.0050
0.1700	5.1816	0.9111	0.0105	0.9485								
0.1740	5.3035										0.0200	
0.1740	5.3035				0.9738							
0.1790	5.4559					0.9718	0.9716	-0.0179	0.0283	0.0183		0.0045
0.1800	5.4864	0.9373	0.0109	0.9620								
0.1840	5.6083										0.0173	
0.1840	5.6083				0.9834							
0.1890	5.7607					0.9830	0.9829	-0.0113	0.0247	0.0166		0.0038
0.1900	5.7912	0.9607	0.0113	0.9739								
0.1940	5.9131										0.0147	
0.1940	5.9131				0.9927							
0.1990	6.0655					0.9956	0.9955	-0.0121	0.0220	0.0149		0.0027
0.2000	6.0960	0.9809	0.0116	0.9840								
0.2040	6.2179										0.0121	
0.2040	6.2179				1.0020							

\+ CROSS WIRE PROBE
\++ SINGLE WIRE PROBE
\+++ PITOT-STATIC

TABLE 25 (continued)

Y (FT.)	Y (CM.)	CP (TOATL)	CP (STATIC)	Q/UO +++	Q/UO ++	Q/UO +	U/UO +	V/UO +	URMS/UO +	VRMS/UO +	WRMS/UO +	-2UV/UO**2 +
0.2090	6.3703					1.0072	1.0071	-C.0124	0.0165	C.C127		C.C018
0.2100	6.4CC8	0.9935	0.0117	0.9904								
0.2140	6.5227										0.C085	
0.2140	6.5227				1.0039							
0.2190	6.6751					1.0120	1.0120	-C.0047	0.0116	C.CC98		0.CC08
0.2200	6.7C56	0.9991	0.0118	0.9931								
0.2240	6.8275										0.0077	
0.2240	6.8275				1.0049							
0.2290	6.9799					1.0082	1.0082	-0.0033	0.0067	C.CC84		C.CC05
0.2300	7.0104	1.0021	0.0119	0.9946								
0.2340	7.1323										0.0058	
0.2340	7.1323				1.0089							
0.2390	7.2847					1.0166	1.0165	-0.0104	0.0C46	C.CC69		0.CC03
0.2400	7.3152	1.0034	0.0120	0.9952								
0.2440	7.4371										0.CC57	
0.2440	7.4371				1.0100							
0.2490	7.5895					1.0131	1.0131	-0.0087	0.0050	0.CC59		0.CC02
0.2500	7.6200	1.0034	0.0120	0.9951								
0.2600	7.9248	-0.C600	0.0120	C.9951								

+ CROSS WIRE PROBE
++ SINGLE WIRE PROBE
+++ PITOT-STATIC

TABLE 26 PROFILES AT X/L = 2.472

Y (FT.)	Y (CM.)	CP (TOATL)	CP (STATIC)	Q/UO +++	Q/UO ++	Q/UO +	U/UO +	V/UO +	URMS/UO +	VRMS/UO +	WRMS/UO +	-2OUV/UO**2 +
0.0000	0.0000										0.0263	
0.0000	0.0000					0.8080	0.8079	0.0129	0.0408	0.0368		0.0042
0.0000	0.0000				0.8105							
0.0000	0.0000	0.6313	0.0000	0.7945								
0.0020	0.0610										0.0262	
0.0020	0.0610					0.8095	0.8094	0.0125	0.0401	0.0363		0.0043
0.0020	0.0610				0.8110							
0.0040	0.1219				0.8120							
0.0100	0.3048	0.6326	0.0010	0.7947								
0.0120	0.3658										0.0254	
0.0120	0.3658					0.8105	0.8104	0.0116	0.0383	0.0363		0.0088
0.0120	0.3658				0.8106							
0.0200	0.6096	0.6368	0.0010	0.7974								
0.0220	0.6706										0.0252	
0.0220	0.6706					0.8128	0.8128	0.0082	0.0380	0.0353		0.0081
0.0220	0.6706				0.8129							
0.0300	0.9144	0.6465	0.0010	0.8034								
0.0320	0.9754										0.0251	
0.0320	0.9754					0.8120	0.8120	0.0053	0.0387	0.0351		0.0079
0.0320	0.9754				0.8196							
0.0400	1.2192	0.6562	0.0010	0.8094								
0.0420	1.2802										0.0255	
0.0420	1.2802					0.8212	0.8212	0.0042	0.0409	0.0350		0.0093
0.0420	1.2802				0.8253							
0.0500	1.5240	0.6768	0.0010	0.8221								
0.0520	1.5850										0.0260	
0.0520	1.5850					0.8286	0.8286	0.0038	0.0414	0.0339		0.0109
0.0520	1.5850				0.8290							
0.0600	1.8288	0.6906	0.0010	0.8304								
0.0620	1.8898										0.0268	
0.0620	1.8898					0.8412	0.8412	0.0008	0.0436	0.0335		0.0119
0.0620	1.8898				0.8424							
0.0700	2.1336	0.7099	0.0010	0.8420								
0.0720	2.1946										0.0283	
0.0720	2.1946					0.8442	0.8442	0.0002	0.0450	0.0332		0.0130
0.0720	2.1946				0.8545							
0.0800	2.4384	0.7319	0.0010	0.8549								
0.0820	2.4994										0.0295	
0.0820	2.4994					0.8572	0.8572	-0.0024	0.0452	0.0323		0.0130
0.0820	2.4994				0.8661							
0.0900	2.7432	0.7540	0.0020	0.8672								
0.0920	2.8042										0.0304	
0.0920	2.8042					0.8704	0.8704	-0.0031	0.0450	0.0315		0.0127
0.0920	2.8042				0.8774							
0.1000	3.0480	0.7748	0.0020	0.8791								
0.1020	3.1090										0.0302	
0.1020	3.1090					0.8876	0.8876	-0.0010	0.0449	0.0307		0.0132
0.1020	3.1090				0.8820							
0.1100	3.3528	0.7940	0.0020	0.8899								
0.1120	3.4138										0.0300	

+ CROSS WIRE PROBE
++ SINGLE WIRE PROBE
+++ PITOT-STATIC

TABLE 26 (continued)

Y (FT.)	Y (CM.)	CP (TOTAL)	CP (STATIC)	Q/UO +++	Q/UO ++	Q/UO +	U/UO +	V/UO +	URMS/UO +	VRMS/UO +	WRMS/UO +	-2UV/UO**2 +
0.1120	3.4138					0.8971	0.8971	-0.0018	0.0440	0.0300		0.0120
0.1120	3.4138				0.8979							
0.1200	3.6576	0.6161	0.0020	0.9023								
0.1220	3.7186										0.0302	
0.1220	3.7186					0.9105	0.9105	-0.0032	0.0437	0.0294		0.0110
0.1220	3.7186				0.9042							
0.1300	3.9624	0.8355	0.0020	0.9130								
0.1320	4.0234										0.0305	
0.1320	4.0234					0.9194	0.9194	-0.0036	0.0425	0.0283		0.0100
0.1320	4.0234				0.9094							
0.1400	4.2672	0.8547	0.0020	0.9234								
0.1420	4.3282										0.0301	
0.1420	4.3282					0.9327	0.9327	0.0001	0.0411	0.0272		0.0096
0.1420	4.3282				0.9222							
0.1500	4.5720	0.8726	0.0020	0.9331								
0.1520	4.6330										0.0292	
0.1520	4.6330					0.9430	0.9430	0.0002	0.0396	0.0260		0.0088
0.1520	4.6330				0.9292							
0.1600	4.8768	0.8906	0.0020	0.9427								
0.1620	4.9378										0.0278	
0.1620	4.9378					0.9473	0.9473	-0.0016	0.0381	0.0250		0.0080
0.1620	4.9378				0.9385							
0.1700	5.1816	0.9099	0.0020	0.9528								
0.1720	5.2426										0.0264	
0.1720	5.2426					0.9572	0.9572	0.0014	0.0356	0.0235		0.0068
0.1720	5.2426				0.9498							
0.1800	5.4864	0.9292	0.0030	0.9624								
0.1820	5.5474										0.0244	
0.1820	5.5474					0.9687	0.9687	0.0002	0.0334	0.0220		0.0063
0.1820	5.5474				0.9592							
0.1900	5.7912	0.9443	0.0030	0.9702								
0.1920	5.8522										0.0230	
0.1920	5.8522					0.9706	0.9706	0.0004	0.0315	0.0208		0.0053
0.1920	5.8522				0.9685							
0.2000	6.0960	0.9623	0.0030	0.9794								
0.2020	6.1570										0.0204	
0.2020	6.1570					0.9843	0.9843	0.0017	0.0283	0.0186		0.0046
0.2020	6.1570				0.9787							
0.2100	6.4008	0.9733	0.0040	0.9846								
0.2120	6.4618										0.0182	
0.2120	6.4618					0.9926	0.9926	0.0038	0.0245	0.0170		0.0038
0.2120	6.4618				0.9889							
0.2200	6.7056	0.9857	0.0050	0.9903								
0.2220	6.7666										0.0166	
0.2220	6.7666					0.9974	0.9974	0.0010	0.0211	0.0157		0.0029
0.2220	6.7666				0.9990							
0.2300	7.0104	0.9912	0.0050	0.9931								
0.2320	7.0714										0.0151	
0.2320	7.0714					1.0032	1.0032	0.0029	0.0172	0.0140		0.0023
0.2320	7.0714				1.0023							

+ CROSS WIRE PROBE
++ SINGLE WIRE PROBE
+++ PITOT-STATIC

TABLE 26 (continued)

Y (FT.)	Y (CM.)	CP (TOATL)	CP (STATIC)	C/UO +++	Q/UO ++	Q/UC +	U/UO +	V/UO +	URMS/UC +	VRMS/UC +	WRMS/UC +	-2OUV/UC**2 +
0.2400	7.3152	0.9995	0.0050	0.9972								
0.2420	7.3762										C.C127	
0.2420	7.3762					1.0094	1.0094	C.0034	0.0132	C.C120		C.C016
0.2420	7.3762				1.0030							
0.2500	7.6200	1.C036	0.0050	0.9993								
0.2520	7.6810										C.C11C	
0.2520	7.6810					1.0143	1.0143	0.0025	0.01C0	C.C108		C.C011
0.2520	7.6810				1.0063							
0.2600	7.9248	1.C377	0.0050	1.0013								
0.2620	7.9858										C.CC95	
0.2620	7.9858					1.0168	1.0168	0.0031	0.0087	0.CC96		C.CC07
0.2620	7.9858				1.0077							
0.2720	8.2906										C.C08C	
0.2720	8.2906				1.0023							

\+ CROSS WIRE PROBE
\++ SINGLE WIRE PROBE
\+++ PITOT-STATIC

REPORT DOCUMENTATION PAGE

READ INSTRUCTIONS BEFORE COMPLETING FORM

1. REPORT NUMBER IIHR Report No. 210	2. GOVT ACCESSION NO.
3. RECIPIENT'S CATALOG NUMBER	
4. TITLE (and Subtitle) Thick Axisymmetric Turbulent Boundary Layer and Near Wake of a Low-Drag Body of Revolution	5. TYPE OF REPORT & PERIOD COVERED
	6. PERFORMING ORG. REPORT NUMBER IIHR Report No. 210
7. AUTHOR(s) V.C. Patel and Y.T. Lee	8. CONTRACT OR GRANT NUMBER(s) N00014-75-C-0273
9. PERFORMING ORGANIZATION NAME AND ADDRESS Institute of Hydraulic Research University of Iowa, Iowa City, Iowa 52242	10. PROGRAM ELEMENT, PROJECT, TASK AREA & WORK UNIT NUMBERS
11. CONTROLLING OFFICE NAME AND ADDRESS David W. Taylor Naval Ship Research and Development Center Dept. of the Navy, Bethesda, Maryland 20084	12. REPORT DATE December 1977 13. NUMBER OF PAGES 130
14. MONITORING AGENCY NAME & ADDRESS (if different from Controlling Office)	15. SECURITY CLASS. (of this report) Unclassified 15a. DECLASSIFICATION/DOWNGRADING SCHEDULE

16. DISTRIBUTION STATEMENT (of this Report)

Approved for public release, distribution unlimited

17. DISTRIBUTION STATEMENT (of the abstract entered in Block 20, if different from Report)

18. SUPPLEMENTARY NOTES

19. KEY WORDS (Continue on reverse side if necessary and identify by block number)

Thick turbulent boundary layer and wake, Longitudinal and transverse curvatures, Static-pressure variations, Turbulence models, Calculation procedures, Extra rates of strain.

20. ABSTRACT (Continue on reverse side if necessary and identify by block number)

Detailed measurements of pressure distributions, mean velocity profiles and Reynolds stresses were made in the thick, axisymmetric boundary layer and the near wake of a low-drag body of revolution. The data are presented in graphical as well as tabular form for convenience in later analysis. These measurements shed some light on the joint influence of transverse and longitudinal surface curvatures and pressure gradients on the boundary-layer development and on the manner in which an axisymmetric boundary layer becomes a

fully-developed wake. Apart from giving a complete set of data on such an important flow configuration, the measurements should provide a fairly rigorous test case for some of the recent turbulence closure models which claim a level of generality not achieved by the older phenomenological models. The present data have been used to provide an independent check on the accuracy of the simple, integral boundary-layer method proposed by Patel, and its extension to the calculation of the near wake made by Nakayama, Patel and Landweber. Preliminary calculations have also been performed using the differential equations of the thick axisymmetric turbulent boundary layer and a rate equation for the Reynolds stress derived from the turbulent kinetic-energy equation along the lines suggested by Bradshaw and others. By inclusion of recently proposed modifications to account for the effects of the extra rates of strain on the turbulence length scale arising from longitudinal and transverse surface curvatures, it is shown that the boundary layer in the tail region of a body of revolution is dominated by the extra strain rates and that more research is needed to account for them properly even in the most recent calculation procedures.